THE BEHAVIOUR OF MAGNETOTACTIC BACTERIA IN CHANGING MAGNETIC FIELDS

Graduation committee

prof. dr. J.N. Kok	University of Twente (chairman and secretary)
prof. dr. ir. L. Abelmann	Saarland University (supervisor)
prof. dr. ir. G.J.M. Krijnen	University of Twente (supervisor)
prof. dr.-Ing. M. Nienhaus	Saarland University
prof. dr. A. Luzhetskyy	Saarland University
prof. dr. A. Manz	KIST Europe
prof. dr. J.C.T Eijkel	University of Twente
prof. dr. J.L. Herek	University of Twente

Deans

prof. dr. J.N. Kok	University of Twente, faculty of Electrical Engineering, Mathematics and Computer Science
prof. dr. G. Kickelbick	Saarland University, faculty of Natural Sciences and Technology

UNIVERSITY OF TWENTE.

KIST Europe

Korea Institute of Science and Technology

UNIVERSITÄT DES SAARLANDES

Cover design by Marc Pichel

THE BEHAVIOUR OF MAGNETOTACTIC BACTERIA IN CHANGING MAGNETIC FIELDS

DISSERTATION

to obtain the degree of doctor at the University of Twente,
on the authority of the rector magnificus, prof. dr. T.T.M. Palstra,

and to obtain the degree of doctor at Saarland University,
on the autority of the president, prof. dr. M.J. Schmitt,

on account of the decision of the graduation committee,
to be publicly defended
on Friday, 9 March 2018 at 14:45

by

Marc Philippe Pichel

born on 21 November 1982,
in Rotterdam, the Netherlands

This dissertation is approved by

prof. dr. ir. L. Abelmann   Saarland University (supervisor)
prof. dr. ir. G.J.M. Krijnen University of Twente (supervisor)

Contents

Chapter 1

Introduction

This thesis presents the study I made over the last four years on magneto-tactic bacteria. The motivation for this research was the use of magneto-tactic bacteria in biomedical applications.

1.1 Minimally Invasive Surgery, Drug Delivery and Microrobots

The trauma to patients when undergoing surgery or drug treatment does not only vary greatly, but it can also have an immense impact on recovery time and side effects.

Going a step further, it might be possible to minimise our surgical and drug delivery tools to the microscopic level, while combing several approaches. Imagine a surgical knife that can travel through interstitial fluid, carrying a payload
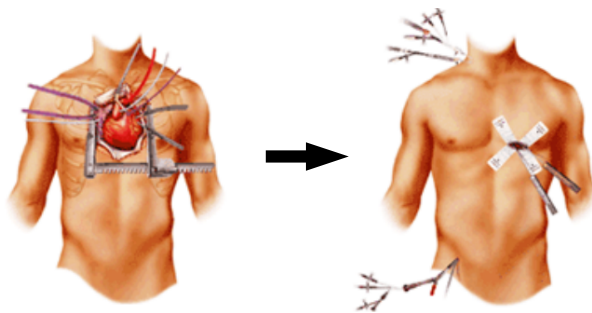
FIGURE 1.1 – *Left: A cartoon showing the impact on a patient during open-heart surgery. Right: A similar situation of a patient undergoing surgery using minimally invasive tools.*

1

FIGURE 1.2 – *An adventure of miniaturisation for the benefit of mankind. And fans of science fiction.*

of drugs which can be steered remotely. Not unlike the 1977 science-fiction movie *the fantastic voyage* as depicted in Figure 1.2.

Typically, our imagination is far ahead of technology. Though we are not that far from miniaturising steerable machines at the microscopic level. Some inspiring examples are the chemically and magnetically driven microrobots which require either an environment incompatible with the human body or both wireless steering and propulsion. An example of engineering at this scale can be seen in Figure 1.3. The direction of movement is determined by an external magnetic field (Solovev et al., 2012) propelled by a chemical catalyst (Schmidt and Eberl, 2001).

Our interests go out to machinery which does not rely on magnetic force, but rather on magnetic torque. The main reason is that the efficiency of using force is very low (Abbott et al., 2009). The force (N) on any microscopic vehicle is

$$\boldsymbol{F} = \nabla(\boldsymbol{m} \cdot \boldsymbol{B}), \tag{1.1}$$

where $\boldsymbol{m}$ (Am^2) is the magnetic dipole moment of the vehicle in question and $\boldsymbol{B}$ (T) is the applied magnetic field. The available field strength to pull an object drops off exponentially. This means that when trying to control an object at a depth of several centimeters requires giant magnetic setups. This is not the case with torque (Nm), which is

$$\boldsymbol{\Gamma} = \boldsymbol{m} \times \boldsymbol{B} \tag{1.2}$$
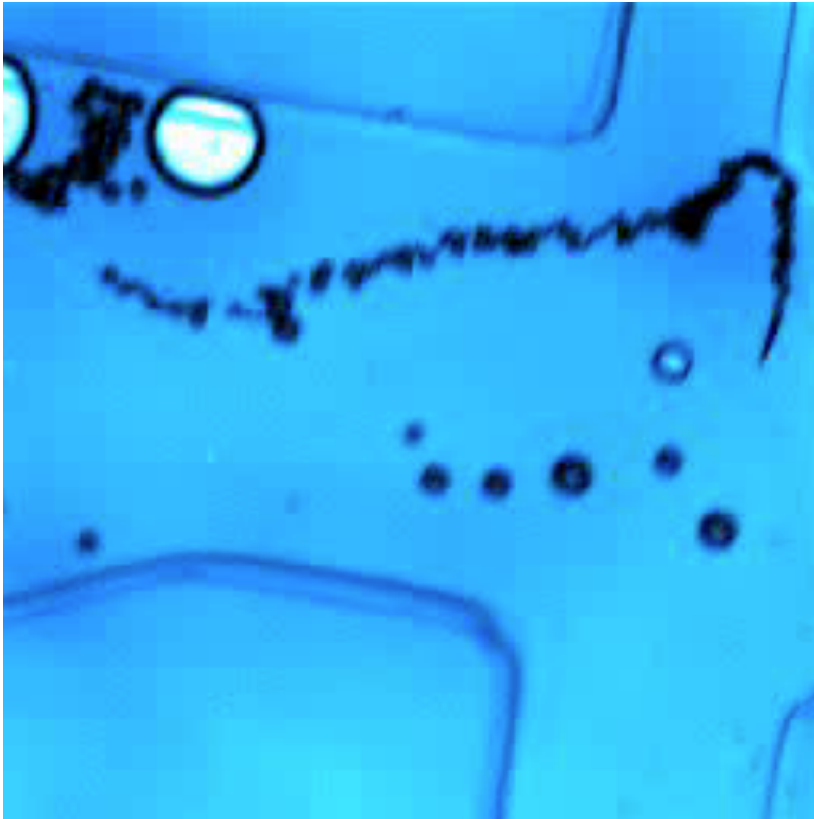
FIGURE 1.3 – *Example of a chemically driven magnetic nanorobot. A platinum catalist inside the robot converts perioxide to oxygen, which propels the robot forward.*

1.2   Magnetotactic Bacteria

As such, magnetotactic bacteria (MTB) have been a common candidate for study due to their many interesting properties. Not only are these organisms highly sensitive to chemical gradients, most notably oxygen, but it is also a naturally occurring magnet field-*sensing* organism. A chain consisting of roughly fifteen 40 nm Fe_3O_4 particles allow MTB to align to magnetic field lines, these are clearly visible under electron micrographs as shown in figure 1.4. It follows that, given a field 100-1000 times stronger than the earth magnetic field, $50\,\mu T$, MTB can be steered to some degree.

FIGURE 1.4 – *Left: A transmission electron micrograph of Magnetospirillum Gryphiswaldense, the MTB used for the majority of this thesis. Iron-oxide nanoparticles can be seen as a dark chain and flagella protruding at the top end (black arrow). Right: The same magnetic chain of particles (white) and flagella (white arrow) can also be seen on scanning electron micrographs of the same species of MTB.*

1.3   Biomimetic Robots

Even though the average velocity of a $5\,\mu$m MTB seems relatively high at $50\,\mu\text{m}\,\text{s}^{-1}$, it pales in comparison to the velocity of the blood in the human body with the exception of capillaries. Figure 1.5 shows an example of those ranges of velocities found in the human body. Furthermore, given that on average the heart with an ejection fraction of $50\,\%$ to $65\,\%$ (Kummer et al., 2010) on average pumps $4\,\text{L}\,\text{min}^{-1}$ to $8\,\text{L}\,\text{min}^{-1}$, it is safe to say that, if MTB would be used as microrobots, they would travel through the entire body within a minute given that an average human has about 5 L of blood (Maceira et al., 2016). If one would consider that for an MTB travelling the distance from heart to your big toe, which could be over 1 m twice, the equivalent of travel distance for a human would be 400000 times our body length, 800 km, in 1 min. Even the world's fastest man, Usain Bolt, sprinting at his topspeed of $44.72\,\text{km}\,\text{h}^{-1}$ would need a little under 20 hours to travel that distance.

1.4   Clinical Setting

In most cases bacteria or other foreign bodies are met with resistance by the immune system, lasting not much longer than several minutes. Compounding the hardship are other physical and chemical parameters like temperature, acidity, salinity, viscosity, etc. which can either perturbate or simply bring a
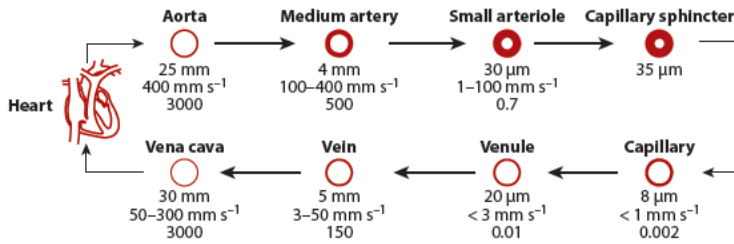
FIGURE 1.5 – *The range of speed of blood depending on vessels diameter. Only in certain cases can MTB flagella compete with and compensate for the speed of the medium they pass through.*

microorganism to a halt (Kumar et al., 2009). As a protective layer against the outside world, humans also possess mucosal layers in places where the regular epithelial layers, skin, are not present. These mucosal layers function as barriers against bacteria, viruses and other hazardous and foreign particles. On top of that, there are organs like the kidneys and the liver, which filter out what is excess or foreign in the body. This also means that certain medicine cannot easily penetrate or remain in our body, with the exclusion of direct injections via hypodermic needles or ingestion.

There are of course natural occurring exceptions, and we seek to exploit their traits for the use of drug delivery systems. To study what these potential biomimetic biorobots could do in the future, we use MTB as a template. We hope that in the future this could lead to new approach for increasing bioavailability and biocompatibility of drug delivery systems.

1.5   Microfluidic platform

As was shown (Erglis et al., 2007) it is possible to measure the magnetic dipole moment or at least make an estimate. Furthermore (Martel and Mohammadi, 2010) demonstrated amazing control over a swarm of MTB, allowing the construction of a microscopic pyramid structure. Combining this knowledge with the power of microfluidics, we attempt to observe individual MTBs more carefully.

1.6   Goal

The purpose of this research is guided by the following interests:

- Explore compatibility of MTB in microfluidic systems
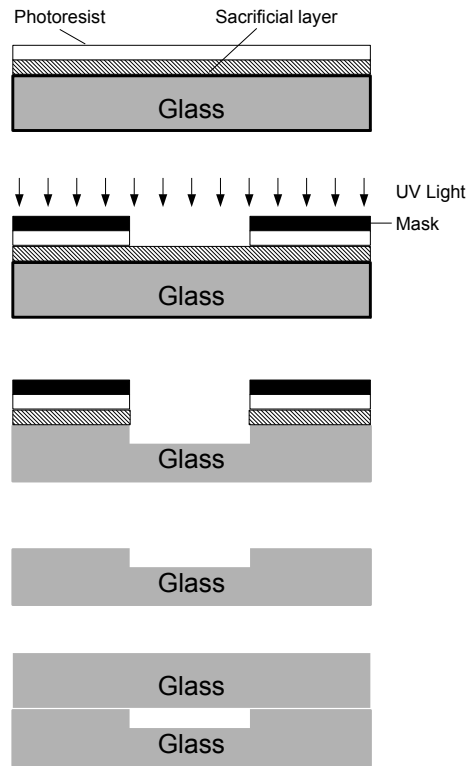
FIGURE 1.6 – *The workflow for fabrication of microfludic chips. In essence, our chips consists of two layers of glass. One patterned and one with etched inlet and outlet holes.*

- Observe behaviour of MTB under varying magnetic field strengths and directions
- Compare their behaviour to simulated datasets
- Explore other systems which might aid in expanding drug delivery research

1.7   Research question

Given the proper constraints to keep MTB in field-of-view, the main question is:

What can we learn about biophysical properties of MTB by observing single or bulk responses to changing magnetic fields?

This lead to several subquestions:

- Does the response (speed) of MTB to changing orientations of a magnetic field, depend on the magnetic field strength?
- How does their behaviour compare to existing theoretical models?
- Is there any potential in using static microfluidic chips instead of flow-based chips?
- Can any physical traits, other than magnetic properties, be derived from observations of single or bulk MTB?

1.8   Things to come

Before analysing bulk and individual properties of MTB at the microscopic level, we first look at the behaviour of an MTB model at the macroscopic level in **chapter 2: Micro- and Macroscopic Drag Torque of MTB**. Most notably the rotational drag, which is a crucial parameter in predicting U-turn paths described in the subsequent chapter. Translational drag has already been described in (Rodenborn et al., 2012), therefore our focus is only on the rotational component. The results from this chapter show that specific trait changes do affect rotational drag, however it does not exceed an order of magnitude in difference.

Next we look into the microscopic regime in **chapter 3: Rotational drag and rate of rotation of magneto-tactic bacteria**. This chapter describes the construction of a microfluidic chip platform to keeps the MTB in focus, which allows the MTB to be magnetically steered in two dimensions. Through the use of a rotating magnetic field U-turn trajectories are generated. These fields facilitate the analysis of the drag torque of MTBs. Results of this chapter show that MTB are susceptible to changes in magnetic field strength, up to a limited range where saturation takes place. It also shows that theoretical models and experimental results agree to a certain degree.

In **chapter 4: Longterm observation of MTB** we delve further into the single MTB observations, by increasing the observation time from several minutes in chapter 3 to several hours. During this period several MTB were observed and tracked for up to 90 minutes. Results from this chapter show a curious change in the MTB behaviour over a longer period of time. Whether this is due to fatigue or the effects of observing the MTB, remains unclear.

In **chapter 5: Real-time observation of MTB traits and growth** we continue to investigate the long term behaviour of MTB, but now in bulk. MTB are observed using a spectrophotometer, utilising similar principles as generic O.D.-meters in biological laboratories. With the exception that our device also provides a controllable magnetic coil system in three orthogonal directions. This allows us to measure continuously while applying magnetic fields in varying strength and orientations. Results show similar response of the bulk, com-

parable to results found in chapter 3. Additionally, traits such as speed, magnetic moment or rotational drag of MTB can be derived from the bulk analysis when using U-turn technique demonstrated in chapter 3.

As an outlook to the possiblities of MTB in minimally invasive medical procedures, we take a first step towards drug delivery applications. In **chapter 6: MTB and Mucus** we investigate the behaviour of MTB in the vicinity of human pulmonary mucus. These preliminary results show perturbation of MTB and reduced motility when moving at the interface of the growth medium and mucus.

Chapter 2

Micro- and Macroscopic Drag Torque of MTB

Abstract

In this study we modelled, simulated and measured the drag torque of 3D-printed models based on traits of *Magnetospirillum Gryphiswaldense* at a mesoscopic scale. Several trait differences were introduced to ascertain the contribution to rotational drag when compared to the base model.

The work in this chapter was executed in close cooperation with my colleagues. My specific contribution was to set up the cultivation of *Magnetospirillum Gryphiswaldense* in our laboratory, the design of the experimental setup, to prepare (TEM, SEM) samples for observation of MTB traits and supervise Alveena Mir, who designed the majority of the 3D printer models and performed the structuring of result data. The fit of our dataset to the polynomial was done in close cooperation with Tijmen Hageman.

2.1   Introduction

Bacteria have long been a source of inspiration for micro robotic design and self-driven motors (Nelson et al., 2010). Though accurate, the model used for estimation of rotational drag or shape factor of an MTB are not completely accurate. When looking at the difference in morphology, it could be speculated that the additional drag of an MTB is partially due to the size and frequency of the windings. This does not only apply to microorganisms with spirillum shapes, but also micro robots utilising similar morphology. In this study we attempt to measure the contribution of morphological traits of MTB to rotational drag at the macroscopic scale, as an analogy to the microscopic scale. How much magnetic torque is needed for steering an average MTB can be approximated using this approach.

2.1.1   Prior state-of-art

Rodenborn *et al.* investigated the contribution of morphological traits to drag of a spirillum shaped 3D model, compared to resistive force and slender body theory of Lighthill and Johnson *et al.* (Rodenborn et al., 2012). However, this only applies to translational drag. Instead we intend to focus on rotational drag as used in prediction of U-turn patterns by (Erglis et al., 2007).

2.1.2   Organisation of paper

In this paper we present a thorough experimental analysis of rotational drag of 3D printed models based on the morphology of magnetotactic bacteria macroscopic swimmers. We show the effects of changes in traits of the external morphology through an analysis of the rotational drag. These relations can help update our knowledge on predicting the drag of a specific shape factor of a spirillum shaped bacteria. We hope this can lead to more accurate control of MTB in the micro-robotics field.

2.2   Theory

2.2.1   Rotational drag

The rotational drag of an MTB is often approximated using a description for a prolate spheroid, rotating around it's minor axis. Though this model is accurate, it is not the true shape of the MTB. Furthermore, previous findings have shown that the difference in rotational drag can be observed when relying only on theoretical models (Erglis et al., 2007).

One could approximate the MTB by a prolate spheroid (Figure 2.1, top). The rotational drag coefficient for this shape has a simple expression (Berg, 1993)

$$f_{\text{p, theory}} = \frac{\eta \pi L^3}{3\ln(\frac{2L}{W}) - \frac{3}{2}} \qquad (2.1)$$

Where L is the bacteria length and W the bacteria width. This approximation does not encompass other traits of MTB such as helix amplitude (H) and number of windings (N). Therefore we introduce a correction, defined as a dimensionless factor α_{corr}.

$$\alpha_{\text{corr}}(L, W, H, N) = \frac{f_{\text{MTB}}(L, W, H, N)}{f_{\text{p, theory}}(L, W, H, N)} \qquad (2.2)$$

Since the bacteria are small and rotated slowly, the flow is in the laminar flow regime. Therefore, the correction will only depend on the relative dimensions. We propose to use the bacteria length L as the scaling factor, so $w = W/L$
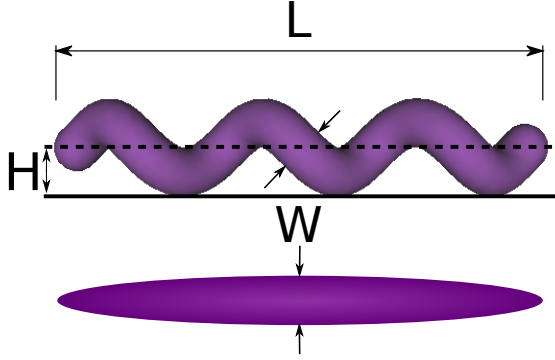
FIGURE 2.1 – *A schematic example of a the MTB (spirilium) (top) and prolate spheroid (bottom) shape. Relevant dimensions used for defining the (rotational) drag profile of a prolate spheroid, length, L, and width, W, according to Berg 1993. Additionally the MTB shape includes helical amplitude, H, and number of windings per length unit, L, the latter of which is not shown.*

and $h = H/L$. Over the parameter range investigated, the correction can be accurately approximated by a a three-dimensional linear fit:

$$\alpha_{\text{corr,poly}}(w, h, N) = a_0 + a_1 w + a_2 h + a_3 N \tag{2.3}$$

Macroscopic Analogy

Measuring the drag profile of these models at micro scale is a difficult task, since it requires production of all our models at the microscale. Microfabrication is limited in capacity when it comes to mimicking the shape and traits of MTB or other microorganisms. Therefor we limit our approach to the macroscopic scale at which we approximate the laminar conditions by adjusting for a Reynolds number below the value of Re=10, as shown to be reliable for Stokes flow approximations by Dennis *et al.* (Dennis et al., 1980). Inertial forces therefore do not play a significant role. The ratio between the viscous and inertial forces is characterized by the Reynolds number Re, which for rotation at an angular velocity of ω [rad/s] is

$$Re = \frac{L^2\omega}{4\nu}, \tag{2.4}$$

where L is the characteristic length (in case of our macroscopic models, the length of the bacterium and prolate spheroid), ν the kinematic viscosity of the liquid (m^2). Experiments by Dennis *et al.* (Dennis et al., 1980) show that a Stokes flow approximation for the drag torque is accurate up to Re=10, allowing

TABLE 2.1 – *By increasing the kinematic viscocity ν of the medium and reducing the rotational velocity, the Reynolds number of the macroscale models can be kept below one.*

	MTB	3D Model
L	2.5 μm	5 cm
W	0.25 μm	0.5 cm
ω	20 rad/s	2.6 rad/s
ν	1.0×10^{-6} m^2/s	5.7×10^{-3} m^2/s
Re	10^{-4}	0.3

experiments to remain outside the turbulent regime. An overview of all values at both scales can be seen in 2.1.

2.3 Experimental

2.3.1 Part Design

Parts were designed using freeware (OPENScad). SEM and TEM images of *Magnetospirillum Gryphiswaldense* were used to estimate the amount of windings per length unit of the base spirillum model. From which other variations. The 3D printed parts were made of PLA and subsequently drilled to fit the spindle used for all experiments. A variation of models can be seen in Figure 2.2.

2.3.2 Setup

All measurements were done using a rheometer (Brookfield DV-III Ultra). 3-D models were connected to the base spindle instead of the standard measuring tool. Subsequently, all samples were suspended in 5000 mPa s silicone oil (Calsil IP 5000 from Caldic, Belgium), as seen in Figure 2.3. The density of the silicon oil was assumed to have the literature value of 878 kg/m^3 , leading to a kinematic viscosity of 5.7×10^{-3} m^2/s.

2.3.3 Calibration and drag effects

Initial calibration to find a conversion factor from the relative torque measured by the rheometer to actual torque was done using a 3D printed sphere. As seen in Figure 2.4, the relation between torque and rotational velocity is linear, indicating that we are clearly in the laminar flow regime. The calibration factor is , which is in agreement with the manufacturers specification of 7.19 N m %$^{-1}$.

Additionally, we have observed an increase in drag when the size of the 3D printed models reach the outer dimensions of the containment unit. It can be seen in Figure 2.5 that the drag effect increases based on interaction with

FIGURE 2.2 – *Different shapes of models (from left to right): prolate spheroid, high helicity, high width, great length and high number of windings per length unit.*
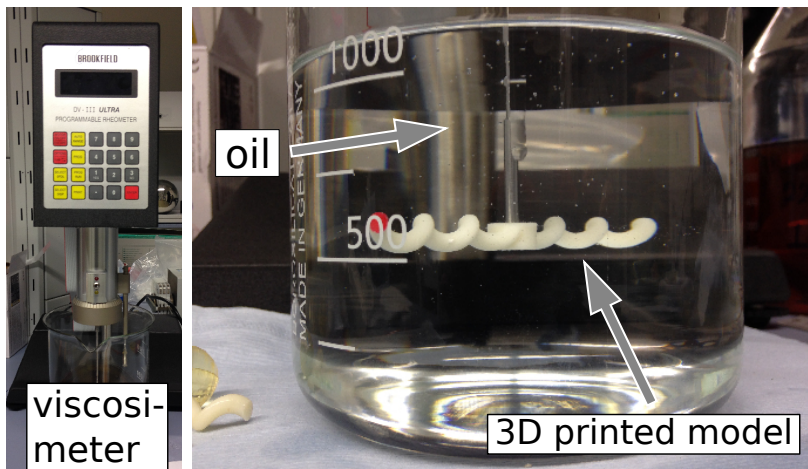
FIGURE 2.3 – *Setup used for all measurements.*
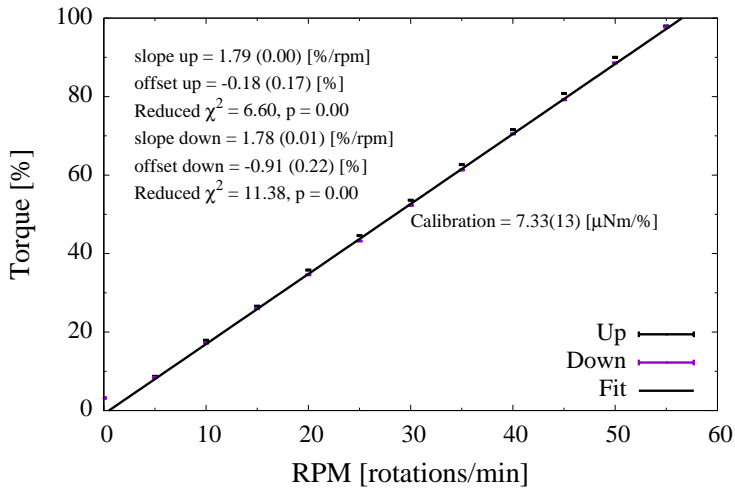
FIGURE 2.4 – *The calibration of a* 2 cm *sphere based on the drag profile for a sphere gives a slope of* 7.33 N m *for each % of the measured torque.*

the side walls, indicating that our environment might be a too confined for our larger models. Also for a short model, the deviation from theory becomes significant. This is most likely due to the additional cylindrical support that was needed to obtain a sturdy connection to the shaft. Based on this measurement, we decided to use models of 5.5 cm for the linear fit only.

2.4 Results

2.5 Measurement results

Various bacterium shapes were 3D printed to obtain measurement points. The basic shape consist of L=5.5 cm, W=5 mm, H=5 mm, D=55 m^{-1}. While keeping three of these variables fixed, the fourth was varied with a total of 25 shapes, based on the extrema found in figures 2.6, 2.7 and 2.8.

Eight additional shapes were constructed where two variables were changed at the same time, using the most extreme values for the variables as can be seen in figures 2.6, 2.7 and 2.8.

The effect of change in width is minimal, as can be seen in figure 2.6. The value of α_{corr} remains near constant and lies between 1.42 to 1.48

The helical shape is not part of the spheroid model. As a result, the helix amplitude has a significant effect on the correction (figure 2.7). The value of
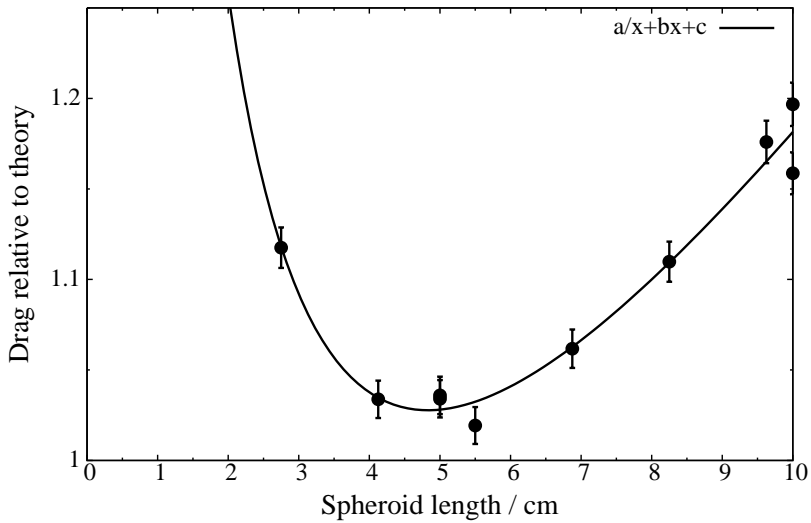
FIGURE 2.5 – *Relative drag as function of MTB aspect ratio (length-to-width), increases as the model reaches the same length as the diameter of the tank.*

α_{corr} lies in the range of 1.19 to 1.60

Similarly, the number of windings are also absent in the prolate spheroid. It also harbours the strongest effect of all traits on the correction number (figure 2.8), length not included. The value of α_{corr} increases with nearly 50 % between the ranges of 1.32 to 1.80

While not all traits contribute an equal amount to the increase of α_{corr}, it is evident that all traits should be taken into account when estimating rotational drag.

2.5.1   Model fit

Over the range of parameters varied, the change in correction factor is very close to linear with the parameter values. For simplicity, we therefore to a the three-dimensional linear function (Equation 2.3). The fitting coefficients are a_0=1.03, a_1=0.255, a_3=2.69 and a_4=0.0507. The value of a_0 is slightly larger than the expected value of one (For w, h and N equal zero, the model is identical to a prolate spheroid). This seems to be in agreement with the observation of figure 2.5, where the correction between an exact spheroid and theory also has a minimum that is close to, but slightly above unity (1.01 to 1.02)

The average absolute error between the measurement points and the fit is 0.015. Sixteen additional shapes were constructed, but now varying two para-
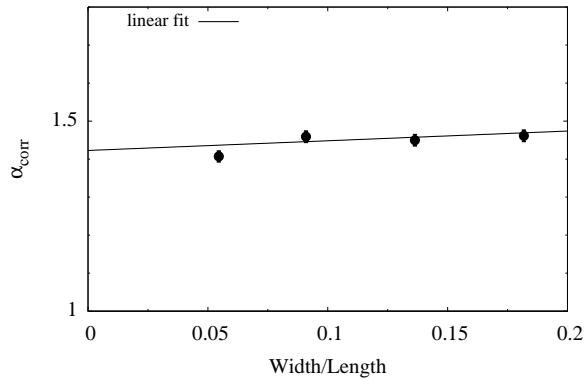
FIGURE 2.6 – *Correction of the rotational drag relative to the spheroid model as function of width over length ratio, for a length of* 5.5 cm, *helical amplitude of* 0.5 cm *and three windings, and the fit to the linear model.*
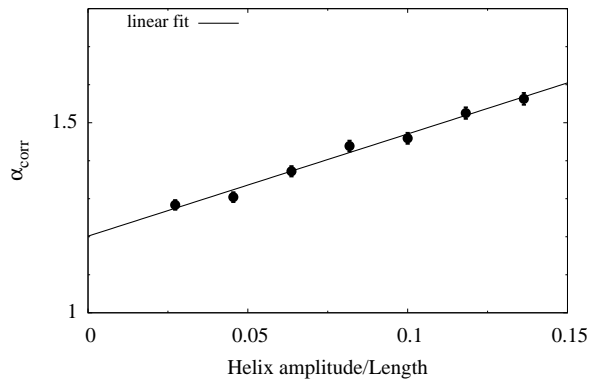
FIGURE 2.7 – *Correction of the rotational drag relative to the spheroid model as function of helix amplitude over width, for a length of* 5.5 cm, *width of* 0.5 cm *and three windings, and the fit to the linear model.*
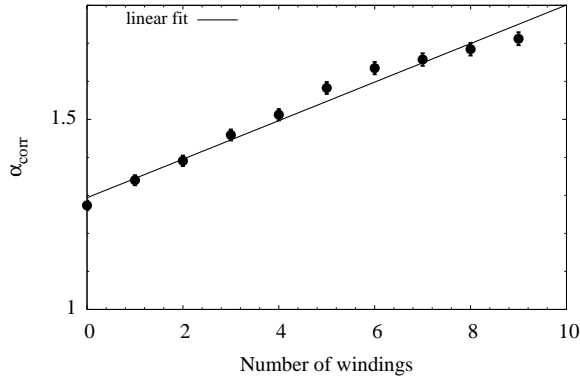
FIGURE 2.8 – *Correction of the rotational drag relative to the spheroid model as function of number of windings, for a length of* 5.5 cm*, width of* 0.5 cm *and helix amplitude of* 0.5 cm*, and the fit to the linear model.*

meters at the same time. The average absolute error between the polynomial and measured values is 0.09, indicating that the fit is quite good.

2.6   Discussion

When inspecting the measurement data, there appears some scatter in the results. This amount of scatter cannot be explained by measurement noise, which was much smaller. Reproducibility of the 3D printed objects is very good, and also unlikely to be the source of the scatter. We suspect that cause lies in the duration and repetition of the experiments, which took place over several weeks. This might have led to temperature variations, and subsequent changes in the viscosity. Additionally, during this this period the silicone oil was exposed to the room atmosphere. Minor evaporation, which might affect the dynamic viscosity in the long term, was not accounted for in our calculations.

Over the parameter space investigated, the linear polynomial approximation is fairly accurate. The increased drag due to the helical structure, as compared to prolate spheriod, is at maximum 1.7. When it comes to order of magnitude estimation, as stated in the introduction, the approximation through a prolate spheroid (f_p) is sufficient.

When we want to control the bacteria accurately in the microscopic domain, an error of 13 % to 80 % is significant. This underestimation of drag will lead to an equal underestimation of the magnetic field strength required to achieve the desired torque to steer the MTB. This will affect response time as well as energy consumption up to a higher degree due to the exponential drop-off of magnetic field strength at further distances in general.

It should be noted that we only investigated the rotational drag of the MTB body, but not the additional drag caused by the flagella. Since the flagella are flexible, with unknown elasticity, the additional drag is difficult to estimate. This could be part of future work in this area.

MTB species come in all different shapes and sizes, but most do not look like prolate spheroids. Instead they are more commonly cocci, spiral or bacili shaped, but can also vary in emergent or bulk properties depending on species (Berlanga, 2010). It would be possible to calculate a α_{corr} for each trait or shape of a specific species, in relation to the drag coefficient of a prolate spheroid.

2.7   Conclusion

We analysed the relation between the shape of spiral shapes magneto-tactic bacteria and their rotational drag coefficient. For this, we realized a range of centimeter sized 3D printed models with varying length, width, helix amplitude and winding density. Using a modified viscosimeter, we measured the torque as a function of rotation speed. In order to maintain laminar flow, we used silicon oil with a dynamic viscosity 5000 times higher than water and rotated the models ten times slower than their microscopic originals.

The measured rotational drag coefficients were normalized to that of a prolate spheroid of equal length and width, to obtain a correction factor α_{corr}. This correction factor ranges from 1.19 to 1.80, depending on trait. So one underestimates the drag considerably if no traits are taken into consideration.

The effect of a change in width on the correction factor is minimal, since the width is incorporated in the spheroid approximation.

In contrast, the helical shape is not captured by the spheroid approximation. Consequently, the correction factor increases with an increase in helix amplitude, as well as with increasing number of windings.

The drag should approach the value of the spheroid model if the helical shape is removed and the width is reduced to zero. Our measurements however show a small residual correction (1.03), which we attribute to the drag of the cylindrical part required to connect the model to the shaft.

Over the parameter range investigated, the relation between the correction factor and the variables can be approximated by a three-dimensional linear relationship. This leads to a simple formula for the rotational drag, which is of importance to the biophysics community working with spirilium shaped bacteria.

Chapter 3

Rotational drag and rate of rotation of magneto-tactic bacteria

Abstract

In this study we modelled, simulated and measured the U-turn trajectories of individual magnetotactic bacteria under application of rotating magnetic fields, ranging in amplitude from 1 to 12 mT . The model is based on the balance between rotational drag and magnetic torque. For accurate verification of this model, bacteria were observed inside 5 μm high microfluidic channels, so that they remained in focus during the entire trajectory. From analysis of hundreds of trajectories and accurate measurements of bacteria and magnetosome chain dimensions, we confirm that the model is correct within measurement error. The resulting average rate of rotation of *Magnetospirillum Gryphiswaldense* is 0.74(3) rad/mTs.

The work in this chapter was performed in close cooperation with my colleagues. My specific contribution was to set up the cultivation of *Magnetospirillum Gryphiswaldense* in our laboratory, and to prepare (TEM, SEM, light microscope) samples for observation and I designed and fabricated the 3D printer models for drag measurements. The magnetic torque model was developed by Leon Abelmann, and the subsequent trajectory calculations by Tijmen Hageman. The microscope imaging and off-line image analysis was performed by Tijmen Hageman. Afterwards, I performed the manual part of the tracking of the U-turns.

3.1   Introduction

Magnetotactic bacteria (Blakemore et al., 1979) (MTB[*]) possess an internal chain of magnetosome vesicles (Komeili et al., 2004) which biomineralise nanometer sized magnetic crystals (Fe_3O_4 or Fe_3S_4 (Baumgartner and Faivre, 2011;

---

[*]Throughout this paper we will use the acronym MTB to indicate the single bacterium as well as multiple bacteria

Lins et al., 2005; Uebe and Schüler, 2016)), encompassed by a membrane (magnetosome) (Gorby et al., 1988). This magnetosome chain (MC) acts much like a compass needle. The magnetic torque acting on the MC aligns the bacteria with the earth magnetic field (Erglis et al., 2007). This is a form of magnetoception (Kirschvink et al., 2001), working in conjunction with aero-taxis (Frankel et al., 1997). At high latitudes the earth's magnetic field is not only aligned North-South, but also substantially inclined with respect to the earth's surface (Maus et al., 2010). The MTB are therefore aligned vertically, which converts a three-dimensional search for the optimal (oxygen) conditions into a more efficient one-dimensional search (Esquivel and Lins de Barros, 1986) (gravitational forces do not play a significant role at the scale of a bacterium). This gives MTB an evolutionary advantage over non-magnetic bacteria in environments with stationary chemical gradients more or less perpendicular to the water surface.

In this paper we address the question of how the MTB of type *Magnetosprilillum Gryphiswaldense* (MSR-1) respond to varying magnitudes of the external field, in particular a field that is rotating. Even though the response of individual magneto-tactic bacteria to an external magnetic field has been modelled and observed (Bahaj and James, 1993; Bahaj et al., 1996; Cebers, 2011; Erglis et al., 2007; van Kampen, 1995), there has been no thorough observation of the dependence on the field strength. The existing models predict a linear relation between the angular velocity of the bacterium and the field strength, but this has not been confirmed experimentally. Nor has there been an analysis of the spread in response over the population of bacteria. The main reason for the absence of experimental data is that the depth of focus at the magnification required prohibits the observation of multiple bacteria in parallel. In this paper, we introduce microfluidic chips with a channel depth of only 5 μm, which ensures that all bacteria in the field of view remain in focus.

The second motivation for studying the response of MTB to external magnetic fields, is that they are an ideal model system for self propelled medical microrobotics (Abbott et al., 2009; Menciassi et al., 2007). Medical microrobotics is a novel form of minimally invasive surgery (MIS), in which one tries to reduce the patient's surgical trauma while enabling clinicians to reach deep seated locations within the human body (Abayazid et al., 2013; Felfoul et al., 2016; Nelson et al., 2004).

The current approach in medical microrobotics is to insert the miniaturized tools needed for a medical procedure into the patient through a small insertion or orifice. By reducing the size of these tools a larger range of natural pathways becomes available. Currently, these tools are mechanically connected to the outside world. If this connection can be removed, so that the tools become untethered, (autonomous) manoeuvring through the veins and arteries of the body becomes possible (Dankelman et al., 2011).

If the size and/or application of these untethered systems inside the human body prohibits the storage of energy for propulsion, the energy has to be harvested from the environment. One solution is the use of alternating magnetic fields (Abbott et al., 2009). This method is simple, but although impressive pro-

gress has been made, it is appallingly inefficient. Only a fraction, 10^{-12}, of the supplied energy field is actually used by the microrobot. This is not a problem for microscopy experiments, but will become a serious issue if the microrobots are to be controlled deep inside the human body. The efficiency would increase dramatically if the microrobot could harvest its energy from the surrounding liquid. In human blood, energy is abundant and used by all cells for respiration.

For self-propelled objects, only the direction of motion needs to be controlled by the external magnetic field. There is no need for field gradients to apply forces, so the field is allowed to be weaker and uniform when solely using magnetic torque (Nelson et al., 2010). Compared to systems that derive their energy for propulsion from the magnetic field, the field can be small in magnitude and only needs to vary slowly. As a result, the energy requirements are low and overheating problems can be avoided.

MTB provide a perfect biokleptic model to test concepts and study the behaviour of self-propelled micro-objects steered by external magnetic fields (Khalil et al., 2013). The direction of the motion of an MTB is modified by the application of a magnetic field at an angle with the easy axis of magnetization of the magnetosome. The resulting magnetic torque causes a rotation of the MTB at a speed that is determined by the balance between the magnetic torque and the rotational drag torque. Under the application of a uniform rotating field, the bacteria follow U-turn trajectories (Bahaj and James, 1993; Reufer et al., 2014; Yang et al., 2012).

The magnetic torque is often modelled by assuming that the magnetic element is a permanent magnet with dipole moment $\boldsymbol{m}$ [Am^2] on which the magnetic field $\boldsymbol{B}$ [T] exerts a torque $\boldsymbol{\Gamma} = \boldsymbol{m} \times \boldsymbol{B}$ [Nm]. This simple model suggests that the torque increases linearly with the field strength, where it is assumed that the atomic dipoles are rigidly fixed to the lattice, and hardly rotate at all. This is usually only the case for very small magnetic fields.

In general one should consider a change in the magnetic energy as a function of the magnetization direction with respect to the object (magnetic anisotropy). This is correctly suggested by Erglis *et al.* for magnetotactic bacteria (Erglis et al., 2007). An estimation of the magnetic dipole moment can be obtained by studying the dynamics of MTB (Bahaj et al., 1996).

Recent studies of the dynamics of MTB in a rotating magnetic field show that a random walk is still present regardless of the presence of a rotating field (Cebers, 2011; Smid et al., 2015). The formation and control of aggregates of MTB in both two- and three-dimensional control systems has been achieved *in vitro* (De Lanauze et al., 2014; Martel and Mohammadi, 2010; Martel et al., 2009) as well as *in vivo* (Felfoul et al., 2016), showing that MTB can use the natural hypoxic state surrounding cancerous tissue for targeted drug delivery.

Despite these impressive results, successful control of individual MTB is much less reported. This is because many experiments suffer from a limited depth of focus of the microscope system, leading to a loss of tracking. A collateral problem is overheating of the electromagnets in experiments that take longer than a few minutes. We recently demonstrated the effect of varying field

strengths on the control of magneto-tactic bacteria (Hassan et al., 2016). In the present paper we provide the theoretical framework and systematically analyse the influence of the magnetic field on the trajectories of individual MTB. This knowledge will contribute to more efficient control of individual MTB, and ultimately self-propelled robotic systems in general.

We present a thorough theoretical analysis of the magnetic and drag torques on MTB. This model is used to derive values for the proportionality between the average rate of rotation and the magnetic field during a U-turn trajectory under a magnetic field reversal. The theory is used to predict U-turn trajectories of MTB, which are the basis for our experimental procedures.

Lastly, we present statistically significant experimental results which verify our theoretical approach and employ a realistic range of magnetic field strength and rotational speed of the applied magnetic field to minimize energy input.

3.2 Theory

In our experiment, the MTB are subjected to a magnetic field $\boldsymbol{B}$ [T] of constant magnitude rotating over 180°. The magnetic field excerts a torque on the magnetosome chain with magnetic moment $\boldsymbol{m}$ [Am^2], which causes the MTB to rotate around the axis $\boldsymbol{m} \times \boldsymbol{B}$. The angular velocity is restricted by viscous drag. As a result, the MTB perfrom a U-turn under 180° rotation of the magnetic field. In appendix A we show that for magnetic fields below 12 mT, the ratio between MTB velocity v [m/s] and U-turn diameter D [m] can be approximated within 2 % by

$$\frac{v}{D} = \gamma B, \tag{3.1}$$

where γ [rad/Ts] can be linked to the magnetic moment m and drag coefficient f_b [Nms],

$$\gamma = \frac{m}{\pi f_\mathrm{b}}. \tag{3.2}$$

Since the 180° rotation of the magnetic field takes place in a finite time, an optimum field values exists for which the average rate of rotation of the MTB is maximum. This optimum field value is inversely proportional to the rotation time.

3.3 Experimental

3.3.1 Magnetotactic bacteria cultivation

A culture of *Magnetospirillum Gryphiswaldense* was used for the magnetic moment study. The cultures were inoculated in MSGM medium ATCC 1653 according to with an oxygen concentration of 1 % to 5 %. The bacteria were cultivated at 21 °C for 2 days to 5 days for optimal chain growth (Katzmann et al., 2013).
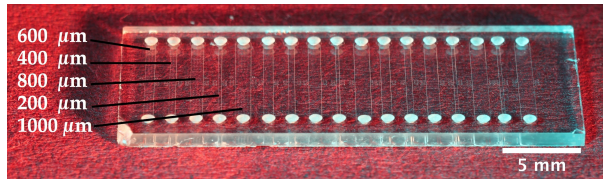
FIGURE 3.1 – *Top: A* 5 µm *deep microfluidic chip with various channel widths of 200, 400, 600, 800 and 1000* µm.

The sampling was done using a magnetic "racetrack" separation, as described in (Wolfe et al., 1987).

3.3.2 Dynamic viscosity of growth medium

The kinematic viscosity of the freshly prepared growth medium was determined with an Ubbelohde viscometer with a capillary diameter of 0.63(1) mm (Si Analytics 50110). The viscometer was calibrated with deionized water, assuming it has a kinematic viscosity of 0.98(1) mm^2/s at 21.0(5) °C. At that temperature, the growth medium has a kinematic viscosity of 0.994(17) mm^2/s. The density of the growth medium was 1.009(2) g/cm^3, measured by weighing 1 ml of it on a balance. The dynamic viscosity of the growth medium is therefore 1.004(19) mPas, which is, within measurement error, identical to water (1.002 mPas).

3.3.3 Microfluidic Chips

Microfluidic chips with a channel depth of 5 µm were constructed by lithography, HF etching in glass and subsequent thermal bonding. The fabrication process is identical to the one described in (Park et al., 2015). Figure 3.1 shows the resulting structures, consisting of straight channels with inlets on both sides. By means of these shallow channels, the MTBs are kept within the field of focus during microscopic observation, so as to prevent out-of-plane focus while tracking. The channel width was 200 µm or more, so that the area over which U-turns could be observed was only limited by the field of view of the microscope. The chips are positioned on a microcrope slide with the access holes down. A very thin layer of vasiline is applied between the chip and the microscope slide to obtain an tight seal so that oxygen cannot diffuse into the channel.

3.3.4 Magnetic Manipulation Setup

A schematic of the full setup, excluding the computer used for the acquisition of the images, is shown in figure 3.2. A permanent NdFeB magnet (5 mm × 5 mm × 10 mm, grade N42) is mounted on a stepper motor (Silverpak 17CE, Lin Engineering) below the microfluidic chip. The direction of the field can be adjusted with a
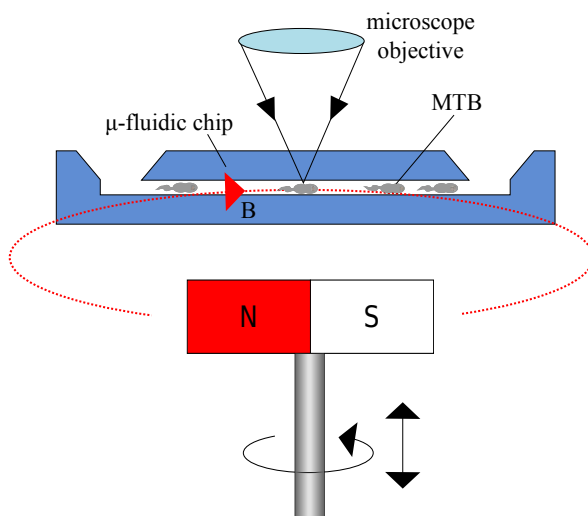
FIGURE 3.2 – *The setup used to measure the MTB U-turns. (a) Reflective microscope, (b) microfluidic chip and (c) a permanent magnet mounted on (d) a stepper motor.*

precision of 51 200 steps for a full rotation, at a rotation time of 130 ms with a constant acceleration of 745 rads^{-2}. The field strength is adjusted using a lab-jack, with a positioning accuracy of 0.5 mm.

The data acquisition was done by a Flea3 digital camera (1328×1048 at 100 fps, FL3-U3-13S2M-CS, Point Grey) mounted on a Zeiss Axiotron 2 microscope with a 20× objective.

During the experiments, a group of MTB was observed while periodically (every two seconds) rotating the magnetic field. This was recorded for field magnitudes ranging from 1 mT to 12 mT. Offline image processing techniques were used to track the bacteria and subtract their velocity and U-turn diameter.

The error in our measurements of the magnetic field is fundamental to determining the responsiveness of the MTB. Therefore we measured the magnetic fields at specific heights using a Hall meter (Metrolab THM1176). The results can be seen in figure 3.3.

The placement of the tip of the Hall meter was at the location of the microfluidic chip, assuming the field strength inside the chip's chamber equals that at the tip. It should be noted that the center of the magnet was aligned with the center of rotation of the motor, therefore the measurements were only done with a stationary magnet on top of an inactive motor. Errors in the estimation
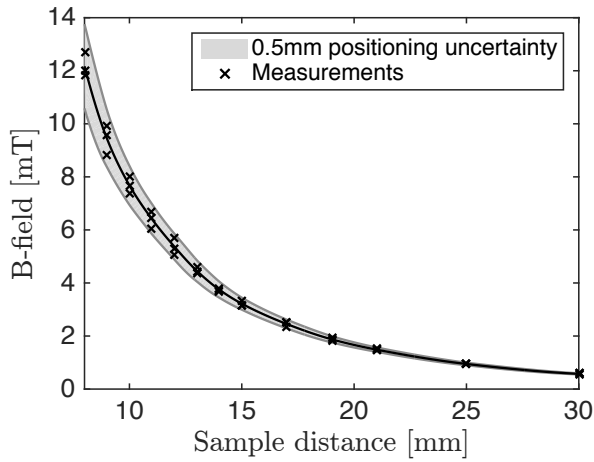
FIGURE 3.3 – *Magnetic field strength as a function of distance of the magnet to the microfluidic chip.*

of the magnetic field strength due to misalignment of the magnetic center from our measurements therefore cannot be excluded.

The rotation profile of the motorized magnet was investigated by recording its motion by a digital camera at 120 fps and evaluating its time-dependent angle by manually drawing tangent lines. Figure 3.4 shows that the profile accurately fits a constant-acceleration model with an acceleration of $745\,\mathrm{rads}^{-2}$, resulting in a total rotation time of 130 ms.

3.3.5   Macroscopic Drag Setup

Macro-scale drag measurements were performed using a Brookfield DV-III Ultra viscometer. During the experiment, we measured the torque required to rotate different centimeter sized models of bacteria and simple shapes in silicone oil (Figure 3.5). In order to keep the Reynolds number less than one, silicone oil of 5000 mPas (Calsil IP 5000 from Caldic, Belgium) was used as a medium to generate enough drag. Furthermore, the parts were rotated at speeds below 30 rpm. The models were realized by 3D printing. The designs can be found in the accompanying material.

3.3.6   Image Processing

The analysis of the data was done using in-house detection and tracking scripts written in MATLAB®. The process is illustrated in figure 3.6. In the detection step, static objects and non-uniform illumination artefacts are removed by sub-
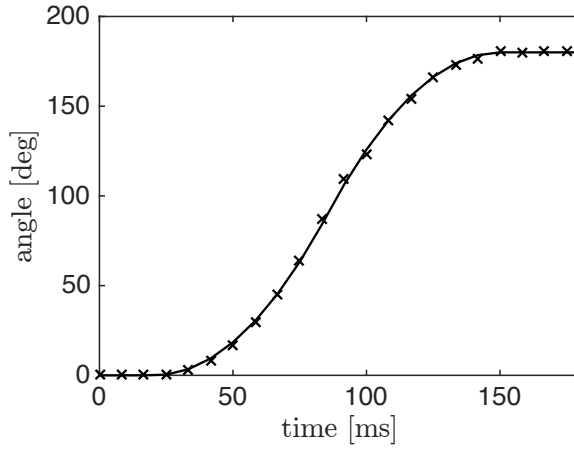
FIGURE 3.4 – *The measured angle of the motorized magnet accurately fits a constant-acceleration model with a total rotation period of* 130 ms.
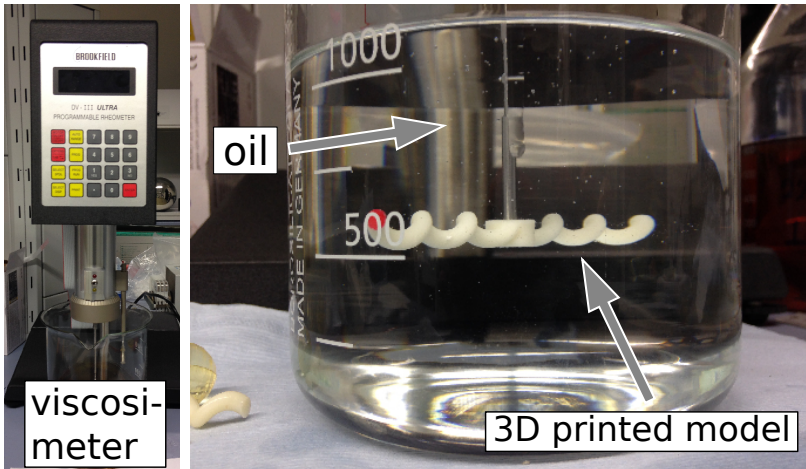

FIGURE 3.5 – *The viscometer setup used to measure the rotational drag of macroscopic spheroid and helical structures. 3D printed models were mounted on a shaft and rotated in a high viscosity silicone oil (5 Pas). A video of the experiment is available as additional material (DragMeasurements.mp4).*
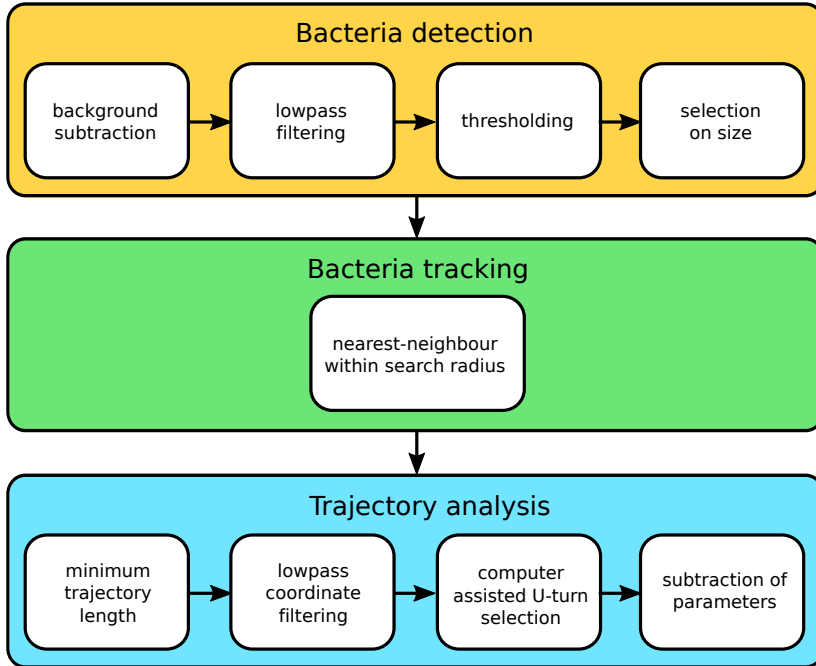
FIGURE 3.6 – *The process of bacteria detection, tracking, and subsequent analysis.*

tracting a background image constructed by averaging 30 frames spread along the video. High-frequency noise is reduced using a Gaussian lowpass filter. A binary image is then obtained using a thresholding operation, followed by selection on a minimum and maximum area size. The centers-of-mass of the remaining blobs are compared in subsequent frames, and woven to trajectories based on a nearest-neighbor search within a search radius 3.6. A sequence of preprocessing steps can be seen in figure 3.7. The software used is available under additional material.

Subsequently, the post-processing step involves the semi-automated selection of the MTB trajectories of interest for the purpose of analysis. The U-turn parameters of interest analyzed are the velocity v, the diameter D of the U-turn, and the time t. A typical result of the post-processing step can be seen in figure 3.8.

3.4 Results and discussions

The model developed in section A.1 predicts the trajectories of MTB under a changing magnetic field: in particular, the average rate of rotation over a U-
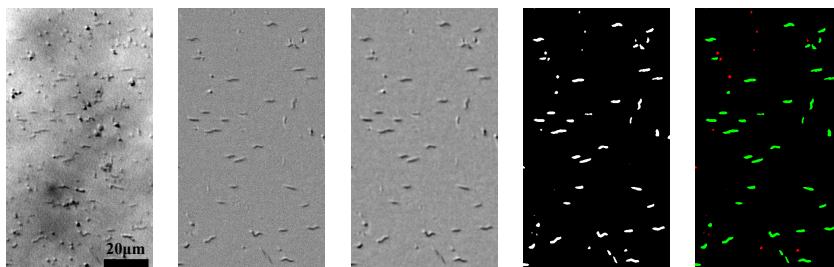
FIGURE 3.7 – *Pre-processing filter steps: (a) raw, (b) background subtraction, (c) low pass filtering, (d) thresholding resulting in a binary image, (e) size selectivity. A video is available as additional material (MTBImageProc.mp4)*
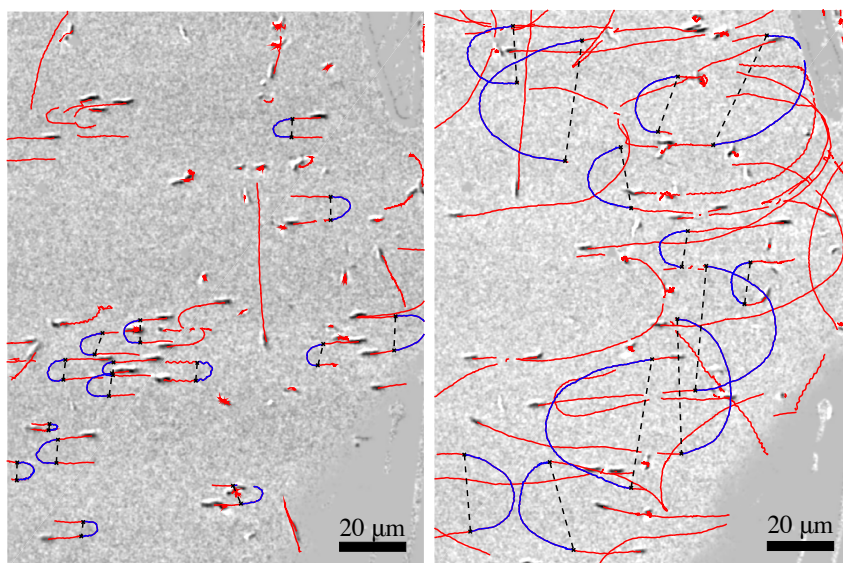
FIGURE 3.8 – *Trajectory during image post-processing at a magnetic field strength of* 12.2 mT *(left) and* 1.5 mT *(right). Selection procedure of analyzed U-turns, showing selected U-turns in blue and unanalyzed trajectories in red. The black dotted line connects two manually selected points of a given U-turn trajectory, from which the distance in the y-direction, or the U-turn diameter, is determined.*

turn. To validate the model, the essential model parameters are determined in section 3.4.1, after which the average rate of rotation is measured and compared to theory in section 3.4.2.

3.4.1 Estimate of model parameters

The rate of rotation of an MTB under a rotating magnetic field is determined by the ratio between the rotational drag torque and the magnetic torque. Both will be discussed in the following, after which the average rate of rotation will be estimated.

Estimate of rotational drag torque

To determine the rotational drag torque, the outer shape of the MTB was measured by both optical microscopy and scanning electron microscopy (SEM). The drag coefficient was estimated from a macroscale drag viscosity measurement.

**Outer dimensions of the bacteria**   The length L of the bacteria is measured from the same optical images as used for the trajectory analysis (figures 3.8). Scanning electron microscopy (SEM) would in principle give higher precision per bacterium, but due to the lower number of bacteria per image the estimate of the average length and distribution would have a higher error. Moreover, using the video footage ensures that the radius of curvature and the length of the bacteria are measured on the same bacterium.

A typical MSR-1 has a length of 5.0(2) μm. The length distribution is shown in Figure 3.10. These values agree with values reported in the literature (Bazylinski and Frankel, 2004; Faivre et al., 2010; Schleifer et al., 1991).

The width W of the bacteria is too small to be determined by optical microscopy, and needs to be determined from SEM images, see figure 3.9. A typical bacterium has a width of 240(6) nm. The main issue with SEM images is whether a biological structure is still intact or perhaps collapsed due to dehydration, which might cause overestimation of the width. The latter might be as high as $\pi/2$ if the bacterial membrane has completely collapsed. Fortunately, the drag coefficient scales much more strongly with the length than with the width (equation A.24). For a typical bacterium, the overestimation of the width by using SEM leads at most to an overestimation of the drag by 18 %.

Table 3.1 lists the values of the outer dimensions L and W, including the measurement error and standard deviation over the measured population.

Rotational Drag   From the outer dimensions of the bacteria, the rotational drag torque can be estimated. The bacterial shape correction factor, equation (A.25), was determined by macro-scale experiments with 3D printed models of an MTB in a viscosimeter using high viscosity silicone oil (see section 3.3.5). Figure 3.11 shows the measured torque as a function of the rotational speed for prolate spheroids and spiral shaped 3D printed bodies of two different lengths. The
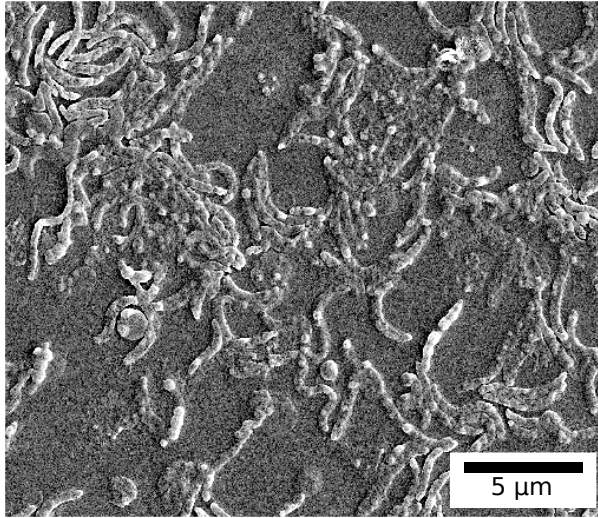
FIGURE 3.9 – *Scanning electron microscopy images of* Magnetospirillum Gryphiswaldense. *Separated MTB were selected for width measurements.*
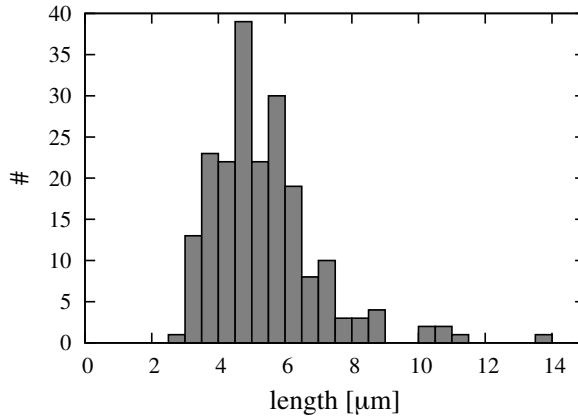

FIGURE 3.10 – *Number of magnetotactic bacteria (MTB) as a function of the length of the MTB as measured by optical microscopy.*
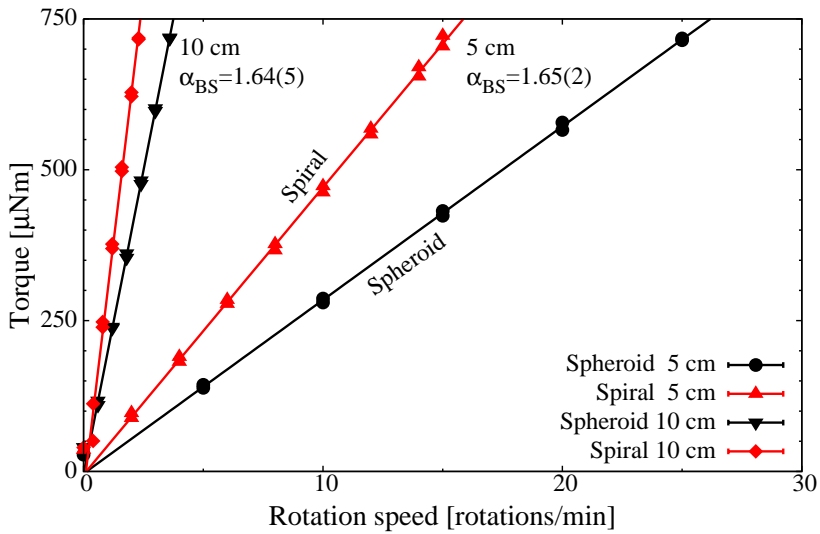
FIGURE 3.11 – *Rotational drag torque versus angular rotation speed of 3D printed prolate spheroids and MTB models of lengths* 5 *and* 10 cm. *The curves are linear, indicating that the flow around the objects is laminar. Irrespective of the length, the spiral shaped MTB model has a drag that is* 1.64(5) *higher than a prolate spheroid of equal overall length and diameter.*

relation between the torque and the speed is linear, so we are clearly in the laminar flow regime. This is in agreement with an estimated Reynolds number of less than 0.3 for this experiment (equation A.22). Independently of the size, the spiral shaped MTB models have a drag coefficient that is 1.64(5) times higher (α_{BS}) than that of a spheroid of equal overall length and diameter.

Using the same experimental configuration, we can obtain an estimate of the effect of the channel walls on the rotational drag by changing the distance between the 3D printed model and the bottom of the container. Figure 3.12 shows the relative increase in drag when the spiral shape approaches the wall. This experiment was performed on a 5 cm long, 5 mm diameter spiral at 8 rpm. To visualise the increase, the reciprocal of the distance normalised to the length of the bacteria is used on the bottom horizontal axis. The normalised length is shown on the top axes. Note that when plotted in this way, the slope approaches unity at larger distances.

For an increase over 5 %, the model has to approach the wall at a distance smaller than $L/3$, where L is the length of the bacteria. For very long bacteria of 10 µm, this distance is already reached in the middle of the 5 µm high channel. Since there are two channel walls on either side at the same distance, we estimate that the additional drag for bacteria swimming in the centre of the
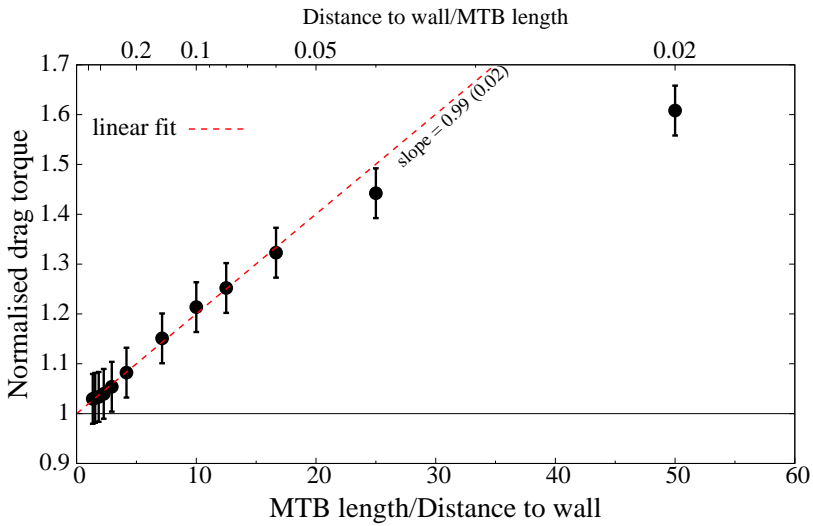
FIGURE 3.12 – *Increase in rotational drag as a function of the distance between the 3D printed spiral and the bottom of the container. The distance is normalized to the length of the bacteria (*5 cm*). The torque is normalized to the extrapolated value for infinite distance (displayed as "linear fit").*

channel is less than 15 %. If the spiral model approaches the wall, the drag rapidly increases. At $L/50$, the drag increases by 60 %. It is tempting to translate this effect to real MTB. It should be noted however that the 3D printed models are rigid and stationary, whereas the MTB are probably more flexible and mobile. Intuitively, one might expect a lower drag.

From the bacterial dimensions, we can estimate a mean rotational drag coefficient, f_b, of 67(7) zNms. Since the relation between the rotational drag and the bacterial dimensions is highly nonlinear, a Monte Carlo method was used to estimate the error and variation of f_b. For these calculations, the length of the bacteria was assumed to be Gaussian distributed with parameters as indicated in table 3.1. The code for the Monte Carlo calculation is available as additional material.

Due to the nonlinearity, the resulting distribution of f_b is asymmetric. So rather than the standard deviation, the 10 % to 90 % cut-off values of the distribution are given in table 3.2). Most of the MTB are estimated to have a drag coefficient in the range of 30 to 120 zNms.

TABLE 3.1 – *Characteristics of magnetotactic bacteria. Length L and width W and amount n, radius r and center-to-center distance a of the crystals in the magnetosomes. The error indicated on the means is the standard error (standard deviation/square root of the total number of samples).*

	L	W	n	r	a
	[µm]	[nm]		[nm]	[nm]
mean	5.0(2)	240(6)	16(2)	20(1)	56(1)
stddev	1	28	6	5	8

TABLE 3.2 – *From the values of table 3.1, the drag coefficient f_b, demagnetisation factors ΔN, magnetic moment m, maximum magnetic torque Γ_{max}, and proportionality factor γ are estimated ($v/D = \gamma B$). The input parameters are assumed to obey a Gaussian distribution with standard deviations as in table 3.1. Using a Monte Carlo method, the standard error of the calculated parameters, and the 10 %–90 % cut-offs in the distribution, are calculated.*

	f_b	ΔN	m	Γ_{max}	γ_{theory}	γ_{exp}
	[zNms]		[fAm^2]	[aNm]	[rad/mTs]	[rad/mTs]
mean	67(7)	0.10(2)	0.25(05)	7(3)	1.2(3)	0.74(3)
10%	31	0.03	0.07	0.7	0.3	
90%	124	0.27	0.57	41	3.6	

Estimate of magnetic torque

Figure 3.13 shows typical transmission electron microscopy images (TEM) of magnetosome chains. From these images, we obtain the magnetosome count n, radius r, and center-to-center distance a, which are listed as well in table 3.1. These values agree with those reported in the literature (Faivre et al., 2010; Pósfai et al., 2007) and lie within the range of single-domain magnets (Faivre, 2015). We have found no significant relation between the inter-magnetosome distance and the chain length, see figure 3.14.

From these values the demagnetisation factor ΔN, the magnetic moment m, and the maximum torque Γ_{max} are calculated using the model from section A.1.1, and tabulated in table 3.2. Again, the standard deviations of the values and the 10%- and 90 % cut-off values are determined from Monte Carlo simulations.

Average rate of rotation

From the drag coefficient f_b and the maximum torque Γ_{max}, the ratio γ between the average rate of rotation and the magnetic field strength can be obtained us-
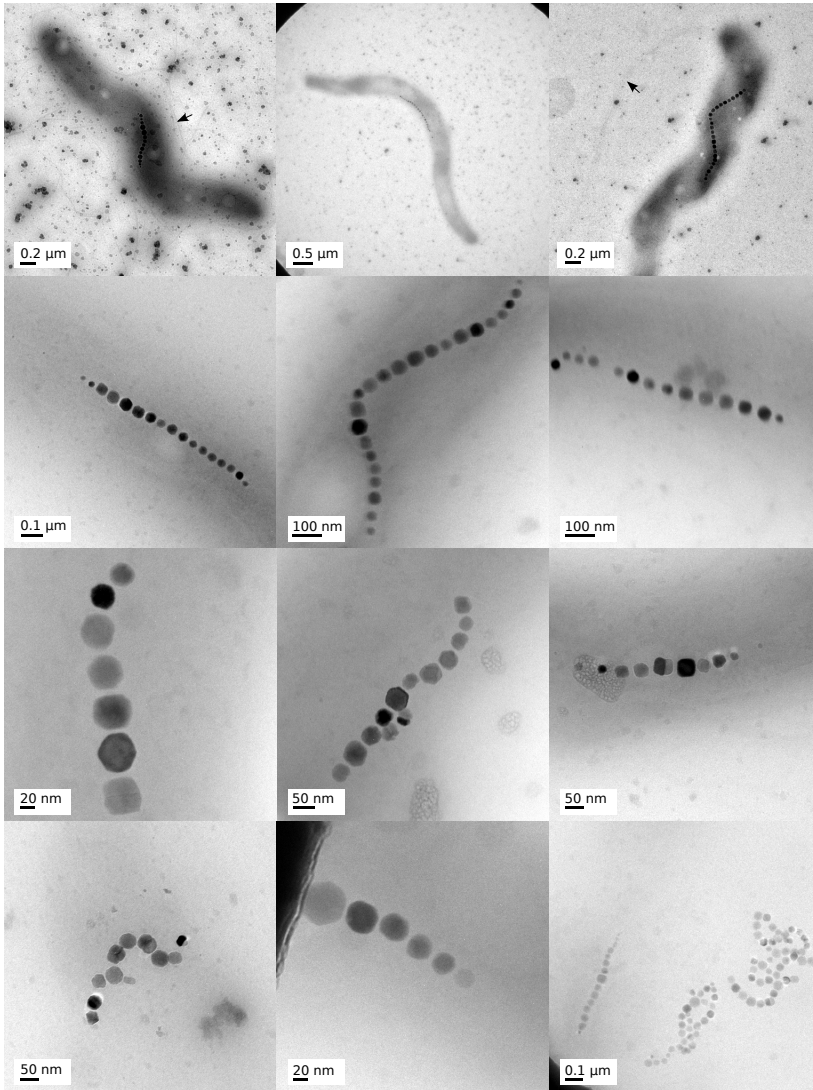
FIGURE 3.13 – *Transmission electron micrographs of MSR-1, magnetosomes and chains. The top row shows typical full scale bacteria, where black arrows indicate the flagella. Compared to the second row, the third row shows shorter chains with a higher variety in size distribution of magnetic nanoparticles due to an immaturity of the chain (Uebe and Schüler, 2016). The bottom row shows irregular chains and overlapping groups of expelled chains due to the formation of aggregates, making it hard or impossible to distinguish individual chains.*
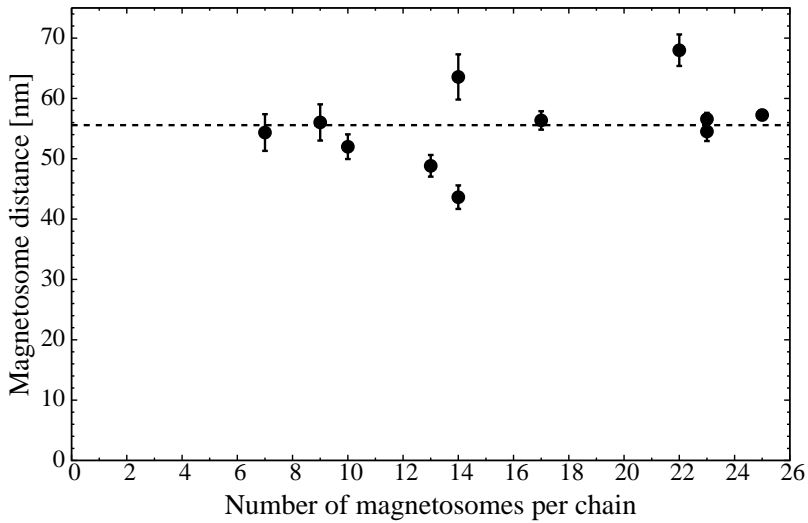
FIGURE 3.14 – *Distance between magnetite particles as a function of the number of particles in the chain. The mean of the entire sample group is indicated with a dashed line at* 56(1) nm. *Vertical error bars represent the standard error of each individual chain.*

ing equation A.30. This value is listed as γ_{theory} in table 3.2, and has a convenient value of approximately 1 rad/mTs. So in the earth's magnetic field (0.04 mT), the rate of rotation of an MSR-1 is approxmately 0.04 rad/s. A U-turn will take at least 78 s.

Average Velocity

The MTBs' velocity was determined from the full set of 174 analyzed bacteria trajectories. This set has a mean velocity of 49.5(7) µm/s with a standard deviation σ of 8.6 µm/s (figure 3.15). Using the value for the average rate of rotation γ of approximately 1 rad/mTs, this speed leads to a U-turn in the earth's magnetic field of about 1 mm (equation A.30).

The average velocity of the bacteria is close to the value reported by Popp for *Magnetospirillum Gryphiswaldensen* in an oxygen gradient free environment (42(4) µm/s (Popp et al., 2014)), and much higher than that reported by Lefevre for bacteria in the vicinity of an oxic-anoxic zone (13 µm/s to 23 µm/s (Lefèvre et al., 2014)). This suggests that there is no oxygen gradient, which is in agreement with the fact that we seal the chip before observation.

Depending on the choice of binning, one might recognise a dip in the velocity distribution. Similar dips have been found in previous research, which
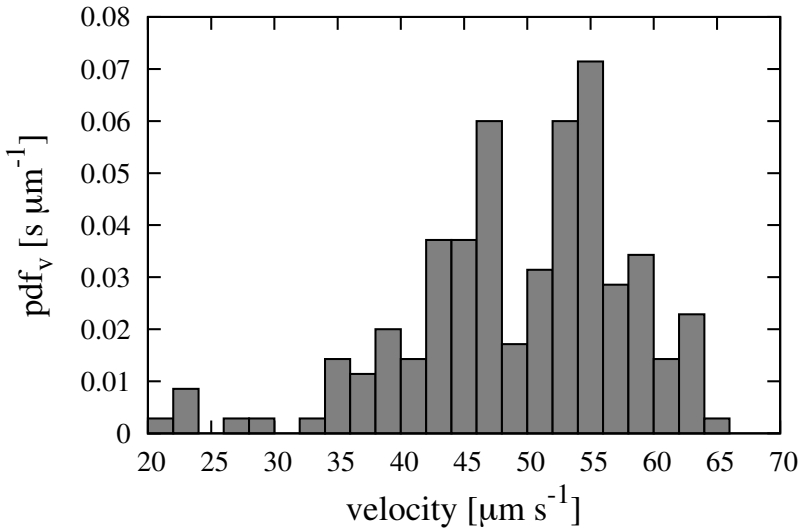
FIGURE 3.15 – *Probability density function for the MTB velocity distribution for* 174 *observed MTB.*

were attributed to different swimming modes (Reufer et al., 2014). There might as well be possible wall-effects on bacteria caused by the restricted space in the microfluidic chip (Magariyama et al., 2005).

The measured velocity during U-turns as a function of the magnetic field strength is shown in figure 3.16. The vertical error bars display the standard error of the velocity within the group. The size of the sample group is depicted above the vertical error bars. For every sample group containing less than ten bacteria, the standard deviation of the entire population was used instead. The error in the magnetic field is due to positioning error, as described in section 3.3.4.

On the scale of the graph, the deviation from the mean velocity is seemingly large, especially below 2 mT. This deviation is however not statistically significant. The reduced χ^2 of the fit to the field-independent model is very close to unity (0.67), with a high Q-value of 0.77 (the probability that χ^2 would even exceed that value by chance, see Press *et al.*, chapter 15 (Press et al., 1992)). Within the standard errors obtained in this measurement, and for the range of field values applied, we can conclude that the velocity of the MTB is independent of the applied magnetic field, as expected.
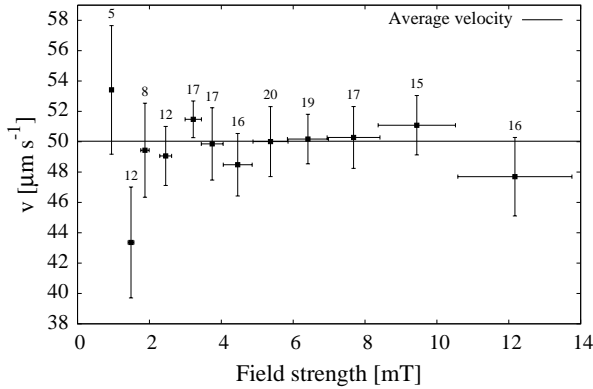
FIGURE 3.16 – *Average MTB velocity as function of the applied magnetic field. The vertical error bars indicate the standard error calculated from the number of bacteria indicated above the error bar.*

3.4.2 Trajectories

The diameter D of the U-turn was measured from the trajectories as in figure 3.8. From these values and the measured velocity v for each individual bacterium, the average rate of rotation v/D can be calculated. Figure 3.17 shows this average rate of rotation as a function of the applied magnetic field, B. The error bars are defined as in figure 3.16.

The data points are fitted to the U-turn trajectory model simulations of section A.1.2. The fit is shown as a solid black line, with the proportionality factor γ_{exp} equal to 0.74(03) rad/mTs. The reduced χ^2 of the fit is (2.88), and the Q-value (0.000 86)

Figure 3.17 shows that the observed average rate of rotation in low fields is higher than the model fit in comparison with the measurement error. We neglected the effect of the (earth's) magnetic background field. As discussed before, at this field strength, however, the average rate of rotation is on the order of 40 mrad/s and the corresponding diameter of a U-turn is on the order of 1 mm. The background field can therefore not be the cause of any deviation at low field strengths. Tracking during the pre-processing step under low fields leads to an overlap between the trajectories, which affect the post-processing step. Due to the manual selection in the post-processing, illustrated in figure 3.8, the preference for uninterrupted and often shorter trajectories may have led (for lower fields) to a selection bias to smaller curvatures. The deviation from the linear fit below 2 mT could therefore be attributed to human bias ("cherry picking").

If we neglect trajectories below 2 mT for this reason, the fits improve (drastically) for both the velocity and average rate of rotation. Fitting datapoints over
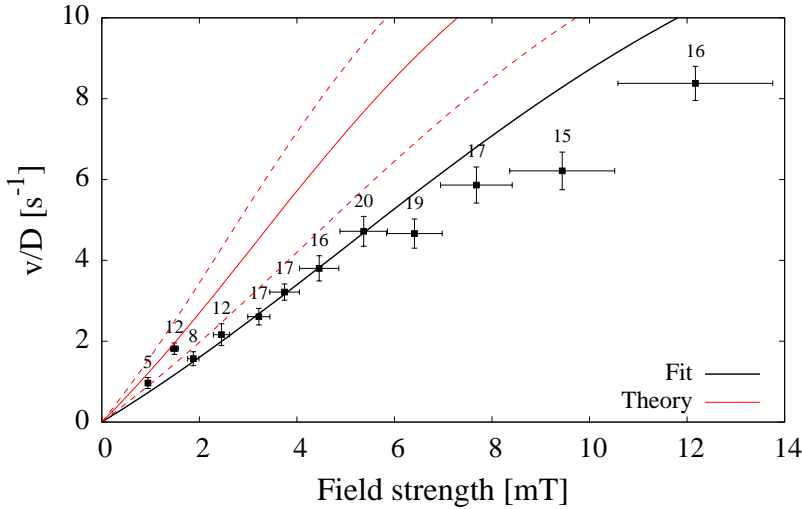
FIGURE 3.17 – *The average rate of rotation, v/D, as a function of the applied magnetic field, B. Vertical error bars display the standard error calculated for the number of MTB denoted above the error bars. For remaining sample groups, containing less than 10 bacteria samples, the standard deviation of the entire population is used instead. The black solid line is the fit of the model to the measured data, resulting in γ_{exp} =0.74(3) rad/mTs. The solid red line is the model prediction, using the γ_{theory} derived from the bacteria and magnetosome dimensions, with the dotted red lines indicating the error on the estimate (1.2(3) rad/mTs).*

the range of 2 m to 12 mT (eight degrees of freedom) decreases the reduced χ^2 of the velocity from 0.67 to 0.42. Furthermore, the Q-value of 0.77 is increased to 0.91, a slight increase in likelihood that our datapoints fall within the limits of the model.

Similarly, the reduced χ^2 of the average rate of rotation is lowered from 2.88 to 1.03 and the Q-value from 0.00086 to 0.41, a drastic change in likelihood of the fit. We therefore assume that these results validate the model with the exclusion of outliers below 2 mT.

At high fields, the observed average rate of rotation seems to be on the low side, although within the error bounds. For the high field range, the diameter of a U-turn is on the order of 5 μm and reversal times are on the order of 100 ms. The resolving power of our setup of 180 nm/pixel and time resolution of 100 frames/s are sufficient to capture these events, so cannot explain the apparent deviation.

A second option is that the weakest bacteria reach the saturation torque

value. As can been seen in figure A.4, this would only be the case for about 10 % to 20 % of the population, and the difference with the linear model would only be about 20 %. The combined effect would therefore be less than 2 %, which is too low to explain the reduction at higher field. To solve this issue experiments as a fuction of the applied field on an individual bacterium, preferably at higher field values, will be required. Unfortunately, this is outside the range of possiblities of our experimental setup.

3.5   Discussion

Figure 3.17 shows in red the prediction of the model using the proportionality factor determined from observations of the MTB (the outer dimensions by optical microsopy and SEM, the magnetosome by TEM), γ_{theory}=1.2(3) rad/mTs. The predicted proportionality factor is clearly higher than measured. This is either because we overestimated the magnetic moment or underestimated the rotational drag coeffient. The latter seems more likely. In the the first place, we neglected the influence of the flagella. A coarse estimate using a rigid cylinder model for the flagellum shows that a flagellum could indeed cause this type of increase in drag. Since we lack information on the flexibility of the flagellum, we cannot quantify the additional drag. Secondly, we ignored the finite height of the microfluidic channel. As was shown by the macroscale experiments, the additional drag increases rapidly if a bacterium approaches within a few hundred nanometers of the wall. Since we do not have information about the distance, again quantification is difficult.

Given the above considerations, we are confident that over the observed field range, the MTB trajectories are in fair agreement with our model.

3.6   Conclusion

We studied the response of the magnetotactic bacteria *Magnetospirillum Gryphiswaldense* to rotation of an external magnetic field *B*, ranging in amplitude from 1 mT up to 12 mT.

Our magnetic model shows that the torque on the MTB is linear in the applied field up to 10 mT, after which the torque starts to saturate for an increasing part of the population.

Our theoretical analysis of bacterial trajectories shows that the bacteria perform a U-turn under 180° rotation of the external field, but not at a constant angular velocity. The diameter, *D*, of the U-turn increases with an increase in the velocity *v* of the bacteria. The average rate of rotation, *v*/*D*, for an instantaneously reversing field is linear within 2 % in the applied field up to 12 mT.

If the applied field is rotated over 180° in a finite time, the average rate of rotation is higher at low field values than it was for an instantaneous reversal. Given a field rotation time, an optimum field value exists at which the rate

of rotation is approximately 18 % higher than for instantaneous reversal. This optimum field value is inversely proportional to the field rotation time.

The rotational drag coefficient for an MTB was estimated from drag rotation experiments in a highly viscous fluid, using a macroscale 3D printed MTB model. The spiral shape of the body of an MTB has a 64(5) % higher drag than a spheroid with equal length and diameter, which has been the default model in the literature up to now. Furthermore, the added drag from the channel wall was found to be negligible for an MTB in the center between the walls (less than 10 %), but to increase rapidly when the MTB approaches to within a few hundred nanometers of one of the walls.

From microscope observations, we conclude that the MTB velocity during a U-turn is independent of the applied field. The population of MTB has a non-Gaussian distributed velocity, with an average of 49.5(7) μm/s and a standard deviation of 8.6 μm/s. As predicted by our model, the average rate of rotation is linear in the external magnetic field within the measured range of 1 mT to 12 mT. The proportionality factor $\gamma = v/DB$ equals 0.74(3) rad/mTs. The predicted theoretical value is 1.2(3) rad/mTs, which is based on measurements of the parameters needed for the model, such as the size of the bacteria and their magnetosomes from optical microscopy, SEM, and TEM images. The number of parameters and their nonlinear relation with the proportionality factor causes the relatively large error in the estimate.

These findings finally prove that the generally accepted linear model for the response of MTB to external magnetic fields is correct within the errors caused by the estimation of the model parameters if the field values are below 12 mT. At higher values, torque saturation will occur.

This result is of importance to the control engineering community. The knowledge of the relation between the angular velocity and the field strength (γ) can be used to design energy efficient control algorithms that prevent the use of excessive field strengths. Furthermore, a better understanding of the magnetic behavior will lead to more accurate predictions of the dynamic response of MTB for potential applications in micro-surgery, as drug carriers, or for drug delivery.

Chapter 4

Longterm observation of MTB

Abstract

In this study we controlled and observed individual magnetotactic bacteria, *Magnetospirillum Gryphiswaldense*, under application of a rotating magnetic field at 1.5 mT . For accurate tracking bacteria were observed inside 5 μm high microfluidic channels, so that they remained in focus during the entire trajectory. From analysis of over 4 hours of trajectories and accurate measurements of bacteria motion, we can confirm that it is possible to control *Magnetospirillum Gryphiswaldense* for a period of up to 90 minutes. Furthermore, it is possible to distinguish modes of motility based on the changes in the velocity of the MTB.

The work in this chapter was performed in close cooperation with my colleagues. My specific contribution was to set up the cultivation of *Magnetospirillum Gryphiswaldense* in our laboratory, to prepare (TEM, SEM, cuvette) samples for observation, the design of a microfluidic chip, perform an equal part of the experiment and participate in inception of experimental design. The image processing and tracking of trajectories and analysis thereof was done by Tijmen Hageman.

4.1 Introduction

Energy consumption and capacity can be a challenging aspect of micro-robotics. Either energy has to be supplied by a medium that is incompatible with the human body (Schmidt and Eberl, 2001) or the setup required to drive the microrobot generates fields which utilise a fraction of the energy used to attempt to control small magnetic objects (Nelson et al., 2010). Unlike mechanical microrobots, MTB possess rotary motors as seen in Figure 4.1 Molecular motor of MTB utilize the proton motive force (PMF).

MSR-1 is a common candidate for biophysical investigation of motility and magnetic response. Figure 4.1 shows a sample of the culture.
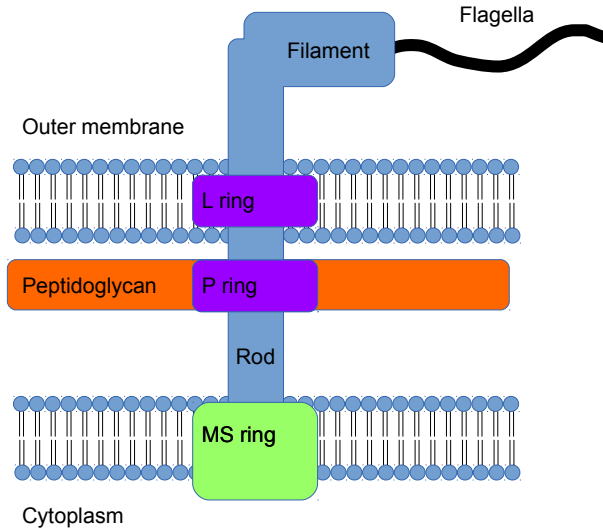
FIGURE 4.1 – *MTB rotary motor. Adapted from (Mandadapu et al., 2015)*

In this paper we attempt to address the viability of measuring changing traits of individual MTB over several hours inside a microfluidic chip. Namely, the direction and speed of a given MTB over time.

This question has relevance for microrobotics. In case of biorobotic or biomimetic approaches to microsurgery or controllable drug delivery systems, the bacteria-like robot will have to move over long distances and over extended periods of time.

Even though observing MTB trajectories and reversals with scrutiny has been shown before, the time of observation was limited by the fact that the MTB run out-of-focus (Erglis et al., 2007; Reufer et al., 2014). This also limited the analysis of other long term changes related to velocity, size, magnetic response, etc. Simulations of wandering centers of MTB in rotating magnetic fields as well as reversals have also been simulated to show potential trajectories, but have not been confirmed experimentally for periods longer than 200 seconds (Cebers, 2011).

In this chapter, we observed the MTB inside a microfluidic chip with a channel height of only 5 μm, which keep the MTB in the focal region of the microsope. In addition, the MTB is forced to perform an eight figure trajectory, which keeps it within the field of view of the camera. In this way, only a minor corrections
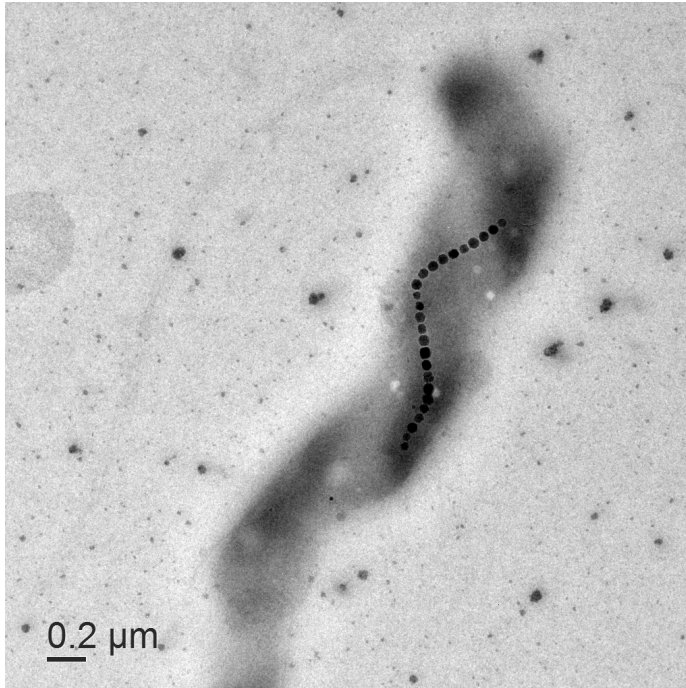
FIGURE 4.2 – *A scanning electron microscope image of MTB with iron-oxide nanoparticles (white) organised in a chain.*

and patience are required to observe the bacteria for hours.

4.2 Experimental

4.2.1 Magnetotactic bacteria cultivation

Magnetospirillum Gryphiswaldense was used as candidate for tracking and controlling. Cultures were inoculated in MSGM medium ATCC (1653) with an oxygen concentration of 1 % to 5 %, with an adjusted pH of 7.0. The bacteria were cultivated at 26 °C for 5 days to 7 days. The sampling was done using a magnetic "racetrack" separation method as described in (Wolfe et al., 1987).

4.2.2 Microfluidic Chip

A macroscopic photo of the chip and region of interest for observation can be seen in Figure 4.3. During the experiment a magnetic field provided an 8-pattern loop, which was only interrupted for temporary manual control. Due to drift and sudden reversals, MTB were steered back to the center of our field
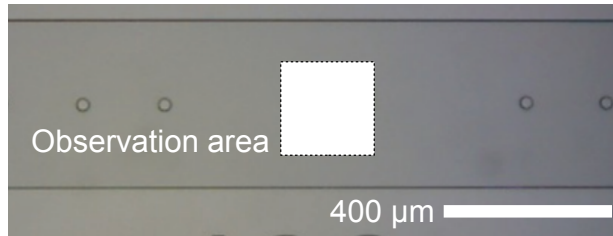
FIGURE 4.3 – *Light microscope image of the microfluidic channel and the observed area (white). MTB were redirected before drifting out of the center of the field of view.*

of vision during the entire experiment. The tracking results of a typical recentering process can be seen in Figure 4.4.

4.2.3   Setup

Figure 4.5 shows the experimental setup. A chip filled with bacteria was placed in a reflected light microscope (Zeiss Axiotron II) with 20× magnification. For long-term observation the bacteria would need to remain in the field of view, which was realised by magnetic control, as seen in figure 4.4. Fields were generated by a motorised permanent magnet placed underneath the sample. This magnet is magnetised orthogonal to the axis of rotation, such that it creates an in-plane magnetic field on the location of the sample of which the angle can be controlled. The motor (Silverpack 17C) was programmed to loop in an 8-shaped trajectory, so that the bacteria, on average, will not move its position. It further allowed temporary manual override to compensate any drift of bacteria. Data was recorded at 10 fps on a resolution of 1328x1024 for a period of 5 h by a Point Grey FL3-U3-13S2M-CS camera. During this period, a single bacterium was tracked at a time. When this bacterium would stop being motile, the magnetic field would be directed parallel to the microfluidic channel in order to find and trap a new one.

4.2.4   Image Processing

The image sequence was processed offline to extract the coordinates of the bacteria of interest. The low-contrast nature of the image required pre-processing steps. Subsequently, we performed background subtraction, lowpass filtering, thresholding and finally selecting the resulting blobs based on size. The center of gravity was registered at the bacteria position. A nearest-neighbour algorithm
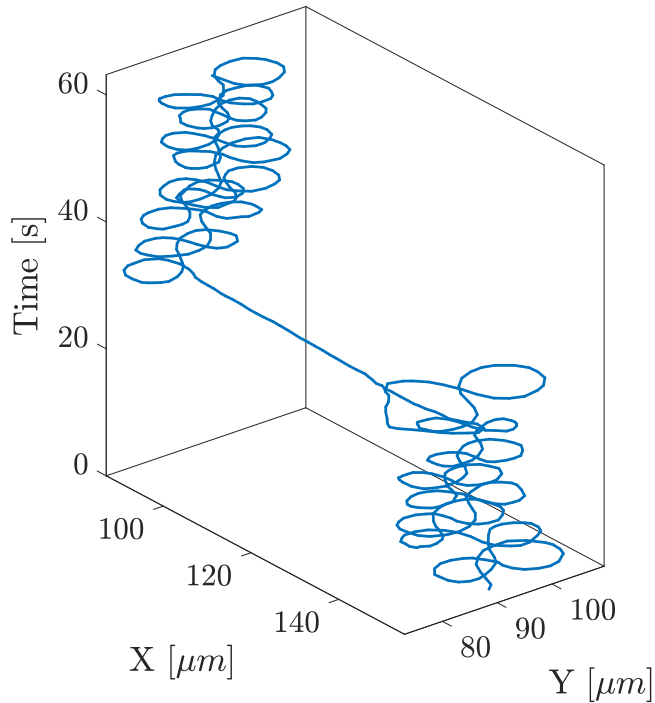
FIGURE 4.4 – *Re-centering manouver to keep a given MTB in the field of view. The long straight path indicates a manual correction between 8-pattern loop sequences.*

with maximum search radius was used to build trajectories from the detected bacteria. The resulting trajectories were manually cleaned. The velocity was calculated from the trajectories.

4.3   Results

4.3.1   Long term tracking

Fig 4.6 shows the velocity of a selection of MTB as a function of time. In all cases, the MTB initially show a a constant velocity, after which the velocity gradually decreases with time. The initial velocity and the duration of the period of constant velocity varies. For the fast moving bacteria (number 3, 5 and 6 in the sequence), the rate of decrease in velocity is similar.
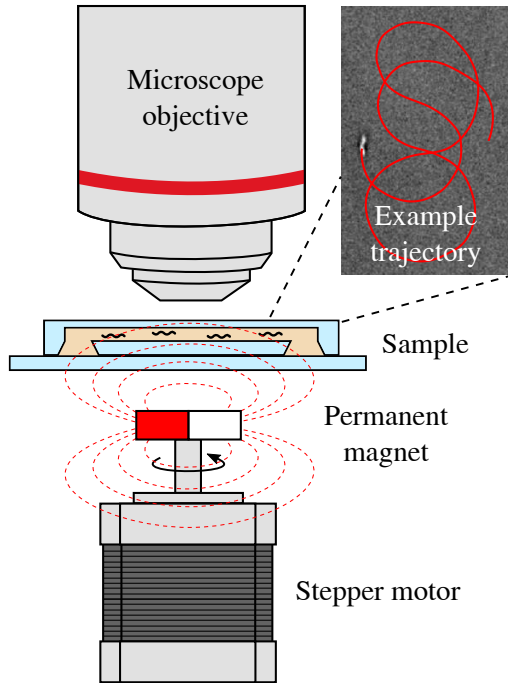
FIGURE 4.5 – *A sample of MTB is inserted in a sealed microfluidic chip and observed under a reflected light microscope. A motorized magnet located under the sample generates in-plane magnetic fields, used to keep the bacteria in the field of view.*
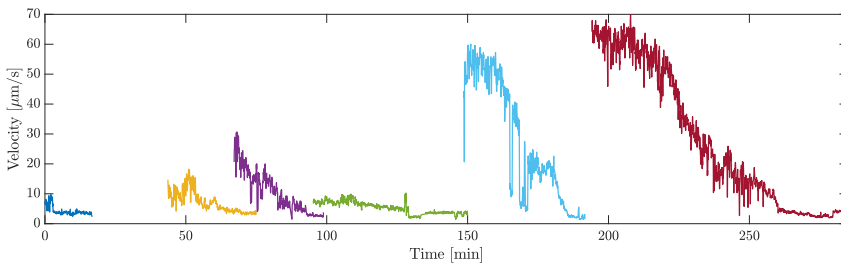

FIGURE 4.6 – *The (low-pass filtered) velocity of six bacteria over time. The velocity of all bacteria decreases with time, but the duration varies from a few minutes up to almost one hour.*
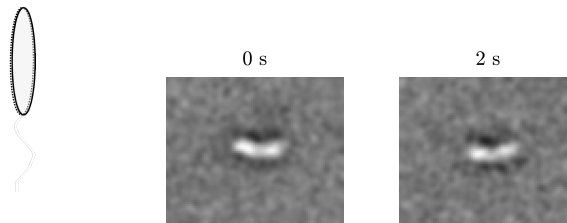
FIGURE 4.7 – *Due to the nature of image processing, MTB which come to a full stop are no longer detected by the tracking algorithm. These images show a lack of motion of what we define as non-motile MTB.*
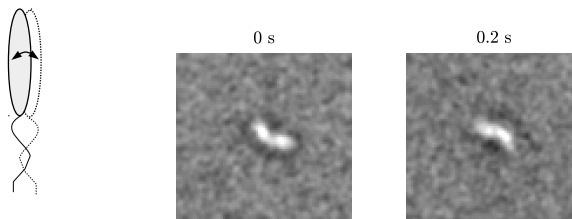

FIGURE 4.8 – *An image sequence of an MTB rotating about the minor axis. It is uncertain from observation why this takes place. It does however correlate with a drop in velocity.*

4.3.2   Modes of motile behaviour

During the tracking period, several modes of motility were observed. They are defined as follows: Full stop or non-motile (Figure 4.7), rotation around minor axis (Figure 4.8), rotation around major axis (Figure 4.9) and rotation around point (Figure 4.10). Both non- and magnetic MTB displayed this behaviour. Magnetic MTB follow the rotation of the field where non-magnetic MTB simply seem to drill or rotate. It is however clearly a different mode of motility than is common in run-and-tumble or nutrient seeking behaviour found in literature. We suspect this is related to confinement in the micro-fluidic environment.

Additionally, reversals were observed with seemingly no regularity. These occur with unpredictable intervals and mostly pose difficulties when manually controlling MTB. The velocity or rotation direction of the MTB flagella is not under manual control and therefor requires on-the-fly correction when steering MTB through a microfluidic chamber. As is evident from the trajectory, there is also a clear drop in velocity as described in section A.1. The drop in velocity can be seen in Figure 4.11 as dropping from $50\,\mu m\,s^{-1}$ (red) to $5\,\mu m\,s^{-1}$ (blue).
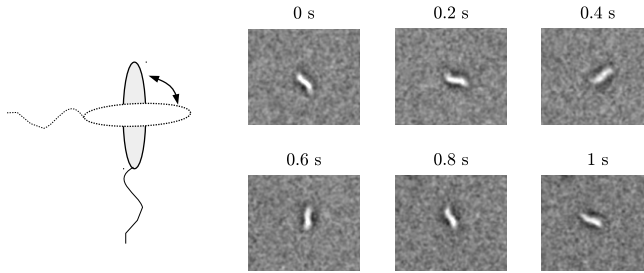
FIGURE 4.9 – *This image sequence displays what we categorise as magnetic and non-motile MTB. The resulting velocity is in the order of magnitude of the background noise and therefor hard to distinguish.*
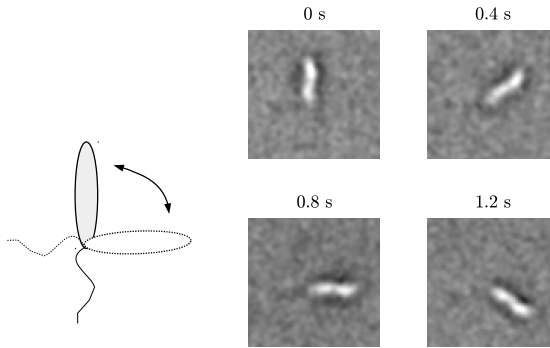
FIGURE 4.10 – *A sequence of MTB most likely stuck on the glass at either end near the flagella. The rotation around the tip is a result of a lack of freedom.*

4.4   Discussion

4.4.1   Decline in velocity

In each case of a long term control sequence we observe a decline in velocity. Though it is unclear why this happens, several reasons for this decline come to mind.

It could be possible that direct lighting from our observation is heating up the samples we are observing. No noticeable increase in chip temperature was observed however. Since the thermal conductivity of glass is high it does not support a high thermal gradient. It is therefore unlikely that the observation area increases significantly in temperature.

We assume that local ion depletion is also not a problem, since in some cases when an MTB comes to a halt, other non-magnetic ones still cross the screen without problem.
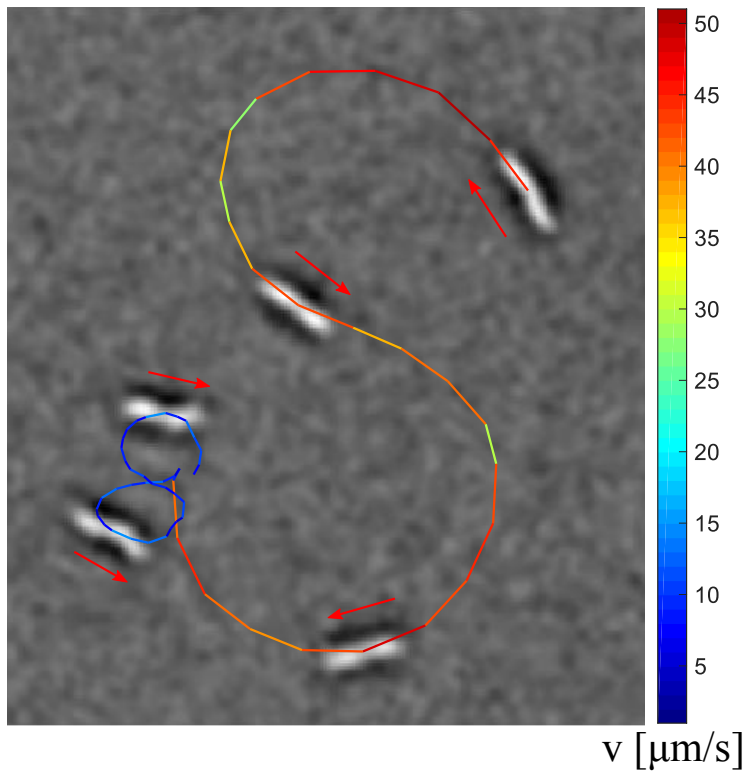
FIGURE 4.11 – *Reversal trajectory taking place over the course of 10 seconds.*

Perhaps the MTB stop in all activity prior to cell division. Clear size changes however are not visible, even after observing the bacteria for a long period after they stop. Moreover, the time before division of MTB is several hours. It would be very accidental if all bacteria observed would be close to division.

One might suggest the reduction in velocity is simply due to fatigue of some sort. Perhaps the flagellar motor has intervals of activity over such a long period of time. The efficiency of the flagellar motors is reported to be near 100 % (Kinosita et al., 2000). If fatigue would arise within such short time, it is hard to imagine how MTB would survive in a natural environment where they need to travel over tens of centimeters.

To us, the most likely cause for the reduction in motility is damage by light. In the microscope, we focus a very bright LED light source of 450 nm wavelength on the field of view. This high intensity light source might damage the bacteria under observation. Only the MTB that is observed is affected. The other MTB which appear later in the field of view during the 260 minute observation remain

unaffected until we utilise them for observation.

4.5   Conclusion

We observed magneto-tactic bacteria inside a microfluidic chip for a total of 260 min. During this time individual MTB were tracked and controlled for a minimum duration of 20 min.

From these experiments we learned that each MTB displayed five modes of motility, namely: Locomotion, rotation around the major axis, rotation around the minor axis, rotation around the tip and non-motility.

Furthermore, it is possible to distinguish reversal events from unobstructed movement, which can be traced back to both inversion of the speed as well as a drop in velocity from around 50 to $5\,\mu\mathrm{m\,s^{-1}}$. No consistent occurrence has been found in these reversals.

The duration of control sequences, where the MTB would follow manual steering or an open-loop instruction, lasted up to 90 min. Every observation of a single MTB showed a slow decline in velocity followed by a full stop.

When dropping below a critical velocity, near to or simply non-motility, the algorithm either loses tracking of the MTB in question due to background filtering or the error in position determination overshadows any motion the MTB might display.

The complex behaviour that was observed poses a challenge for the control of magneto-tactic bacteria inside a microfluidic chip under microscope observation, and will have implications for the design of control loops.

Chapter 5

Real-time observation of MTB traits and growth

Abstract

We designed and built an optical-density (OD) based machine, and used it to automatically monitor the growth and magnetosome development of *Magnetospirillum Gryphiswaldense* (MSR-1) with high temporal resolution. The machine measures the optical density over time while cycling through magnetic field settings generated by coils placed around the sample, exploiting the orientation-dependent scattering of MSR-1. We quantified the bacteria density via OD, the relative and absolute amount of magnetic MTB via the differential OD signal at orthogonal magnetic field orientations, and their response to external fields (magneto-fluidic dynamics) via the step response of the OD. Additionally, the angle-dependent scattering of MSR-1 was measured and parameterised. The device offers automation of otherwise labour-intensive operations at a measurement rate of 10 mHz.

The work in this chapter was performed in close cooperation with my colleagues. My specific contribution was to set up the cultivation of *Magnetospirillum Gryphiswaldense* in our laboratory, to prepare (TEM, SEM, cuvette) samples for observation and participate in inception of experimental design for which I performed comparative measurements with off-the-shelf equipment. The design, programming and construction of the OD based machine was done by Tijmen Hageman. Subsequent signal analysis, both online and offline, was done by Tijmen Hageman.

5.1 Introduction

Magnetotactic bacteria (MTB) possess the property to align with external magnetic fields due to their internal chain of magnetic nanocrystals (magnetosomes). (Blakemore et al., 1979) In nature they utilize this ability to more efficiently search for their desired habitat in the oxic-anoxic transition zone; align-

ing with the earth magnetic field transforms a three-dimensional search into a one-dimensional search.

The growth of these organisms been extensively researched, and they are known to be difficult to cultivate. (Ban et al., 2010; Geelhoed et al., 2010; Heyen and Schüler, 2003; Katzmann et al., 2013; Li et al., 2009; Liu et al., 2010; Moisescu et al., 2011; Schüler and Baeuerlein, 1998; Yang et al., 2001a,b, 2013) Also the development of magnetosomes has been thoroughly investigated. (Faivre et al., 2010; Heyen and Schüler, 2003; Katzmann et al., 2013; Lefèvre et al., 2009; Li et al., 2009; Moisescu et al., 2011; Schüler and Baeuerlein, 1998; Yang et al., 2001a, 2013) It has been found that the oxygen concentration is extremely important for both growth types. Several strains have proven to grow magnetosomes only in low-oxygen (microaerobic) conditions. At the same time, a too low and too high oxygen level prevents growth of the organisms. (Heyen and Schüler, 2003; Katzmann et al., 2013; Schüler and Baeuerlein, 1998). Growth and Fe uptake of *Magnetospirillium Gryphiswaldense* (MSR-1) was found to be most optimal at a temperature of 28° and a pH of 7. (Katzmann et al., 2013; Moisescu et al., 2011). Other groups have investigated the influence of growth medium composition on the growth and magnetosome formation. (Ban et al., 2010; Lefèvre et al., 2009; Liu et al., 2010; Yang et al., 2001a,b)

In the literature, bacterium concentration is often measured by optical density (Heyen and Schüler, 2003; Katzmann et al., 2013; Li et al., 2009; Schüler and Baeuerlein, 1998; Yang et al., 2001a,b, 2013), dry weight analysis (Geelhoed et al., 2010; Heyen and Schüler, 2003; Liu et al., 2010) and using counting chambers (Yang et al., 2001a,b). The magnetosome growth is studied by transmission electron microscopy (TEM) (Ban et al., 2010; Katzmann et al., 2013; Lefèvre et al., 2009; Li et al., 2009; Yang et al., 2013), spectrometry (Liu et al., 2010; Moisescu et al., 2011; Yang et al., 2001b) or by a light scattering method exploiting the fact that spirillium-type bacteria have a different optical density under different orientation, yielding parameter C_{mag}. (Faivre et al., 2010; Katzmann et al., 2013; Schüler and Baeuerlein, 1998; Schüler et al., 1995; Yang et al., 2013) The literature reports several variants of this parameter. (Schüler et al., 1995; Song et al., 2014; Zhao et al., 2007) It provides a loose estimate on the average amount of magnetosomes per bacterium, although the method actually combines several measures; the ratio of magnetic and nonmagnetic bacteria and the magnetosome distribution over the population.

All reported methods have in common that they require manual sampling and analysis. Counting chambers and TEM is time intensive and the latter also requires expensive specialised equipment. All in all these methods are labour-intensive and yield low temporal resolution.

We attempt to solve these problems by introducing an automated optical density meter which performs continuous optical density-based measurements obtaining information about growth in numbers as well as magnetosome development. The device measures the optical density as a measure for growth, C_{mag} as a measure for the ratio of magnetic over nonmagnetic bacteria, D_{mag} as a measure for the absolute amount of magnetic bacteria, and γ as a measure

for the response of MTB to magnetic fields, indirectly a measure for the average magnetic dipole moment.

5.2 Theory

With increasing concentration of bacteria, the absorption or optical density (OD) of the sample will increase. We define the OD as:

$$OD = \log_{10}\left(\frac{I_0}{I_s}\right), \tag{5.1}$$

where I_0 is the unobstructed light intensity signal and I_s is the signal strength after absorption. MSR-1 absorb more light when aligned to the light beam ($OD_{\parallel}$) compared to orthogonal positioning ($OD_{\perp}$). This property allows us to measure the C_{mag}, the standard for qualitatively determining the ratio of magnetic and nonmagnetic bacteria in a sample (Schüler et al., 1995):

$$C_{\mathrm{mag}} = \frac{OD_{\parallel}}{OD_{\perp}} \tag{5.2}$$

This method provides a ratio only, and does not provide a measure for the absolute amount of magnetic bacteria. For completeness we propose a simple differential measure which, in contrast, can:

$$D_{\mathrm{mag}} = OD_{\parallel} - OD_{\perp}. \tag{5.3}$$

The transition between the orientation extrema can be modelled with an angle-dependent absorption factor $g(\theta)$:

$$OD(\theta) = OD_{\perp} + g(\theta)\left(OD_{\parallel} - OD_{\perp}\right). \tag{5.4}$$

The response of bacteria to external fields by means of U-turns and rotations has been modelled and used to determine their properties (Pichel et al., 2018; Esquivel and Lins de Barros, 1986; Zahn et al., 2017). Alignment of a bacterium to an external magnetic field with angle $\theta(t)$ can be described by the following differential equation:

$$f\frac{\partial\theta(t)}{\partial t} + mB\sin\left(\theta(t)\right) = 0, \tag{5.5}$$

where f [N m s] represents the drag coefficient, m [Am^2] the magnetic dipole moment of the bacterium, and B [T] the magnetic field strength. Initially we assume the bacterium to be orthogonal to the magnetic field $\theta(0) = \pi/2$. Solving for θ yields:

$$\theta(t) = 2\cot^{-1}\left(e^{\frac{mB}{f}t}\right). \tag{5.6}$$

The angle can be indirectly estimated by the measured optical density as described by equation 5.4. The settling time of this transition period is characterised by time constant $\tau = f/mB$. As in Pichel et al. (2018), we characterise the response of MTB to magnetic fields by γ [rad s^{-1} T^{-1}]:

$$\gamma = \frac{m}{\pi f} = \frac{1}{\pi \tau B}. \tag{5.7}$$

So far we have left out rotational Brownian motion as a disturbing influence on the orientation of bacteria. There is an interplay between temperature-driven rotational diffusion which prevent full alignment of MTB with the external field. The angular distribution of MTB $b(\theta)$ in a static magnetic field is fully determined by the ratio of magnetic and thermal energy according to Maxwell-Boltzmann statistics (Bryant et al., 2007):

$$
\begin{aligned}
b(\theta) &= \frac{\int_0^{2\pi} e^{\frac{mB}{kT}\cos\theta} \sin(\theta) d\phi}{\int e^{\frac{mB}{kT}\cos\theta} d\Omega} \\
&= \frac{1}{2} \frac{mB}{kT} \frac{\sin(\theta)}{\sinh(\frac{mB}{kT})} e^{\frac{mB}{kT}\cos\theta},
\end{aligned} \tag{5.8}
$$

where k [J K^{-1}] is the Boltzmann constant and and T [K] the temperature. The average angle can be obtained via the integral $\int_0^{\pi} b(\theta)\theta d\theta$. As it is hard to solve analytically a numerical approach has been taken. Figure 5.1 shows the angular distribution of MTB as per equation 5.8 for various magnetic field strengths, assuming a dipole moment of 0.25 fA m^2 as reported in our earlier work (Pichel et al., 2018) and room temperature (300 K). Not surprisingly, the bacteria distribution becomes more narrow and more concentrated as the field amplitude increases. Additionally, perfect alignment of MTB with the field is very rare, as for very small angles there is no magnetic torque and Brownian motion is dominant. In the right figure we see the average angle as a function of the energy ratio. In absence of a field the MTB have random orientation ($\theta_{\text{avg}} = 90°$). For very strong fields, the average angle will saturate to a nonzero asymptote due to saturation of the magnetic torque appearing between 10 mT to 100 mT. (Pichel et al., 2018) The earth magnetic field, approximately 50 µT, is just strong enough to direct only half of all bacteria within 70° of the field. However, the perturbations of rotational diffusion will integrate over time, resulting in an average orientation in the direction of the field.

5.3   Materials and methods

Figure 5.2 gives an overview of the OD meter. A green LED (Cree LC503FPG1-30P-A3, dominant wavelength at 527 nm) transmits light through the sample in a sealed cuvette. Photo diodes measure the intensity of the light source both before and after passing the sample. A window of 1 mm × 5 mm blocks out light that would reach the photo diode indirectly. Two sets of Helmholtz coils are
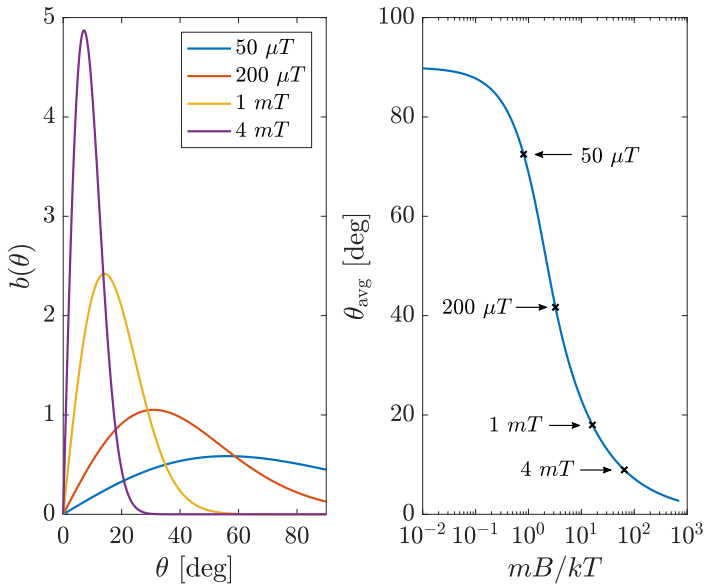
FIGURE 5.1 – *Left: The angular distribution of Magnetotactic Bacteria (MTB) in a static magnetic field due to angular Brownian diffusion, assuming a reported value for the magnetic dipole moment (*$0.25\,\mathrm{fA\,m}^2$*) (Pichel et al., 2018) and room temperature (*300 K*). Right: the average angle of MTB as a function of the ratio of magnetic and thermal energy, along with values corresponding to the left graph.*

placed around the sample to generate a magnetic field at any angle with respect to the light beam. The measured current of the photo diode is converted to a voltage and amplified (LT1880 opamp), after which it is digitized at 20 Hz with 16-bit precision, yielding a resolution of 31 μV (ADS1115 analog-to-digital converter). Both coil actuation and data acquisition was timed using Arduino hardware.

The electronic noise was characterised by measuring the response of an empty cuvette for 13 min. After correcting the measured signal by the intensity of the light source (using the signal from the reference diode), the noise is characterised by a standard deviation of 30(1) μV, yielding a signal-to-noise ratio of 85 dB.

The magnetic fields generated by the coils were measured by a Metrolab THM1176 three-axis hall magnetometer and corrected carefully for misalignment with respect to the orientation of the coils.
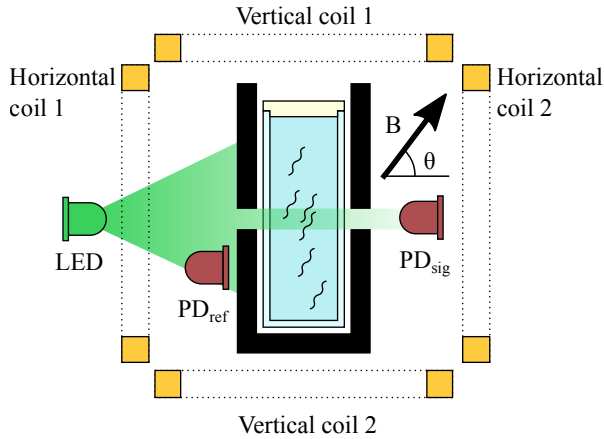
FIGURE 5.2 – *The OD meter transmits a light beam through a sealed sample of magnetotactic bacteria (MTB). The concentration of bacteria and their alignment determines the extent to which the light is absorbed or scattered. Two sets of coils around the sample generate a magnetic field of desired strength and angle. Photo diodes measure the light intensity both before (PD_{ref}) and after the sample (PD_{sig}).*

5.3.1   Angle dependency of OD

The angle-dependent scatter factor was determined by measuring the OD while increasing the angle of the magnetic field with steps of approximately 5°. The magnetic field was at all times over 1 mT. As the OD of the sample is continuously fluctuating due to activity and sedimentation within the cuvette, 20 sweeps were carried out. The resulting curves were normalised to a range of 0 to 1 and averaged.

5.3.2   Cultivation

Liquid cultures of *Magnetospirillum Gryphiswaldense*, strain MSR-1, were grown unagitated at room temperature (21 Celcius in closed 2 mL (Eppendorf) centrifugation tubes for 4 days to 10 days. Modified spirillum growth medium (ATCC 1653) with an oxygen concentration of 1 % to 3 % was prepared with an adjusted pH of 6.8. The cultures had an average optical density at the end of cultivation of 0.3 (at 550 nm) in the presence of a magnetic field (5 mT) oriented parallel to the light beam. Sampling for experiments was done using chemically sterilized cuvettes (VWR).   After being filled with MSR-1 in liquid solution to leave no head space, the cuvettes were sealed with four layers of UV sterilized parafilm to allow minor air (oxygen) transfer through the membrane.

5.3.3 Growth experiment

Several prepared samples were grown in the OD meter for a period of five days. The magnetic field was set to loop through cycles of 100 s using the following settings:

- Setting 1: 20 s a vertical field of 1.0 mT
- Setting 2: 20 s a horizontal field of 2.9 mT
- Setting 3: 60 s a vertical field of 100 μT

The transition from 1 to 2 uses relative strong fields, guaranteeing reliable estimations of C_{mag}. The transition from 2 to 3 guarantees a relative large time constant, helpful for accurately estimating τ. These settings allow the OD meter to measure the sample parameters with 10 mHz.

Figure 5.3 shows the measured response of a sample of magnetotactic bacteria to a cycle. It visualizes a short settling time of the OD when a strong magnetic field is used (around 25 s). The longer settling time in case of the second transition (around 45 s) is characterised by τ. The transition at 5 s demonstrates the effect of the magnetic field strength on the angular distribution of MTB as visualized in figure 5.1.

The parameters $OD_{\parallel}$ and $OD_{\perp}$ are estimated from the last 9 s of settings 1 and 2, after the signal has settled. The time constant is estimated from fitting the model of equations 5.4 and 5.6 using the sum of squared errors criterion. It uses a fitting window of 45 s. Before fitting, data is lowpass filtered using a rectangular filter in the frequency domain with a cutoff frequency of 9 mHz, in order to minimize influence of low-frequency fluctuations in the sample. Finally, γ is determined using equation 5.7.

5.4 Results

5.4.1 Angle dependency of OD

Figure 5.4 shows the angle-dependent scatter factor $g(\theta)$. It is highest when bacteria are aligned with the light beam and lowest when orthogonal. Parametrising requires a function that is periodic and is symmetric around 0 and 90 degrees. Based on visual inspection, we choose zero derivatives at 0 and 90 degrees. Phenomenologically this can be modelled by a cosine fit using only the even terms (the value in brackets represents the 95 % confidence interval):

$$g(\theta) = \sum_{n=0}^{4} a_n \cos(2n\theta) \tag{5.9}$$

$$\mathbf{a} = [0.376(4)\ 0.445(6)\ 0.104(6)$$
$$0.044(6)\ 0.013(6)]$$
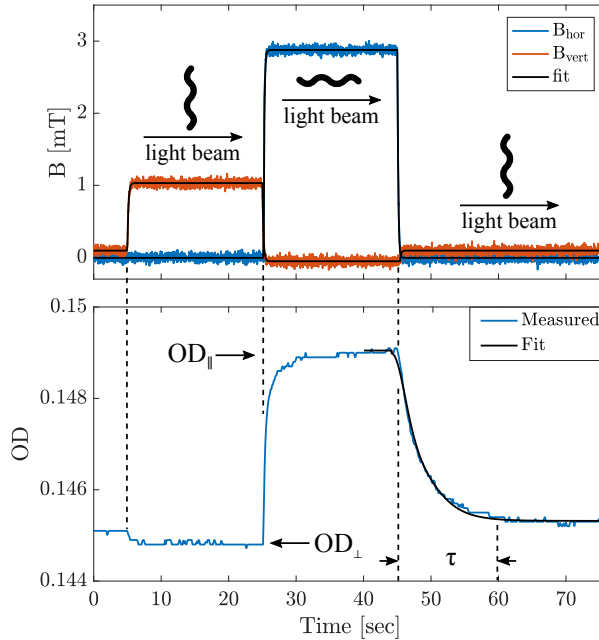
FIGURE 5.3 – *A cycle of the magnetic field in horizontal and vertical direction (top) and the resulting measured response of MTB (bottom). The magnetic field settings direct the MTB from orthogonal orientation with respect to the light beam to parallel orientation and back again. C_{mag} and D_{mag}, proportional to the ratio of magnetic bacteria and their absolute numbers, are calculated from the absorption in parallel ($OD_{\parallel}$) and orthogonal ($OD_{\perp}$) orientations. The time constant τ quantifies the alignment speed of the MTB to the field transition.*

5.4.2   Growth curve

Figure 5.5 shows the measured parameters of a sample of MTB over time; the OD, D_{mag}, D_{mag} and γ. The growth is characterised by a lag phase (L), exponential phase (E), stationary phase (S), magnetic growth phase (M) and an undefined phase (X). The magnetic growth phase is defined independently of OD, and overlaps with other phases (in this case the stationary phase). The sample initially is characterised by a low OD in the lag phase, but by a relative high C_{mag}. Although the fraction of magnetic bacteria is high, the absolute number is low, characterised by a low D_{mag}. As the sample enters the exponential growth phase, the C_{mag} plummets while D_{mag} is unaffected. This indicates that the amount of bacteria increases (as reflected in the OD) but the amount of magnetic bacteria does not. Subsequently in the stationary phase, the OD, C_{mag} and D_{mag} remain relative stable. Only after approximately two days, in the mag-
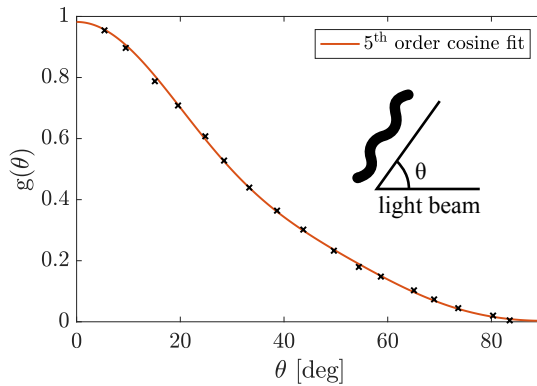
FIGURE 5.4 – *The optical density of MTB is dependent on orientation; it is highest when bacteria are aligned with the light beam and lowest when they are aligned orthogonal. The angle-dependent scatter factor $g(\theta)$ shows a nonlinear dependence on orientation.*

netic growth phase, the amount of magnetic bacteria increases, reflected in both the C_{mag} and D_{mag}, while the OD is not significantly affected. After approximately 3.3 days the amount of magnetic bacteria decreases, while the OD keeps increasing. This phenomenon could be caused by a contamination, or by migration of bacteria within the cuvette.

The measured γ starts off relative low, and starts increasing once in the magnetic growth phase. Surprisingly, it continues to increase when the amount of magnetic bacteria declines. The average form factor of bacteria and medium viscosity is unlikely to change over time. Therefore, the continuing growth can be explained by an increased average magnetic dipole moment, or a higher average amount of iron oxide crystals per bacterium. It is not possible to determine γ accurately before the start of the magnetic growth phase because the amplitude of the alternating OD signal is too low, as depicted in figure 5.3.

The growth profile of MTB is very sensitive to repeated experiments under slightly different conditions. Additional growth curves can be observed in Appendix B.

5.5 Discussion

5.5.1 Repeatability and representability

The observed results provide a clear insight in the growth pattern of MTB with unparalleled temporal resolution. It is unknown, however, to which extent the measured parameters are representative for the entire population residing in

the cuvette. Because of the selective size of the photo diode the observation area is restricted to a small window. Only the response of bacteria in that window is measured. An uneven, time-dependent distribution of MTB in the cuvette will result in a non-representative measurement. Additionally, it is possible an oxygen gradient forms in the sample, contributing to a band formation that may enter and leave the observation area and enhances the uneven distribution of MTB. Indeed, the OD is fluctuating over time after the stationary phase has been reached (figure 5.5).

5.5.2   Response of MTB to magnetic fields

Estimation of γ is based on a model of a single bacterium. The measured OD, however, is a bulk parameter; it is generated by bacteria that are responding with various degrees of speed to a changing magnetic field direction. The single-bacterium model is fitted to a signal consisting from both slow and fast aligning bacteria, which introduces an error. A second error results from the fact that not all bacteria are perfectly aligned with the magnetic field, but fluctuate around a mean orientation.   This effect becomes stronger for bacteria with a low magnetic dipole moment, or for magnetic fields with low amplitude. This phenomenon explains why there is a change in OD from setting 3 to 1; in both cases the fields are directed vertically, but are an order of magnitude apart in field strength.

An additional error in estimating γ results from samples with a significant amount of fluctuation in the measured OD characterised by medium frequencies. These fluctuations are random and cannot be modelled, but do have a significant impact on the goodness of fit.

The values for γ range from $0.44\,\mathrm{rad\,mT^{-1}}$ to $1.41\,\mathrm{rad\,mT^{-1}}$. This agrees with results we obtained in previous work, where we investigated individual bacteria (Pichel et al., 2018). We reported values of $0.74(3)\,\mathrm{rad\,mT^{-1}}$ (determined via bacteria trajectories in microscope observations) and of $1.2(3)\,\mathrm{rad\,mT^{-1}}$ (determined via TEM microscopy of magnetosomes and macroscopic drag models).

5.6   Conclusions

We have constructed an optical density-based (OD) meter which can automatically and continuously measure properties of magnetotactic bacteria (MTB). These properties include the optical density (OD), a measure for the relative amount of magnetic over non-magnetic bacteria (C_{mag}), a measure for the absolute amount of magnetic bacteria (D_{mag}) and a parameter quantifying the alignment speed of bacteria to external magnetic fields (γ).

The angle-dependent optical density of MTB was measured and parametrised. This relation proves to be a non-symmetrical S-curve; the OD is highest when bacteria are aligned with the light beam and lowest when positioned orthogonally.

We obtained growth curves of MTB with high temporal resolution (10 mHz) over a period of 5 days. We clearly distinguished separate growth phases (lag, exponential growth, stationary, and magnetic growth). Initially the sample contained a significant amount of magnetic bacteria, characterised by a relative high C_{mag} and low D_{mag} in the lag phase. The exponential growth phase saw an increase of non-magnetic bacteria only, which reflected in a drop in C_{mag} and a stable D_{mag}. The magnetic growth phase started parallel to the stationary phase, reflected by an increase in both C_{mag} and D_{mag}.

The γ has shown to slowly increase over the span of time, starting at the begin of the magnetic growth phase. As both the viscosity of the medium and the average shape factor of bacteria do not significantly change over time, this increase is proportional to the increase of the average magnetic dipole moment of MTB.

Measurements of growth curves of several samples have shown significant differences between the measured parameters. This demonstrates the need and importance of automated, real-time measurements of these parameters; for the purpose of optimally cultivating bacteria with desired properties, or for measuring the impact of environmental changes on growth each new sample needs to be carefully monitored. This machine requires no manual operations like sampling the culture for OD- and C_{mag} measurements. Additionally it does not require time-consuming, expensive and specialised machinery such as TEM imaging for determining the magnetosome development.

The methods used by the OD meter are not without flaw; the results represent but a sub-population of the sample which might not be representative for the whole. Additionally, model inaccuracies and sample fluctuations occasionally result in non-reliable estimates of γ, as well as for samples characterised by low C_{mag}. Yet, the method offers unparalleled temporal resolution and automated monitoring of MTB. We are convinced it will be an extremely helpful tool in culturing MTB, and possibly for other fields, such as monitoring magnetic particles in fluids.
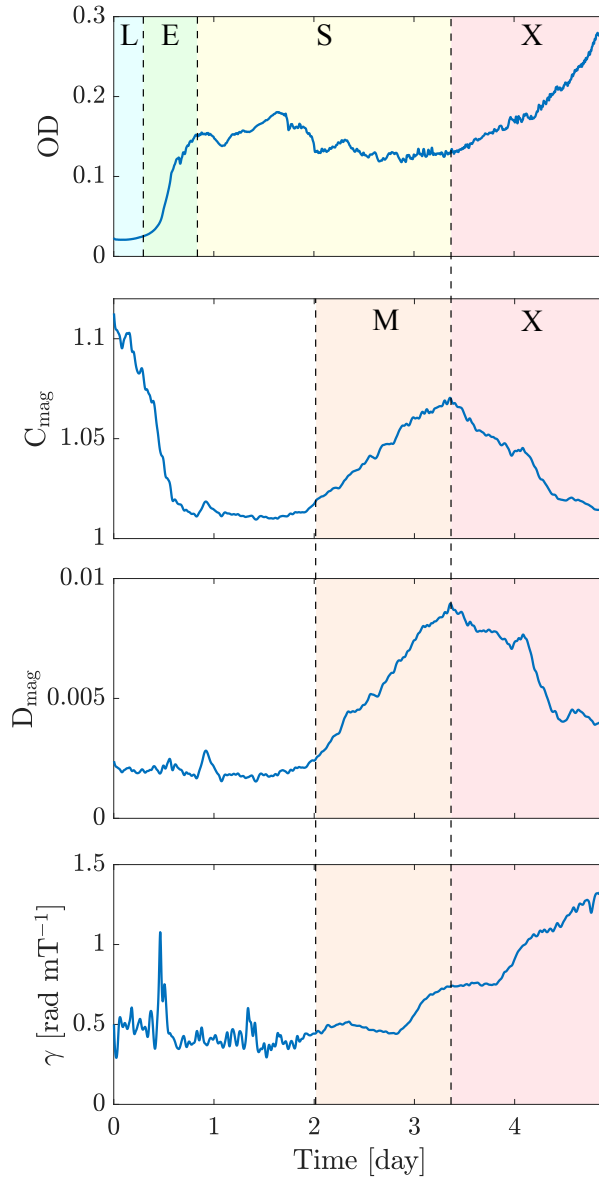
FIGURE 5.5 – *The bacteria colony parameters measured over a span of five days; the optical density (OD), the C_{mag} (quantifying the ratio of magnetic to nonmagnetic bacteria), the D_{mag} (quantifying the amount of magnetic bacteria), and the γ (quantifying how strong the bacteria respond to magnetic fields). The following phases can be identified: lag phase (L), exponential phase (E), stationary phase (S), magnetic growth phase (M) and an undefined phase (X).*

Chapter 6

MTB and Mucus

Abstract

In this study we measured the penetration depth of individual magnetotactic bacteria into human mucus under application of magnetic fields, ranging in amplitude from 1 to 3 mT. The bacteria were observed inside 5 μm high microfluidic channels. The results showed limited penetration of the mucus-medium interface.

The work in this chapter was performed in close cooperation with my colleagues from HIPS, Germany and KIST Europe, Germany. My specific contribution was to set up the cultivation of *Magnetospirillum Gryphiswaldense* in our laboratory, to prepare (TEM, SEM, chip) samples for observation, perform part of the experiments shown and I participated in inception of experimental design. Sample preparation of human mucus was done by Xabi Murgia. Experiments were performed in closed cooperation with Tijmen Hageman, Nuriye Korkmaz and Per Løthman.

6.1   Introduction

Drug delivery through mucosal membranes and natural barriers has been a topic of interest in the last decades. These formidable barriers of nature can be an advantage in keeping out harmful bacteria or other foreign bodies, but also obstruct medicine meant to pass through, lowering efficacy in the process. Several carrier and delivery methods have been proposed over the years. Though many are chemical (lipid-mediated transport, protein binding, etc.) or biological (carrier mediated transport, receptor mediated transport, large and small molecules, etc.) in nature, it is also possible to utilise microrobots for targeting and perhaps drug delivery (Tiwari et al., 2012). At first glance, we are interested in the interaction at the interface between human tissue and the extracellular environment which is where bacteria normally reside.

In this study we attempted to elucidate the physical interaction between magnetotactic bacteria (MTB), *Magnetospirillum Gryphiswaldense* and human
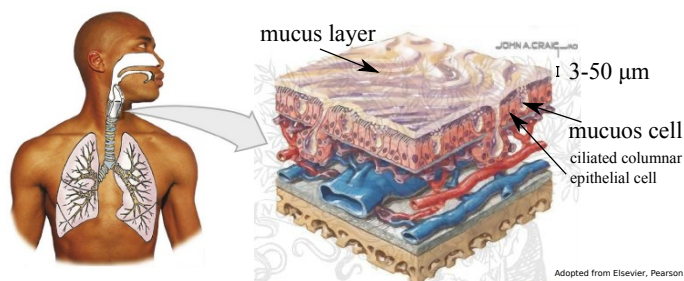
FIGURE 6.1 – *Tracheal mucus lines the epithelial cells of the trachea and lungs. The protective layer is meant to keep out foreign bodies (e.g. bacteria, large inorganic particles like tar from smoke (*100 μm*) (Van Dijk et al., 2011;).*

tracheal mucus. The mucus is derived from pulmonary biopsy tools used in elective surgery procedures. Figure 6.1 shows an the area covered by the same mucus. For this study MTBs were controlled and steered towards the interfaces area between the mucus and the MTB medium.

6.1.1   Prior state-of-art

Drug delivery has been suggested using targeting by MC-1 (Martel et al., 2009) and shown to work to some extent in mice. It proved feasible for MC-1 to navigate to a specific location in mice (Felfoul et al., 2016). Though the multidisciplinary effort and results are impressive, it is limited to intravenous delivery guided by a magnetic system with the purpose of gathering a majority of MTBs in a certain area. What we are interested in, is the specific interaction between the MTB and interfaces that are more viscous than water (0.6 mPas), and less viscous than blood (3.5 mPas) at 37 °C.

6.1.2   Organisation of paper

In our paper we would like to present an open-loop approach to test and observe diffusion of MTBs into human mucosal layers *in vitro*. From experimental results we would like to verify the permeability of human mucus to MTB. These results could be useful for future testing of drug delivery approaches using MTB as a vehicle for delivery.

6.2   Theory

Our point of interest lies at the interface between two miscible liquids: mucus and MTB growth medium. At this interface lies a transition of viscosity between

the mucus and the MTB growth medium. The more viscous a liquid becomes, the slower MTB will be able to move through it, as per Stokes law:

$$\boldsymbol{F}_d = 6\pi\nu R\boldsymbol{v} \tag{6.1}$$

where F_d is the frictional force, or Stokes drag, acting on the interface between the fluid and the MTB, ν is the dynamic viscosity of the liquid, R is the radius (or in this case length) of the MTB and v is the velocity relative to the fluid sufficiently far away from the MTB to that its influence is negligible.

6.3   Experimental

6.3.1   Magnetotactic bacteria cultivation

Liquid cultures of *Magnetospirillum Gryphiswaldense*, were grown unagitated at room temperature (21 Celcius in closed 2 mL (Eppendorf) centrifugation tubes for 3 days to 6 days. Modified spirillum growth medium (ATCC 1653) with an oxygen concentration of 1 % to 5 % was prepared with an adjusted pH of 7.0 for standard cultivation. The cultures had an average optical density at the end of cultivation of approximately 0.2 (at 550 nm) in the presence of a magnetic field of 5 mT oriented parallel to the light beam. Sampling for experiments was done using a chemically sterilzed microfluidic chip.

6.3.2   Microfluidic chip

The microfluidic chips used for our experiments was designed as a static chip with no flow, which can be seen in Figure 6.3.2. Several large outlets and inlets were etched out to allow sampling of mucus in conjunction with liquid culture of MTB. For unobscured observation the channels of the chips were 5 μm deep. The amount of mucus used was kept to a minimum, due to blocking of light at too high concentrations. In some cases this obscured the samples and area of interest.

6.3.3   Setup

The microfluidic chip was mounted on a microscope x-/y-stage. A stepper motor was positioned below the stage which could be manually controlled or provide looped patterns for the MTB to follow. The free stepper motor with magnet and controller can be seen in Figure 6.3. An off-the-shelf lab jack was used to adjust the height of the motor and subsequently strength of the magnetic field. The magnetic field at specific heights was measured at the position of the microfluidic chip using a Hall meter (Metrolab THM1176).
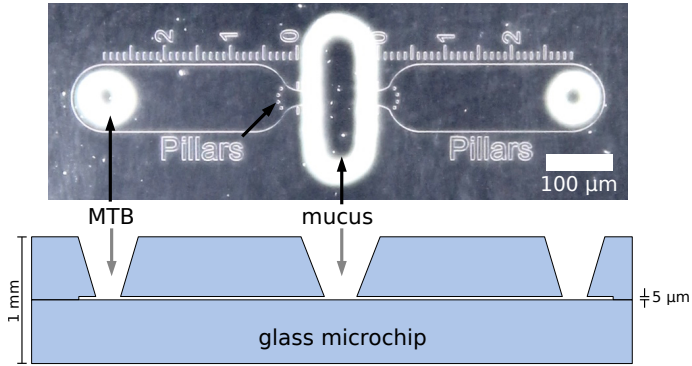
FIGURE 6.2 – *Light microscope image of the microfluidic channel (top) and schematic of the chip cross-sectional layout (bottom)*

FIGURE 6.3 – *The stepper motor that controls the magnet direction is connected to a computer with a game console control. This allows for manual control of the propulsion of a single bacterium.*

6.4   Results

As an initial test, we realized a microfluidic chip with a central access hole (figure 6.3.2) where some of the mucus can be inserted. Subsequently we inserted the growth medium (mostly water) with bacteria in both outer access holes. By means of the magnet system, we control the swimming direction of a single bacterium. Figure 6.4 shows shapshots of a video recording where we directed the bacterium towards the region with mucus. The transition between the medium and the mucus is difficult to identify, and most likely a gradient. We observed
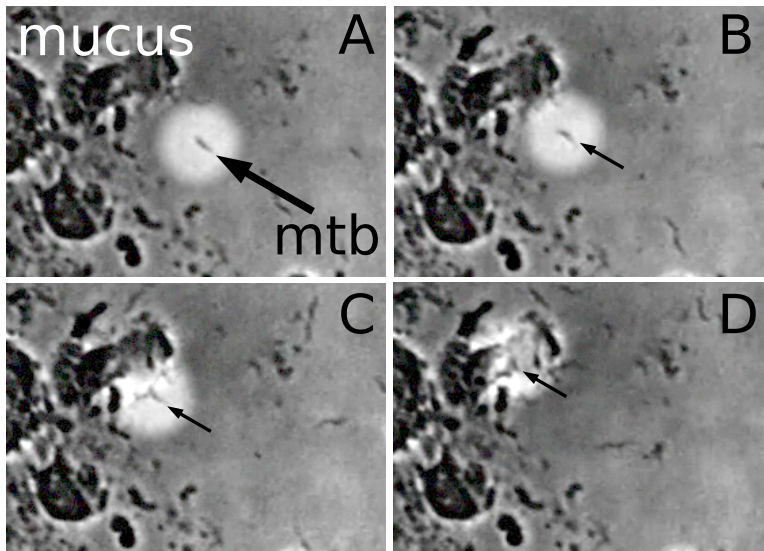
FIGURE 6.4 – *Snapshots of two seconds of an experiment in which a magneto-tactic bacterium was identified (A) and steered towards (B,C) the mucus layer inside the microfluidic chip of figure 6.3.2. The bacterium can be steered for about a body length into the mucous region, where it gets entangled in the mucus for a few seconds (D).*

that the bacterium is able to move very close to the more denser region of the mucus, which appears dark. However, the bacterium is not able to penetrate the darker region. When forced into these darker regions, it either reverses direction or gets entangled for a few seconds.

This experiment shows that a microfluidic system can be successfully used to study the behaviour of bacteria close to interfaces between water and a more dense material. The artificial configuration inside the microfluidic chip is probably very different from the actual situation in the respiratory tract. This initial result shows however that it is not evident that magneto-tactic bacteria can penetrate the mucous layer for more than a few micrometer. Further experiments are required, preferably using artificial mucus with varying density.

6.5   Discussion

With only preliminary data available, it is clear that the mucus is not toxic to MTBs in the short term. This paves a way for follow-up experiments with different types of medium, mucus or MTBs depending on cell viability in co-culture.

6.6   Conclusion

The ability to control the bacteria and to observe them for hours, allowed us to study in detail their interaction with human mucus. Initial experiments show that the bacteria are able to penetrate the mucus for a few micrometer, after which they either reverse or get entangled. Furthermore, cells showed no signs of diminished performance in the vicinity or far away from the mucosal layer for the duration of the experiments (30 mins).

These preliminary results encourage us to study the interaction of magneto-tactic bacteria with barriers of varying viscosity, in order to assess their ability to penetrate biological barriers and deliver therapeutics.

These findings can be of importance to communities focusing on drug delivery at semi-solid and fluid interfaces, looking for a biomimetic approach using an existing and controllable carrier model.

Chapter 7

Conclusion and Outlook

In this thesis we have investigated traits of MTB under influence of changing magnetic fields in micro-fluidic chips and a modified O.D. meter equivalent, to validate a methodology for observing single as well as bulk MTB. This was guided by the following research question:

> What can we learn about biophysical properties of MTB by observing single or bulk responses to changing magnetic fields?

7.1 Bacteria in general

For bacteria (5 µm) in general we have found that the micro-fluidic chip platform serves as an excellent observational tool. The confinement to both narrow channel height and static fluidic setting allows for careful observation of a micro-organism up to several hours. Observation of changes in traits or physical interactions of micro-organisms at biological and -mechanical interfaces over longer periods of time can be easily performed under these conditions.

Long term observations have also revealed a recurring and significant decline in velocity over time. This may be attributed to either fatigue, lack of nutrients, observation conditions or the cell division and proliferation process. Though unclear why, the decline in velocity may pertain to all types of micro-organisms when redirected to do a specific task in an experimental or clinical setting for an extended period of time.

7.2 Magnetotactic bacteria

More specifically, in the case of magnetotactic bacteria, we have found that the size of U-turns can be limited to several micrometers when using field strengths near saturation. At the saturation, due to the self-propelled nature of MTB, the required setup for general use can be limited to a permanent magnet at close range of the micro-fluidic chip.

Furthermore, the measurement of the shape factor, α_{bs}, have shown that the relationship beween the average rate of rotation and the magnetic field strength, γ, are mostly affected by the length. Other attributes, such as width, number of windings or helical amplitude, only contribute a 1.19 to 1.80-fold increase in drag.

This relation can also be observed in bulk if the time resolution is high enough. The O.D. spectrum has the potential to reveal the response time of a culture of MTB at a known magnetic field strength. The shape of the MTB in question is perhaps less relevant than its volume and magnetic moment.

7.3   In microrobotics

Additionally, the results pertaining to the drag profile provide a guideline for the design of micro-robotic agents. The relationship between the average rate of rotation and magnetic field strength ($\alpha \sim B$) dictates that a 10-fold increase in size requires a 1000-fold increase in field strength. These design parameters can significantly reduce the magnetic field, and subsequent energy, required to control a micro-sized therapeutic or robotic agent.

When given a fixed length, the design of secondary morphological traits can be freely adapted when not exceeding the boundaries of the initial length. Larger sized robots will either require a significantly stronger magnetic core or significantly stronger external magnetic fields to compensate for an increase in drag, if the same rate of rotation is desired. Other design space should be dedicated to propulsion and drug delivery systems.

Lastly, from bulk analysis of MTBs it follows that the response time of magnetic particles or robots of the same size might also be observed using a photo spectrometer with a controllable magnetic field. Similarly to MTBs their volume and magnetic moment, rather than morphology, will be the determining factors.

7.4   Outlook

We have found that at low Reynolds numbers size of non-dominant characteristics can matter a lot. The drag increase due to seemingly small feature changes can lead to significant changes in drag. It would of course be possible to simply ignore other features and approach any object with a sphere or rod shape, due to its simplicity. In the future though, these small details in morphology might have to be more clearly defined to create the perfect microrobot or reduce requires for a magnetic field or other means to control the robots wirelessly.

Furthermore, the ability to control a single MTB is not without interruption. Aside from declining velocity in the long term or reversals at any given time, it is still unclear how MTB will respond to the human immune system. Long term experiments done in human blood or a chemical equivalent could prove valuable in determining the controllability of MTB in comparison to our experimental setup.

The current issues make the MTB less reliable when utilised as a drug delivery system when compared to the perfect microrobot, which would ideally follow every command. It does however merit the use of an MTB as a model for such a robot, since it is more easily cultivated in a biological setting than it is (from a control point of view) identically designed and synthetically produced into existence. Aside from aesthetics, the unparalleled performance of the bacterial motor is an additional advantage which is not easily mimicked using mechanical parts.

With the knowledge of the upper boundary of magnetic field strength required for saturation and the limitations of drag, it might be possible in the future to make more functionality-based micro robot designs using the accurate descriptions of what we know about MTB today. At this point in time, it remains impossible to engineer $5\,\mu m$ sized robot which entails a motor that works at nearly 100 % efficiency, moves at $50\,\mu m\,s^{-1}$ and responds to wireless commands by a scientist or surgeon in experimental or clinical setting.

Appendices

Appendix A

Average rate of rotation

A.1 Theory

A.1.1 The Rate of Rotation

The dependence on the field

The magnetic torque Γ [Nm] is equal to the change in total magnetic energy U [J] with changing applied field angle. We consider only the demagnetization and external field energy terms. The demagnetization energy is caused by the magnetic stray field $\boldsymbol{H}_\mathrm{d}$ [A/m] that arises due to the magnetosome magnetization $\boldsymbol{M}$ [A/m]. In principle, one has to integrate the stray field over all space. Fortunately, this integral is mathematically equivalent to (Hubert and Schäfer, 1998)

$$U_\mathrm{d} = \tfrac{1}{2}\mu_0 \int \boldsymbol{M} \cdot \boldsymbol{H}_\mathrm{d}\mathrm{d}V, \tag{A.1}$$

with μ_o the vacuum permeability, $4\pi 10^{-7}$. In this formulation, the integral is conveniently restricted to the volume V of the magnetic material.

The demagnetization energy acts to orient the magnetization so that the external stray field energy is minimized. We can define a shape anisotropy term K [J/m^3] to represent the energy difference between the hard and easy axes of magnetization, which are perpendicular to each other,

$$K = \left(U_\mathrm{d,\,max} - U_\mathrm{d,\,min}\right)/V. \tag{A.2}$$

The external field energy is caused by the externally applied field $\boldsymbol{H}$ [A/m]

$$U_\mathrm{H} = -\mu_0 \int \boldsymbol{M} \cdot \boldsymbol{H}\mathrm{d}V, \tag{A.3}$$
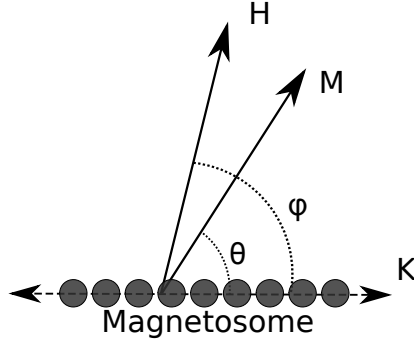
FIGURE A.1 – *Definition of the field angle φ and the magnetization angle θ between the easy axis K, the magnetization M and the magnetic field H.*

and acts to align **M** parallel to **H**. Assuming that the magnetic element of volume V is uniformly magnetized with saturation magnetization M_s [A/m], the total energy can then be expressed as

$$U = KV \sin^2(\theta) - \mu_0 M_s H V \cos(\varphi - \theta). \qquad (A.4)$$

The angles θ and φ are defined as in figure A.1. Normalizing the energy, field, and torque by

$$u = U/KV \qquad (A.5)$$

$$h = \mu_0 HM/2K \qquad (A.6)$$

$$\tau = \Gamma/KV, \qquad (A.7)$$

respectively, the expression for the energy can be simplified to

$$u = \sin^2(\theta) - 2h\cos(\varphi - \theta). \qquad (A.8)$$

The equilibrium magnetization direction is reached for $\partial u/\partial \theta = 0$. The solution for this relationship cannot be expressed in an analytically concise form. The main results are however that for $h < 1/\sqrt{2}$, the maximum torque is reached at the field angle $\varphi_{\max} = \pi/2$,

$$\tau_{\max} = 2h\sqrt{1 - h^2} \qquad \text{for } h \leq 1/\sqrt{2} \qquad (A.9)$$

$$= 1 \qquad \text{for } h > 1/\sqrt{2}. \qquad (A.10)$$

The angle of magnetization at maximum torque can be approximated by

$$\theta_{\max} = h + 0.1h^2 \text{ for } h < 1/\sqrt{2}, \qquad (A.11)$$

where the error is smaller than 5×10^{-3} rad (1.6°) for $h < 0.5$.

For $h > 1$, the field angle $\varphi_{\max}$ at which the maximum torque is reached is smaller than $\pi/2$ and approaches $\pi/4$ for $h \to \infty$. This behaviour can be very well approximated by

$$\varphi_{\max} = \frac{\pi}{4}\left(1 + \frac{2}{3h}\right) \text{ for } h > 1, \tag{A.12}$$

where the error is smaller than $3 \times 10^{-3}\pi$ (0.5°).

In summary, and returning to variables with units, the maximum torque is $\Gamma_{\max} = KV$, which is reached at

$$H > \frac{\sqrt{2}K}{\mu_0 M_s} \tag{A.13}$$

at an angle $\varphi = \pi/2$, which, to a good approximation, decreases linearly with $1/H$ to $\varphi = \pi/4$ at an infinite external field.

Demagnetization factor

The magnetization M_s is a material parameter, so the only variable to be determined is the magnetosome's demagnetization factor. As a first approximation, we can consider the chain of magnetic crystals in the magnetosome as a chain of n dipoles separated at a distance a, each with a dipole moment $m = M_s V$ [Am^2], where V is the volume of each single sphere. We assume that all dipoles are aligned parallel to the field ($\varphi = \theta$) to obtain an upper limit on the torque. (See figure A.1 for the definition of the angles). The magnetic energy for such a dipole chain has been derived by Jacobs and Bean (Jacobs and Bean, 1955), which, rewritten in SI units, is

$$U = \frac{\mu_0 m^2}{4\pi a^3} n K_n \left(1 - 3\cos^2(\theta)\right) +$$
$$\mu_0 n m H \cos(\varphi - \theta) \tag{A.14}$$
$$K_n = \sum_{j=1}^{n} \frac{(n-j)}{nj^3}. \tag{A.15}$$

The maximum torque equals the energy difference between the state where all moments are parallel to the chain ($\theta = 0$) and the state where they are perpendicular to the chain ($\theta = \pi/2$), under the condition that the angle between the moments and the field is zero:

$$\Gamma_{\max} = \frac{3\mu_0 m^2}{4\pi a^3} n K_n. \tag{A.16}$$

For a single dipole $n = 1$, $K_n = 0$ and there is no energy difference, as expected.
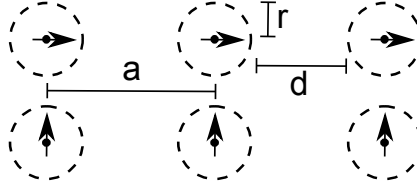
FIGURE A.2 – *Chain of magnetic spheres of radius r, spaced at a distance d, approximated by point dipoles spaced by a distance a = r + d, magnetized along the longitudinal axis of the chain (top) or perpendicular to its longitudinal axis (bottom).*

Combined with equations (A.6) and (A.9), and re-introducing units, the field dependent torque becomes

$$\Gamma = \Gamma_{\text{max}} 2h \sqrt{1 - h^2} \text{ with} \tag{A.17}$$

$$h = \frac{H}{\Delta N M_{\text{s}}}. \tag{A.18}$$

The magnetosome does not consist of point dipoles but should be approximated by spheres with radius r, spaced at a distance of a from each other (figure A.2). We can modify the Jacob and Bean model by introducing the volume of a single sphere V and the magnetization M_s of the magnetite crystal (4.8×10^5 A/m (Witt et al., 2005)),

$$\Gamma_{\text{max}} = \frac{1}{2} \mu_0 M_s^2 n V \Delta N \tag{A.19}$$

$$\Delta N = 2 K_n \left(\frac{r}{a} \right)^3, \tag{A.20}$$

as a correction to equation A.16. This correction is based on the fact that the field of a uniformly magnetized sphere is identical to a dipole field (Griffiths, 1999) outside the sphere, and the average of the magnetic field over a sphere not containing currents is identical to the field at the center of that sphere (Hu, 2000, 2008).

For an infinitely long chain of touching spheres, d=0 and $n \rightarrow \infty$, the difference in demagnetization factors (ΔN) approaches 0.3 (Figure A.3). Approximating the chain by a long cylinder (ΔN=0.5) (Erglis et al., 2007; Hanzlik et al., 1996) therefore overestimates the maximum torque by 40%. Simply taking the total magnetic moment to calculate the torque, as if ΔN=1, would overestimate it by a factor of three.
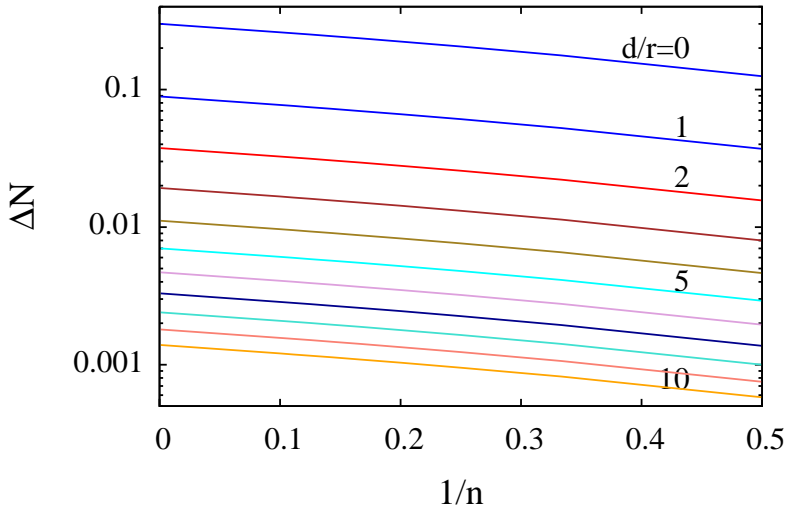
FIGURE A.3 – *Difference in demagnetization factors of a chain of spheres as function of number of spheres n for varying spacing between the spheres d/r.*

Low field approximation

For low values of the field ($h \ll 1$), equation (A.16) can be approximated by

$$\Gamma \approx \Gamma_{\text{max}} 2h = \mu_0 M_s n V H = mB, \qquad (A.21)$$

where m [Am^2] is the total magnetic moment of the magnetosome chain and assuming the permeability of the medium to be equal to vacuum. This approximation is commonly used in the field of MTB studies. Based on the theory presented here, it is now possible to estimate up to which field value this is approximation is valid.

The normalization to the reduced field h is solely dependent on the magnetization and demagnetization factors of the chain. Based on the values for magnetosome morphology (table 3.1), we can estimate the field dependence of the torque. Figure A.4 shows the torque as a function of the field for the range of values tabulated, normalized to the maximum torque. Also shown is the approximation for the case when the magnetization remains aligned with the easy axes. For *Magnetospirillum Gryphiswaldense*, the linear range is valid up to fields of about 10 mT for 90 % of the population.

Drag torque

Magnetotactic bacteria are very small, and rotate at a few revolutions per second only. Inertial forces therefore do not play a significant role. The ratio between
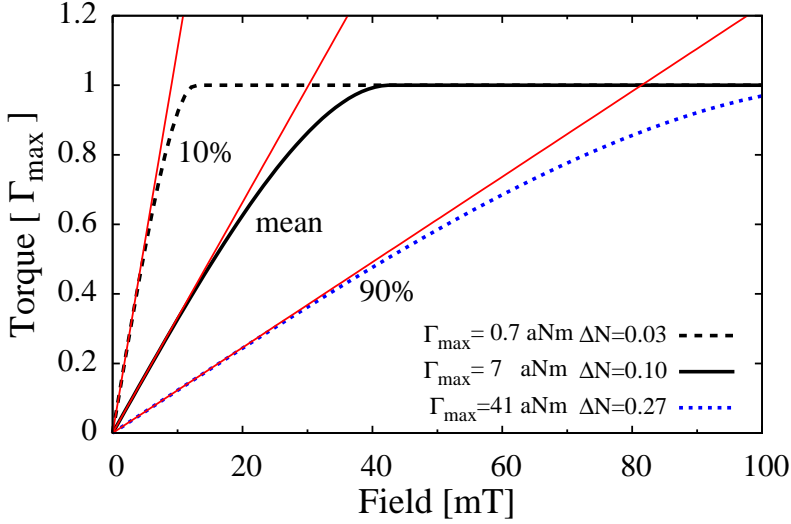
FIGURE A.4 – *Magnetic torque on magnetotactic bacteria, normalized to the maximum torque, as a function of applied field for the average of the population, as well as the* 10 % *and* 90 % *cut-off (see table 3.1). The red solid asymptotes show the linear approximation for* Γ = *mB.*

the viscous and inertial forces is characterized by the Reynolds number *Re*, which for rotation at an angular velocity of ω [rad/s] is

$$Re = \frac{L^2 \rho \omega}{4\eta}, \tag{A.22}$$

where L is the characteristic length (in our case, the length of the bacterium), ρ the density, and η the dynamic viscosity of the liquid (for water, these are, respectively, 10^3 kg/m^3, and 1 mPas). Experiments by Dennis *et al.* (Dennis et al., 1980) show that a Stokes flow approximation for the drag torque is accurate up to *Re*=10. In experiments with bacteria, the Reynolds number is on the order of 10^{-3} and the Stokes flow approximation is certainly allowed. The drag torque is therefore simply given by

$$\Gamma_D = f_b \omega, \tag{A.23}$$

The rotational drag coefficient of the bacterium, f_b, needs to be estimated for the type of MTB studied. In a first approximation, one could consider the MTB to be a rod of length L and diameter W. Unfortunately, there is no simple expression for the rotational drag of a cylinder. Dote (Dote and Kivelson, 1983) gives a numerical estimate of the rotational drag of a cylinder with spherical caps (spherocylinder). Fortunately, for typical MSR-1 dimensions, it can be

shown that a prolate spheroid of equal length and diameter has a rotational drag coefficient that is within 10 % of that value. To a first approximation, one can therefore assume the rotational drag of an MSR-1 to be given by (Berg, 1993)

$$f_e = \frac{\pi \eta L^3}{3 \ln\left(\frac{2L}{W}\right) - \frac{3}{2}}. \tag{A.24}$$

However, the MSR-1 has a spiral shape, so the actual drag will be higher. Rather than resorting to complex finite element simulations, we chose to empirically determine the rotational drag torque by macroscopic experiments with 3D printed bacteria models in a highly viscous medium (Section 3.3.4.). We introduce a bacteria shape correction factor α_{bs} to the spheroid approximation, which is independent of the ratio L/W over the range of typical values for MSR-1 and has a value of about 1.65. The corrected rotational drag coeffient for the bacteria then becomes

$$f_b = \alpha_{bs} f_e. \tag{A.25}$$

Diameter and duration of the U-turn

At the steady-state rate, the magnetic torque is balanced by the rotational drag torque, leading to a rate of rotation of

$$\omega = \frac{\Gamma}{f_b} \approx \frac{mB \sin \phi(t)}{f_b}. \tag{A.26}$$

The approximation is for low field values (see figure A.4), in which case ϕ is the angle between the applied field and the long axis of the bacteria (magnetosome).

The maximum rate of rotation, mB/f_b, is obtained when the field is perpendicular to the long axis of the bacteria. Suppose that we construct a control loop to realize this condition over the entire period of a U-turn. Then the minimum diameter and duration of this loop would be

$$D_{min} = \frac{2 f_b v}{mB} \tag{A.27}$$

$$T_{min} = \frac{\pi f_b}{mB}, \tag{A.28}$$

where D_{min} is the minimum size of a U-turn's diameter and T_{min} is the minimum time of a U-turn. On the other hand, if we reverse the field instantaneously, the torque will vary over the trajectory of the U-turn. Compared to the situation above, the diameter of the U-turn increases by a factor of $\pi/2$:

$$D = \frac{\pi f_b v}{mB}. \tag{A.29}$$

The diameter of the U-turn increases with the velocity of the bacterium. To obtain a description that only depends on the dimensions of the bacteria, we introduce a new parameter v/D [rad/s], which can be interpreted as an average rate of rotation. The relation between the average rate of rotation and the magnetic field B is

$$\frac{v}{D} = \gamma B, \tag{A.30}$$

where the proportionality factor γ [rad/Ts] can be linked to the bacterial magnetic moment m and drag coefficient f_b [Nms],

$$\gamma = \frac{m}{\pi f_b}. \tag{A.31}$$

Note, however, that this expression is only valid in the low field approximation.

The determination of the duration of the U-turn trajectory is complicated by the fact that the magnetic torque starts and ends at zero (at $\theta=0$ or π). In this theoretical situation, the bacteria would never turn at all. Esquivel *et al.* (Esquivel and Lins de Barros, 1986) solve this problem by assuming a disturbance acting on the motion of the bacteria. This disturbance could be due to Brownian motion, as used by Esquivel *et al.*, or due to flagellar propulsion, as we use in the simulations in the following section. Assuming an initial disturbing angle of θ_i, the duration T [s] of the U-turn becomes

$$T = \frac{2f_b}{mB} \ln \frac{2}{\theta_i}. \tag{A.32}$$

A.1.2   U-turn Trajectory Simulations

To check the validity of the analytical approach, we performed simulations. The MTB are approximated by rigid magnetic dipoles with constant lateral velocity v at an orientation of $\theta_x(t)$ and angular velocity of $\omega(t)$ (see figure A.5). They are subject to a magnetic field with magnitude B at an orientation of $\varphi_x(t)$, resulting in a magnetic torque of $\Gamma(t)$. In contrast to the analytical model, it is assumed that flagellar motion causes an additive sinusoidal torque $\Gamma_f(t)$ with amplitude A_f and angular velocity ω_f. These should be in balance with the drag torque: $\Gamma_D = f_b\omega(t)$. The following set of equations link the physical model to the coordinates $x(t)$, $y(t)$:
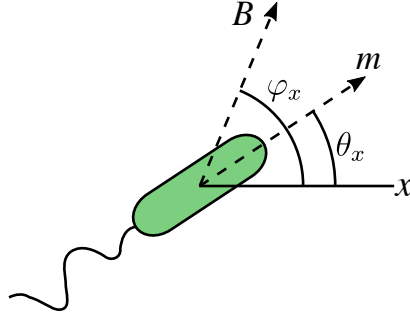
FIGURE A.5 – *Bacterium at angle θ_x with magnetic field at angle φ_x.*

$$x(t) = x(0) + \int_0^t v\cos(\theta_x(t))\mathrm{d}t \tag{A.33}$$

$$y(t) = y(0) + \int_0^t v\sin(\theta_x(t))\mathrm{d}t \tag{A.34}$$

$$\theta_x(t) = \theta_x(0) + \int_0^t \omega(t)\mathrm{d}t \tag{A.35}$$

$$\omega(t) = \frac{1}{f_\mathrm{b}}\left(\Gamma_\mathrm{mag}(t) + \Gamma_\mathrm{flag}(t)\right) \tag{A.36}$$

$$= \frac{mB}{f_\mathrm{b}}\sin(\varphi_x(t) - \theta_x(t)) + \frac{A_\mathrm{f}}{f_\mathrm{b}}\sin(\omega_\mathrm{f}t) \tag{A.37}$$

A linear, closed-form solution of the diameter of the trajectory of the U-turn in the case of an instantaneous field reversal and no flagellar torque is given by equation A.29. This solution is not valid, however, in the case of slowly rotating fields. The experimental magnetic field is considered to rotate according to a constant-acceleration model with a total rotation period of 130 ms (see section 3.3.4). Simulations were carried out with time steps of 10 μs, which is comfortably fast and precise (decreasing this to 1 μs changes the results by approximately 0.01 %). Figure A.6 shows several simulated trajectories subject to fields of various magnitudes, assuming nonzero flagellar torque and realistic MTB parameters.

Figure A.7 shows the simulated v/D as a function of the field magnitude. It can be seen that during an instantaneous field reversal, the solution is nearly identical to the closed-form solution of equation A.29. The difference is caused by the influence of flagellar torque. Introducing a field reversal time T_mag of
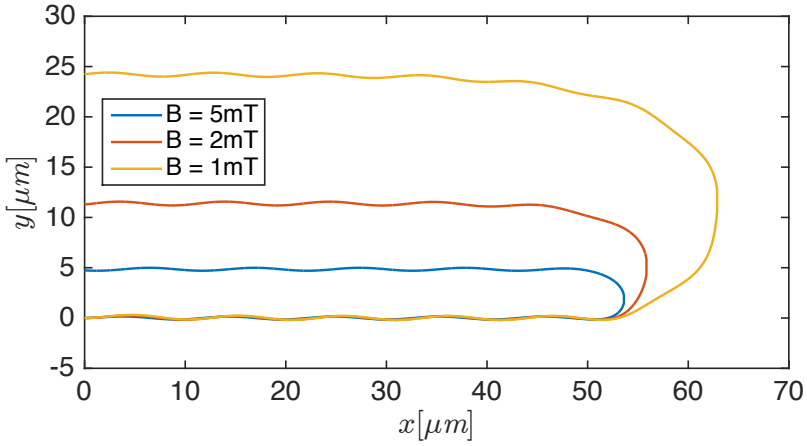
FIGURE A.6 – *Simulated trajectories assuming flagellar torque and a non-instantaneously rotating field for several values of the magnetic field magnitude B. The time step of the simulation is* 10 μs

130 ms into a continuous-acceleration model significantly changes the profile, yielding a similar result for low fields, increasing at moderate fields, and saturating to a maximum value of $16.6\,\mathrm{s}^{-1}$. B_{opt} is defined as the field magnitude at which v/D has the largest difference from the theoretical curve. Figure A.8 shows, from simulations, that the optimal reversal time is inversely proportional to the magnetic field strength. For fields below B_{opt}, v/D can be considered linear with a maximum nonlinearity error of 2 %, independently of T_{mag}.
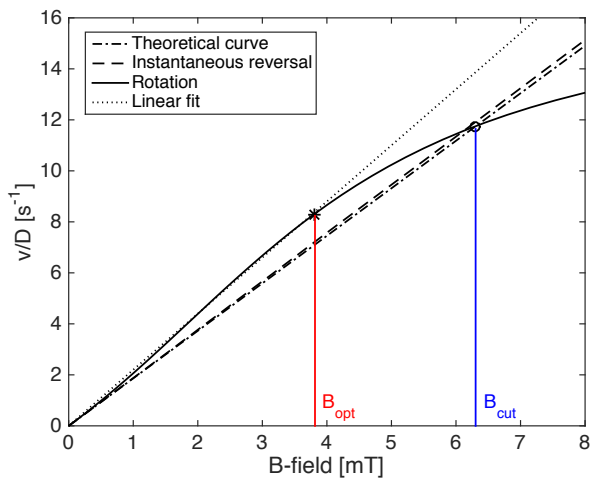
FIGURE A.7 – *Simulated values of v/D for different rotation speeds of the magnetic field, with (red) and without (blue) and flagellar torque, compared with the linear model proposed by Erglis* et al. *(Erglis et al., 2007) (dotted line).*
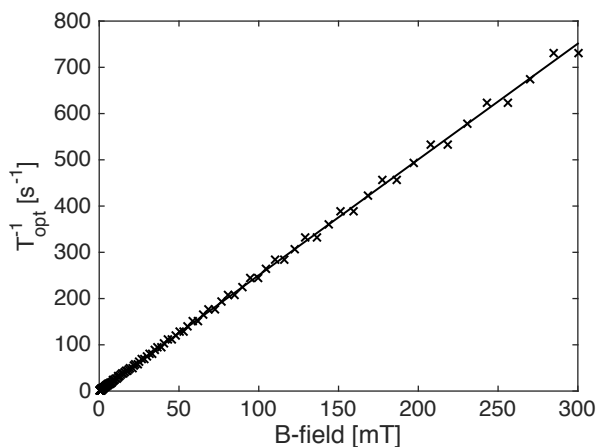

FIGURE A.8 – *Simulated optimum reversal time of the magnetic field as a function of the field strength.*

**Appendix B**

Growth curves measured in the OD meter
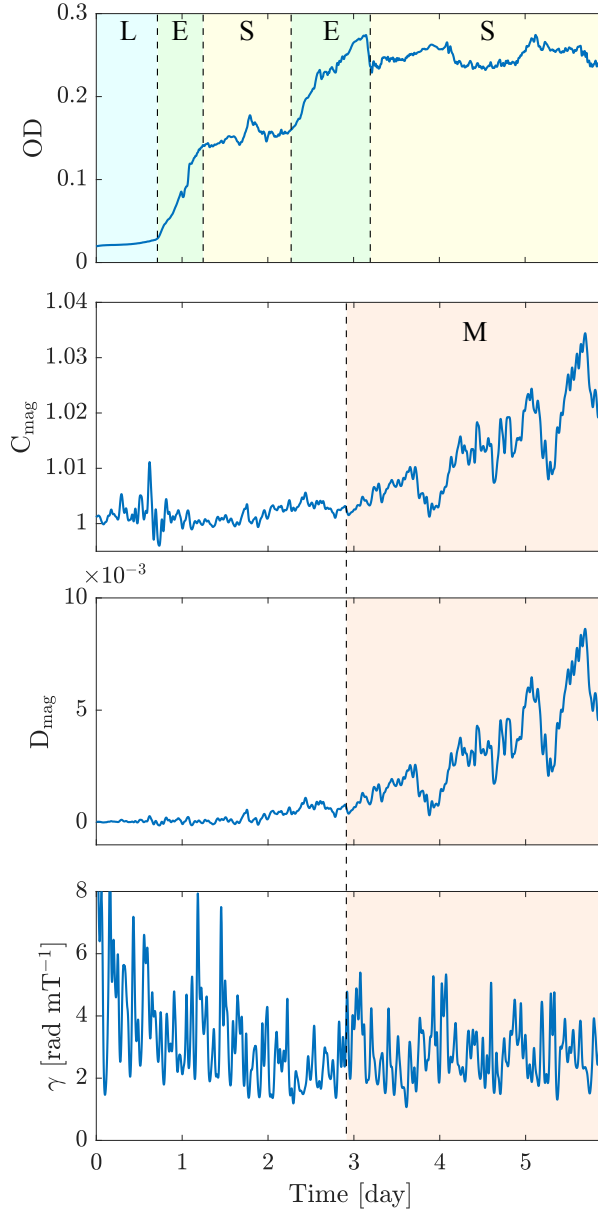
FIGURE B.1 – *Measured growth parameters of a culture of* Magnetospirillum Gryphiswaldense *in the optical density meter. We can identify lag (L), exponential growth (E) and stationary (S) phases. We observe two distinct growth phases (E); these might be actual growth phases, but the second rising slope might also be caused by migration of bacteria within the cuvette. The magnetic growth (M) is independent. There is a lot of noise in the estimation of* γ.
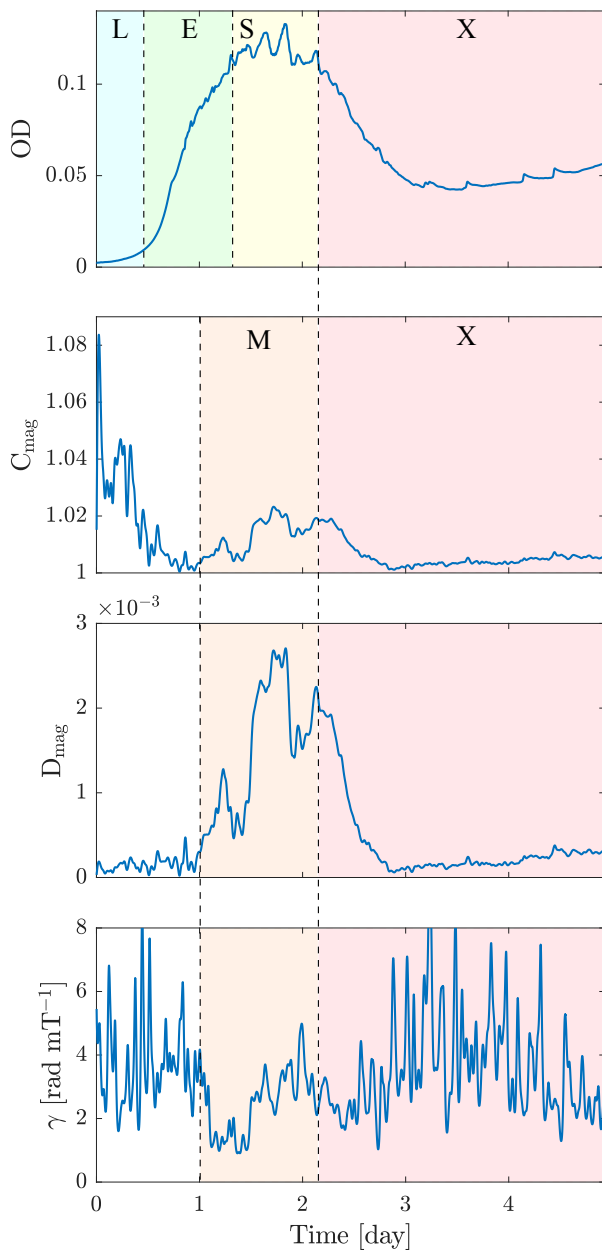
FIGURE B.2 – *Measured growth parameters of a culture of* Magnetospirillum Gryphiswaldense *in the optical density meter. We can identify lag (L), exponential growth (E) and stationary (S) phases, and an undefined phase (X) in which we are not sure what happens. The latter might be caused by cell death or migration of MTB within the cuvette. The magnetic growth (M) is independent. There is a lot of noise in the estimation of* γ.
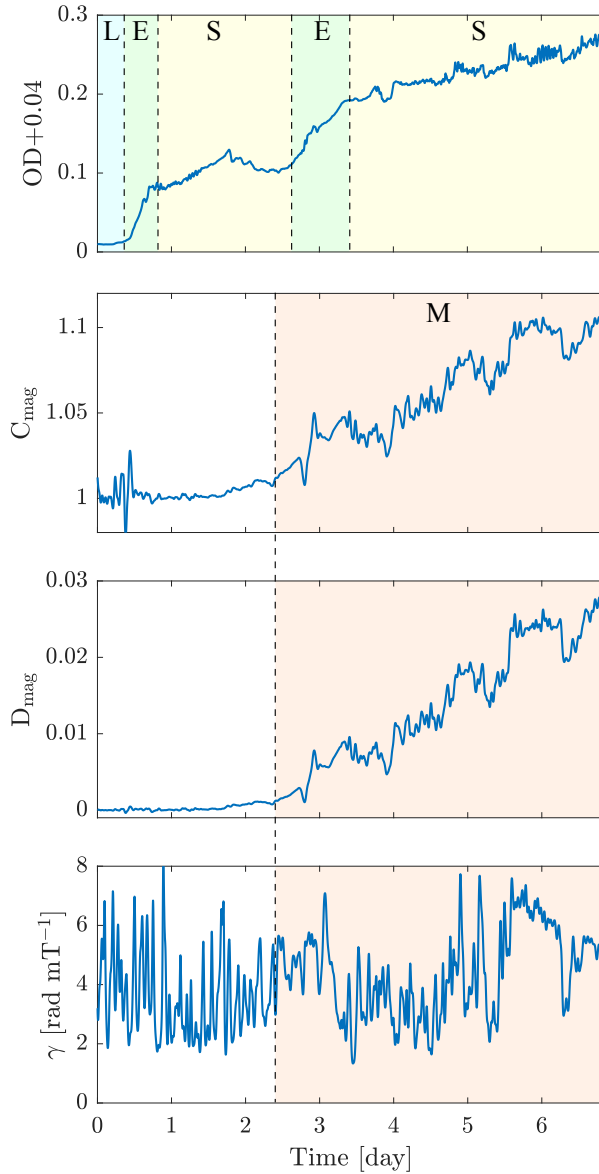
FIGURE B.3 – *Measured growth parameters of a culture of* Magnetospirillum Gryphiswaldense *in the optical density meter. We can identify lag (L), exponential growth (E) and stationary (S) phases. We observe two distinct growth phases (E); these might be actual growth phases, but the second rising slope might also be caused by migration of bacteria within the cuvette. The magnetic growth (M) is independent. There is a lot of noise in the estimation of γ.*

Bibliography

Abayazid M, Roesthuis R J, Reilink R, Misra S, December 2013
  "Integrating deflection models and image feedback for real-time flexible needle steering"
  IEEE transactions on robotics **29**, pp. 542–553

Abbott J J, Cosentino Lagomarsino M, Zhang L, Dong L, Nelson B J, 2009
  "How should microrobots swim?"
  The International Journal of Robotics Research doi: 10.1177/0278364909341658

Bahaj A, James P, 1993
  "Characterisation of magnetotactic bacteria using image processing techniques"
  IEEE Transactions on Magnetics **29**, pp. 3358–3360, doi: 10.1109/20.281175

Bahaj A, James P, Moeschler F, 1996
  "An alternative method for the estimation of the magnetic moment of non-spherical magnetotactic bacteria"
  IEEE Transactions on Magnetics **32**, pp. 5133–5135, doi: 10.1109/20.539514

Ban J, Jiang W, Li Y, Zhang Y, Li J, 2010
  "Functional analysis of hydrogenases and their effects on cell growth and magnetosome synthesis in magnetospirillum gryphiswaldense"
  Chinese Science Bulletin **55**, pp. 1271–1277, doi: 10.1007/s11434-009-0744-8

Baumgartner J, Faivre D, 2011
  "Magnetite biomineralization in bacteria"
  In: W E G Muller, editor, *Molecular Biomineralization, Progress in Molecular and Subcellular Biology*, volume 52, pp. 3–27, Springer Berlin
  ISBN 978-3-642-21229-1, doi: 10.1007/978-3-642-21230-7_1

Bazylinski D, Frankel R, 2004
  "Magnetosome formation in prokaryotes"
  Nature Reviews Microbiology **2**, pp. 217–230, doi: 10.1038/nrmicro842

Berg H C, 1993
  Random Walks in Biology,
  Princeton University Press

Berlanga M, 01 2010
  "Brock biology of microorganisms (11th edn)."
  International Microbiology; Vol. 8, Núm. 2 (2005); 149-150

Blakemore R P, Maratea D, Wolfe R S, 1979
  "Isolation and pure culture of a freshwater magnetic spirillum in chemically defined medium."
  Journal of Bacteriology **140**, pp. 720–729

Bryant H, Sergatskov D, Lovato D, Adolphi N, Larson R, Flynn E, 2007
  "Magnetic needles and superparamagnetic cells"
  Physics in Medicine and Biology **52**, pp. 4009–4025, doi: 10.1088/0031-9155/52/14/001

Cebers A, 2011
  "Diffusion of magnetotactic bacterium in rotating magnetic field"
  Journal of Magnetism and Magnetic Materials **323**, pp. 279–282, doi: 10.1016/j.jmmm.2010.09.017

Dankelman J, van den Dobbelsteen J, Breedveld P, nov. 2011
  "Current technology on minimally invasive surgery and interventional techniques"
  In: *Instrumentation Control and Automation (ICA), 2011 2nd International Conference on*, pp. 12–15, doi: 10.1109/ICA.2011.6130118

De Lanauze D, Felfoul O, Turcot J P, Mohammadi M, Martel S, 2014
  "Three-dimensional remote aggregation and steering of magnetotactic bacteria microrobots for drug delivery applications"
  International Journal of Robotics Research **33**, pp. 359–374, doi: 10.1177/0278364913500543

Dennis S, Singh S, Ingham D, 1980
  "Steady flow due to a rotating sphere at low and moderate reynolds numbers."
  Journal of Fluid Mechanics **101**, pp. 257–279

Dote J, Kivelson D, 1983
  "Hydrodynamic rotational friction coefficients for nonspheroidal particles"
  Journal of Physical Chemistry **87**, pp. 3889–3893

Erglis K, Wen Q, Ose V, Zeltins A, Sharipo A, Janmey P A, Cebers A, 2007
  "Dynamics of magnetotactic bacteria in a rotating magnetic field"
  Biophysical Journal **93**, pp. 1402–1412, doi: 10.1529/biophysj.107.107474

Esquivel D, Lins de Barros H, 1986
  "Motion of magnetotactic microorganisms"
  Journal of Experimental Biology **VOL. 121**, pp. 153–163

Faivre D, 2015
  "Formation of magnetic nanoparticle chains in bacterial systems"
  MRS Bulletin **40**, pp. 509–515, doi: 10.1557/mrs.2015.99

Faivre D, Fischer A, Garcia-Rubio I, Mastrogiacomo G, Gehring A, 2010
  "Development of cellular magnetic dipoles in magnetotactic bacteria"
  Biophysical Journal **99**, pp. 1268–1273, doi: 10.1016/j.bpj.2010.05.034

Felfoul O, Mohammadi M, Taherkhani S b, De Lanauze D, Zhong Xu Y, Loghin D, Essa S d, Jancik S, Houle D, Lafleur M, Gaboury L, Tabrizian M f, Kaou N, Atkin M, Vuong T, Batist G, Beauchemin N, Radzioch D, Martel S, 2016
  "Magneto-aerotactic bacteria deliver drug-containing nanoliposomes to tumour hypoxic regions"
  Nature Nanotechnology **11**, pp. 941–947, doi: 10.1038/nnano.2016.137

Frankel R, Bazylinski D, Johnson M, Taylor B, 1997
  "Magneto-aerotaxis in marine coccoid bacteria"
  Biophysical Journal **73**, pp. 994–1000

Geelhoed J, Kleerebezem R, Sorokin D, Stams A, van Loosdrecht M, 2010
  "Reduced inorganic sulfur oxidation supports autotrophic and mixotrophic growth of magnetospirillum strain j10 and magnetospirillum gryphiswaldense"
  Environmental Microbiology **12**, pp. 1031–1040, doi: 10.1111/j.1462-2920.2009.02148.x

Gorby Y, Beveridge T, Blakemore R, 1988
    "Characterization of the bacterial magnetosome membrane."
    Journal of Bacteriology **170**, pp. 834–841

Griffiths D J, 1999
    Introduction to electrodynamics,
    Prentice Hall, Upper Saddle River, New Jersey, 3rd edition

Hanzlik M, Winklhofer M, Petersen N, 1996
    "Spatial arrangement of chains of magnetosomes in magnetotactic bacteria"
    Earth and Planetary Science Letters **145**, pp. 125–134

Hassan H, Pichel M, Hageman T, Abelmann L, Khalil I S M, 2016
    "Influence of the magnetic field on the two-dimensional control of magnetospirillum gryph-
    iswaldense strain msr-1"
    In: *Proceedings of the IEEE International Conference on Intelligent Robots and Systems (IROS),
    Daejeon, Korea*, pp. 5119–5124,

Heyen U, Schüler D, 2003
    "Growth and magnetosome formation by microaerophilic magnetospirillum strains in an
    oxygen-controlled fermentor"
    Applied Microbiology and Biotechnology **61**, pp. 536–544

Hu B K, 2000
    "Averages of static electric and magnetic fields over a spherical region: A derivation based on
    the mean-value theorem"
    American Journal of Physics **68**, pp. 1058–1060

Hu B K, 2008
    "Averages of static electric and magnetic fields over a spherical region: A derivation based on
    the mean-value theorem"
    arXiv:physics/0002021 [physics.ed-ph]

Hubert A, Schäfer R, 1998
    Magnetic domains: the analysis of magnetic microstructures,
    Springer-Verlag, Berlin, Heidelberg, New-York

Jacobs I, Bean C, 1955
    "An approach to elongated fine-particle magnets"
    Physical Review **100**, pp. 1060–1067, doi: 10.1103/PhysRev.100.1060

van Kampen N, 1995
    "The turning of magnetotactic bacteria"
    Journal of Statistical Physics **80**, pp. 23–33, doi: 10.1007/BF02178351

Katzmann E, Eibauer M, Lin W, Pan Y, Plitzko J, Schuler D, 2013
    "Analysis of magnetosome chains in magnetotactic bacteria by magnetic measurements and
    automated image analysis of electron micrographs"
    Applied and Environmental Microbiology **79**, pp. 7755–7762, doi: 10.1128/AEM.02143-13

Khalil I S M, Pichel M P, Abelmann L, Misra S, May 2013
    "Closed-loop control of magnetotactic bacteria"
    The International Journal of Robotics Research **32**, pp. 637–649, doi:
    10.1177/0278364913479412

Kinosita K, Yasuda R, Noji H, Adachi K, 2000
    "A rotary molecular motor that can work at near 100efficiency."
    Philosophical Transactions of the Royal Society B: Biological Sciences **355(1396),**, p. 473–489.

Kirschvink J, Walker M, Diebel C, 2001
  "Magnetite-based magnetoreception"
  Current Opinion in Neurobiology **11**, pp. 462–467, doi: 10.1016/S0959-4388(00)00235-X

Komeili A, Vali H, Beveridge T, Newman D, 2004
  "Magnetosome vesicles are present before magnetite formation, and mama is required for
  their activation"
  Proceedings of the National Academy of Sciences of the United States of America **101**, pp. 3839–
  3844, doi: 10.1073/pnas.0400391101

Kumar V, Abbas A K, Aster J, 2009
  Robbins and Cotran pathologic basis of disease.,
  St. Louis, Mo: Elsevier Saunders

Kummer M P, Abbott J J, Kratochvil B E, Borer R, Sengul A, Nelson B J, 2010
  "Octomag: An electromagnetic system for 5-dof wireless micromanipulation"
  IEEE TRANSACTIONS ON ROBOTICS **26**, pp. 1006–1017

Lefèvre C, Song T, Yonnet J P, Wu L F, 2009
  "Characterization of bacterial magnetotactic behaviors by using a magnetospectrophotometry
  assay"
  Applied and Environmental Microbiology **75**, pp. 3835–3841, doi: 10.1128/AEM.00165-09

Lefèvre C, Bennet M, Landau L, Vach P, Pignol D, Bazylinski D, Frankel R, Klumpp S, Faivre D, 2014
  "Diversity of magneto-aerotactic behaviors and oxygen sensing mechanisms in cultured mag-
  netotactic bacteria"
  Biophysical Journal **107**, pp. 527–538, doi: 10.1016/j.bpj.2014.05.043

Li J, Pan Y, Chen G, Liu Q, Tian L, Lin W, 2009
  "Magnetite magnetosome and fragmental chain formation of magnetospirillum magneticum
  amb-1: Transmission electron microscopy and magnetic observations"
  Geophysical Journal International **177**, pp. 33–42, doi: 10.1111/j.1365-246X.2009.04043.x

Lins U, McCartney M, Farina M, Frankel R, Buseck P, 2005
  "Habits of magnetosome crystals in coccoid magnetotactic bacteria"
  Applied and Environmental Microbiology **71**, pp. 4902–4905, doi: 10.1128/AEM.71.8.4902-
  4905.2005

Liu J, Notbohm J K, Carpick R W, Turner K T, 2010
  "Method for characterizing nanoscale wear of atomic force microscope tips"
  ACS Nano **4**, pp. 3763–3772, doi: 10.1021/nn100246g

Maceira A M, Cosin-Sales J, Prasad S K, Pennell D J, 2016
  "Characterization of left and right atrial function in healthy volunteers by cardiovascular mag-
  netic resonance"
  Journal of Cardiovascular Magnetic Resonance **18**, p. 64, doi: 10.1186/s12968-016-0284-8

Magariyama Y, Ichiba M, Nakata K, Baba K, Ohtani T, Kudo S, Goto T, 2005
  "Difference in bacterial motion between forward and backward swimming caused by the wall
  effect"
  Biophysical Journal **88**, pp. 3648–3658, doi: 10.1529/biophysj.104.054049

Mandadapu K, JA N, Berry R, Oster G, 2015
  "Mechanics of torque generation in the bacterial flagellar motor."
  Proc Natl Acad Sci U S A **11**

Martel S, Mohammadi M, 2010
  "Using a swarm of self-propelled natural microrobots in the form of flagellated bacteria to perform complex micro-assembly tasks"
  Proceedings - IEEE International Conference on Robotics and Automation pp. 500–505, doi: 10.1109/ROBOT.2010.5509752

Martel S, Mohammadi M, Felfoul O, Lu Z, Pouponneau P, 2009
  "Flagellated magnetotactic bacteria as controlled mri-trackable propulsion and steering systems for medical nanorobots operating in the human microvasculature"
  International Journal of Robotics Research **28**, pp. 571–582, doi: 10.1177/0278364908100924

Maus S, Macmillan S, McLean S, Hamilton B, Thomson A, Nair M, Rollins C, December 2010
  "The us/uk world magnetic model for 2010-2015"
  Technical report, British Geological Survey

Menciassi A, Quirini M, Dario P, 2007
  "Microrobotics for future gastrointestinal endoscopy"
  Minimally Invasive Therapy & Allied Technologies **16**, pp. 91–100

Moisescu C, Bonneville S, Staniland S, Ardelean I, Benning L, 2011
  "Iron uptake kinetics and magnetosome formation by magnetospirillum gryphiswaldense as a function of ph, temperature and dissolved iron availability"
  Geomicrobiology Journal **28**, pp. 590–600, doi: 10.1080/01490451.2011.594146

Nelson B, Kaliakatsos I, Abbott J, 2010
  "Microrobots for minimally invasive medicine"
  Annual Review of Biomedical Engineering **12**, pp. 55–85, doi: 10.1146/annurev-bioeng-010510-103409

Nelson H, Sargent D, Wieand H, Fleshman J, Anvari M, Stryker S, Beart Jr R, Hellinger M, Flanagan Jr R, Peters W, Ota D, 2004
  "A comparison of laparoscopically assisted and open colectomy for colon cancer"
  New England Journal of Medicine **350**, pp. 2050–2059+2114, doi: 10.1056/NEJMoa032651

Park J K, Campos C D M, Neuzil P, Abelmann L, Guijt R M, Manz A, 2015
  "Direct coupling of a free-flow isotachophoresis (ffitp) device with electrospray ionization mass spectrometry (esi-ms)"
  Lab Chip **15**, pp. 3495–3502, doi: 10.1039/C5LC00523J

Pichel M P, Hageman T A G, Khalil I S M, Manz A, Abelmann L, 2018
  "Magnetic response of magnetospirillum gryphiswaldense"
  (under review)

Popp F, Armitage J, Schüler D, 2014
  "Polarity of bacterial magnetotaxis is controlled by aerotaxis through a common sensory pathway"
  Nature Communications **5**, doi: 10.1038/ncomms6398

Pósfai M, Kasama T, Dunin-Borkowski R E, 2007
  "Characterization of bacterial magnetic nanostructures using high-resolution transmission electron microscopy and off-axis electron holography"
  In: D Schüler, editor, *Magnetoreception and Magnetosomes in Bacteria*, pp. 197–225, Springer-Verlag, Berlin, Berlin, Heidelberg
  ISBN 978-3-540-37468-8, doi: 10.1007/7171_044

Press W H, Teukolsky S A, Vetterling W T, Flannery B P, 1992
  Numerical Recipes in C (2nd Ed.): The Art of Scientific Computing,
  Cambridge University Press
  ISBN 0-521-43108-5

Reufer M, Besseling R, Schwarz-Linek J, Martinez V, Morozov A, Arlt J, Trubitsyn D b, Ward F, Poon W, 2014
"Switching of swimming modes in magnetospirillium gryphiswaldense"
Biophysical Journal **106**, pp. 37–46, doi: 10.1016/j.bpj.2013.10.038

Rodenborn B, Chen C H, Swinney H L, Liu B, H Zhang H, 2012
"Propulsion of microorganisms by a helical flagellum"
PNAS **110**

Schleifer K, Schuler D, Spring S, Weizenegger M, Amann R, Ludwig W, Kohler M, 1991
"The genus magnetospirillum gen. nov. description of magnetospirillum gryphiswaldense sp. nov. and transfer of aquaspirillum magnetotacticum to magnetospirillum magnetotacticum comb. nov."
Systematic and Applied Microbiology **14**, pp. 379–385

Schmidt O G, Eberl K, March 2001
"Nanotechnology: Thin solid films roll up into nanotubes"
Nature **410**, pp. 168–168, doi: 10.1038/35065525

Schüler D, Baeuerlein E, 1998
"Dynamics of iron uptake and fe3o4 biomineralization during aerobic and microaerobic growth of magnetospirillum gryphiswaldense"
Journal of Bacteriology **180**, pp. 159–162

Schüler D, Uhl R, Bäuerlein E, 1995
"A simple light scattering method to assay magnetism in magnetospirillum gryphiswaldense"
FEMS Microbiology Letters **132**, pp. 139–145, doi: 10.1016/0378-1097(95)00300-T

Smid P, Shcherbakov V, Petersen N, 2015
"Microscopic observation of magnetic bacteria in the magnetic field of a rotating permanent magnet"
Review of Scientific Instruments **86**, doi: 10.1063/1.4929331

Solovev A A, Xi W, Gracias D H, Harazim S M, Deneke C, Sanchez S, Schmidt O G, 2012
"Self-propelled nanotools"
ACS Nano **6**, pp. 1751–1756, doi: 10.1021/nn204762w

Song T, Zhao L, Wu L F, 2014
"A method for quantitative determination of the number of magnetosomes in magnetotactic bacteria by a spectrophotometer"
IEEE Transactions on Magnetics **50**, doi: 10.1109/TMAG.2014.2323953

Tiwari G, Tiwari R, Sriwastawa B, Bhati L, Pandey S, Pandey P, Bannerjee S K, Jan-Mar 2012
"Drug delivery systems: An updated review"
International Journal of Pharmaceutical Investigation **2**, pp. 2–11, doi: 10.4103/2230-973X.96920

Uebe R, Schüler D, 2016
"Magnetosome biogenesis in magnetotactic bacteria"
Nature Reviews Microbiology **14**, pp. 621–637, doi: 10.1038/nrmicro.2016.99

Van Dijk W, Gopal S, Scheepers P, 2011;
"Nanoparticles in cigarette smoke; real-time undiluted measurements by a scanning mobility particle sizer."
Analytical and Bioanalytical Chemistry. **399(10)**, doi: 10.1007/s00216-011-4701-4.

Witt A, Fabian K, Bleil U, 2005
"Three-dimensional micromagnetic calculations for naturally shaped magnetite: Octahedra and magnetosomes"
Earth and Planetary Science Letters **233**, pp. 311–324, doi: 10.1016/j.epsl.2005.01.043

Wolfe R S, Thauer R K, Pfenning N, 1987
   "A 'capillary racetrack' method for isolation of magnetotactic bacteria"
   FEMS Microbiology Ecology **45**, pp. 31–35

Yang C, Takeyama H, Matsunaga T, 2001a
   "Iron feeding optimization and plasmid stability in production of recombinant bacterial mag-
   netic particles by magnetospirillum magneticum amb-1 in fed-batch culture"
   Journal of Bioscience and Bioengineering **91**, pp. 213–216, doi: 10.1016/S1389-1723(01)80068-2

Yang C, Chen C, Ma Q, Wu L, Song T, 2012
   "Dynamic model and motion mechanism of magnetotactic bacteria with two lateral flagellar
   bundles"
   Journal of Bionic Engineering **9**, pp. 200–210, doi: 10.1016/S1672-6529(11)60108-X

Yang C D, Takeyama H, Tanaka T, Matsunaga T, 2001b
   "Effects of growth medium composition, iron sources and atmospheric oxygen concentrations
   on production of luciferase-bacterial magnetic particle complex by a recombinant magneto-
   spirillum magneticum amb-1"
   Enzyme and Microbial Technology **29**, pp. 13–19, doi: 10.1016/S0141-0229(01)00343-X

Yang Y, Lopez G P, Yellen B B, 2013
   "Tunable assembly of colloidal crystal alloys using magnetic nanoparticle fluids"
   ACS Nano **7**, pp. 2705–2716

Zahn C, Keller S, Toro-Nahuelpan M, Dorscht P, Gross W, Laumann M, Gekle S, Zimmermann W,
   Schüler D, Kress H, 2017
   "Measurement of the magnetic moment of single magnetospirillum gryphiswaldense cells by
   magnetic tweezers"
   Scientific Reports **7**, doi: 10.1038/s41598-017-03756-z

Zhao L, Wu D, Wu L F, Song T, 2007
   "A simple and accurate method for quantification of magnetosomes in magnetotactic bacteria
   by common spectrophotometer"
   Journal of Biochemical and Biophysical Methods **70**, pp. 377–383, doi:
   10.1016/j.jbbm.2006.08.010

Abstract

The observation of behaviour of magnetotactic bacteria (MTB) in changing magnetic fields can give significant direct and indirect information about their traits and biophysical properties. Both single and bulk experiment and analysis were performed in this study.

The single cel experiments were performed inside custom microfluidic chips designed to keep the MTB in focus, while a magnet field was applied using a permanent magnet mounted under a microscope stage. Observation and recording of the response allowed for off-line analysis of the trajectories. This analysis has shown that the cells respond differently to varying magnitudes of magnetic field strength.

Furthermore, from simulations and experiments we have found that the drag of the MTB had been underestimated, which lead to additional macroscopic experiments relating morphological traits to more rotational drag profiles. These experiments were done in a vat of silicone oil using 3D-printed models of varying spheroid- and spirillum-based morphologies. The models were based on scanning electron microscope images of actual MTB. Analysis of these experiments elucidated the contribution of traits not included in existing models for rotational drag.

The bulk analysis was performed in a custom made optical density meter, specifically designed to combine magnetic field orientations with photo spectrometry. From our observation we could derive the magnetic response, both absolute and relative, of a given culture or sample of MTB. Additionally, the response time of a given batch could also be measured, relating the magnetic dipole moment with the rotational drag. This allowed distinguishing between different quality and quantity of cultures, as well as long term and continuous observation of a culture in growth.

In spite of having found new traits by which one can more accurately calculate the rotational drag profile, the length of an object still remains the dominate factor when balancing magnetic torque and drag force. Our model does allow for predicting more accurately the rotational drag of objects with shapes similar to MTB in Stokes flow or under low Reynolds number conditions.

Zusammenfassung

Die Beobachtung des Verhaltens von magnetotaktischen Bakterien (MTB) in wechselnde Magnetfeldern kann signifikante direkte und indirekte Informationen offenlegen über deren Merkmale und physiologische Eigenschaften. Sowohl Einzel- als auch Massenanalyse wurden in der vorliegenden Studie durchgeführt. Die Einzelzell-Experimente wurden in einem mikrofluidischen Chip mit maßgefertigtem Design durchgeführt, in welchem die MTB fokussiert werden konnten während ein Magnetfeld mittels eines permanenten Magneten angelegt wurde, welcher unter dem Mikroskoptisch befestigt war. Beobachtungen und Aufnahme der Reaktionen erlaubte eine offline-Analyse der Bewegungsbahnen. Diese Auswertung zeigte, dass die Zellen unterschiedlich reagierten auf Variation der Magnitude der Magnetfeldstärke. Des Weiteren konnte durch Simulationen und Experimente aufgezeigt werden, dass der Widerstand der MTB unterschätzt wurde, was zu zusätzlichen makroskopische Experimenten führte, um eine Verbindung von morphologischer Eigenschaften und Rotationswiderstandsprofilen darzulegen. Diese Experimente wurden durchgeführt in einem Gefäß mit Silikonöl unter Verwendung verschiedener 3D-gedruckter Modelle von verschiedenen ellipsoid- und spirillum-basierenden Morphologien. Die Modelle begründeten sich auf Elektronenmikroskop-Abbildungen von tatsächlichen MTB. Die Auswertung dieser Experimente konnte zur Aufklärung beitragen, dass Eigenschaften der MTB nicht in existierende Modelle des Rotationswiderstandes berücksichtigt werden. Die Massenanalyse wurde durchgeführt in einem maßangefertigtem Optischen-Dichte-Messer, spezifisch hergestellt um Magnetfeld-Orientierungen mit Photospektrometrie zu kombinieren. Von diesen Beobachtungen konnte der magnetische Gehalt von einer MTB-Kultur und Einzelproben abgeleitet werden, sowohl absolut als auch relativ. Zusätzlich wurde die Reaktionszeit einer verwendeten Charge gemessen werden um den magnetischen dipol-Moment mit dem Rotationswiderstand zu korrelieren. Dies erlaubte eine Unterscheidung zwischen verschiedenen Qualitäten und Quantitäten von Kulturen, als auch Langzeit- und kontinuierliche Beobachtung des Wachstumsverhaltens von diesen. Trotz des Auffindens neuer Eigenschaften durch welche eine genauere Berechnung von Rotationswiderstandsprofilen möglich wurde bleibt die Länge eines Objekts weiterhin der dominierende Faktor im Zusammenspiel von magnetischem Drehmoment und Rotationswiderstandskraft. Unser Modell erlaubt eine genauere Vorhersage des

Rotationswiderstandes von Objekten mit ähnlichen Formen wie MTB in Schleichender Strömung als auch Zuständen von geringen Reynoldszahlen.

Samenvatting

Door het observeren van magnetotactische bacteriën (MTB) onder invloed van controleerbare en wisselende magnetische velden kunnen we boekdelen aan informatie op over hun gedrag en reacties op wisselende magnetische velden ontdekken. In deze thesis is zowel gekeken naar de enkele als een grotere verzameling van MTBs.

De MTB hebben van nature een keten van magnetische deeltjes die ze in staat stelt magneetlijnen te volgen. In het eerste deel proberen we met behulp van deze eigenschap inzicht te bieden over het gedrag van een MTB onder invloed van een inverterend magnetisch veld. Hierbij maken de MTBs, onder invloed van het magnetische veld, een zogeheten *U-turn* waarbij de MTB 180 graden draait. De snelheid en vorm van de baan waarin dit plaatsvindt, vertelt wat over het magnetisch dipool moment en de weerstandscoefficiënt van de MTB. Hieruit blijkt dat de baan van de MTB kan worden voorspeld mits de aangewende magnetisch veldsterkte, de specifieke weerstandscoefficiënt en magnetisch dipool moment van de MTB bekend zijn. Tevens is er een limiet in magnetische veldsterkte vernomen waarbij saturatie plaatsvindt en onderscheid tussen U-turns bij hoge velden lastiger wordt door een limiet in de resolutie van de opstelling.

Vervolgens, naar aanleiding van discrepantie tussen metingen en voorspellingen, hebben wij getracht dieper in te gaan op de aspecten van de rotatiönele frictie van een MTB. Hiervoor zijn er 3-D modellen geprint met verschillende facetes van de MTB met variatie in breedte, amplitude en frequentie van de helix-vorm ten opzichte van de lengte. Hieruit blijkt dat er een onderschatte hoeveelheid frictie is ten gevolge van eerder niet meegenomen variabelen in het bestaande model. Dit resulteerde in een analytisch model dat accurater de rotatiönele frictie kan schatten op basis van eigenschappen van de MTB zelf die men door bijvoorbeeld electron microscopie kan achterhalen.

In het laatste deel wordt het gedrag van de bulk geanalyseerd door middel van een zelfgebouwde photospectrometer in combinatie met een bestuurbare set elektromagneten. Deze observaties leveren ons informatie waarmee we de relatieve en absolute aantallen magnetische MTBs kunnen bepalen in een heterogene cultuur. Dit is een kwantitatieve methode die de kwaliteit van een kweek in enkele seconde maar ook over meerdere dagen kan bepalen. Daarnaast is ook de temporale resolutie van ongekend niveau en laat zien dat er nog veel te

halen valt uit dit onderzoek.

요약

자기장 변화에 따른 주자성 세균 (MTB) 의 행동양상을 관찰한 결과, 생물 물리 학적 특성에 대한 직접적이고 간접적 인 정보를 얻을 수 있었다. 이 연구에서는 단일 및 대량 실험 및 분석이 모두 수행되었다.

단일 세균을 이용한 실험은 현미경에 장착 된 영구 자석을 사용하여 자석 필 드가 적용되는 동안 MTB의 초점을 유지하도록 자체 제작된 맞춤형 미세 유체 칩 내부에서 수행되었다. 이 시스템은 단일 세균의 다양한 반응에 대한 관찰 및 기록은 궤적 추적을 위한 오프라인 분석을 가능하도록 하였다. 이 분석은 세포가 다양한 세기의 자기장 강도에 다르게 반응한다는 것을 보여주었다.

또한, 시뮬레이션과 실험을 통해 우리는 MTB의 항력이 과소 평가되었다는 사실을 발견했다. 이 러한 새로운 사실은 형태학적 특성과 더 많은 회전 항력 프 로파일을 관련시키는 추가적인 거시적 실험을 추가하도록 유도하였다. 따라서, 실제 MTB의 주사 전자 현미경을 통한 결과를 기반으로. 다양한 타원형 및 나 선형 기반 형태의 실리콘 기름을 이용한 3D 인쇄 모델을 이용하여 새 시스템을 제작하였다. 이 시스템을 이용한 실험의 결과는 회전 항력에 대한 기존 모델에 포함되지 않은 새로운 모델을 제시하였다.

대량 분석은 자체 제작된 광학 밀도 측정기에서 수행되었으며, 특히 자기장 방향과 광 분광법을 결합하도록 설계되었다. 앞에서 열거한 시스템을 바탕으 로 한 실험을 수행한 결과, 배양이나 MTB샘플에 관한 표본의 절대 및 상대적인 자기적 함량에 대한 수치를 도출 할 수 있었다. 또한, 위 대량배양 모델에 대한 반응도를 관측한 결과, 이는 자기 쌍극자 모멘트와 회전 항력과 관련이 있음을 시사하였다. 이것은 MTB의 배양에 관한 질적 양적 표준화 및 장기간 걸친 배양 기간 동안의 실시간 관측이 가능한 시스템을 제시하였다.

이번 연구를 통하여, MTB의 회전 항력을 보다 정확히 프로파일을 계산할 수 있는 새로운 특성을 발견 했음에도 불구하고, 자기 화전력과 항력 사이의 균형을 유지할 수 있는 조건을 만족시킬 수 있는 대상의 길이는 여전히 주요한 요소로 작용될 것으로 간주된다. 또한, 스톡스 흐름 또는 낮은 레이놀즈 수 조건에서 의 MTB와 유사한 모양을 가진 물체의 회전 저항을 더 정확하게 예측할 수 있는 시스템을 구축하였다.

Acknowledgments

The author would like to thank the following people for their valuable comments, discussions and encouragement during the entirety of the thesis duration.

Leon, I sadly miss the words to thank you properly without saying what many before me probably thought. Similar to Tijmen's situation, someone once told me that the most important decision you make during a PhD is to find the right supervisor. For many reasons that has been you. You have been a fantastic boss, a critical mind to look up to, a shaper of my mind, supervisor for the past four years, a caring person and, most importantly in my case, a very patient human being. Thank you for the relentless support you have offered, for the scientific and fun discussions, for the many things you have taught me in words and drawings, and for forcing me to think more critically about life in the past and most certainly in the future. I even got to meet one of the Mythbusters, which took some time to sink it, but was one of the most inspiring moments in my life. I have many things to be thankful for and hope to someday return the favour. Thank you for believing in me when I could not.

Tijmen, it has been a long time working side by side. At least that is what it says on paper, because it feels like it flew by! Aside from being one of the few dutch people to talk to at KIST, you have also been a fellow PhD student going to similar struggles and highs. Yet I am often the one turning to you for help. No doubt this is because you invite people to trust in and rely on you. Seeing how you have handled obstacles up close, has made me a better person in so many ways. Your patience seems to know no bounds, yet you can speak up when things really matter. I really admire that in you and hope to get to that level of thinking one day. Many thanks also for being my paranymph! As I said before, without you I doubt I would have ever made it this far, so a fitting end to these last few years. Most of all though, I look forward to all the adventures we will undertake together in the future!

Vanessa, where should I start? I feel like we went through hell and back, together! The Tough Mudder races seem like a distraction from the weight of doing a PhD. We talked just moments before I wrote this, so everything that I want to tell you, you already know. Our lingua franca may consists mostly of hugs and smiles, but I would like to believe our friendship is based on a mutual understanding between human beings. I miss you a lot and I hope I get to see

I would also like to thank all the people at GUC in Egypt with whom I have worked and laughed together. Nermeen, thank you for the Koshari and warm hospitality. Islam, thank you for the supervision during my master project and discussions over the last years leading into this milestone. Thank you to all the students and teachers from GUC I've had the pleasure and honour of working with; Heba, Osama, Abdelmomen, Karim, Ola, Noura, Maram, Negi, Abelrahman, Mohamed and Elwi. Shukran!

Thank you all, members of the committee, for taking my thesis into consideration and making this defence possible; Leon Abelmann, Gijs Krijnen, Jennifer Herek, Joost Kok, Andreas Manz, Matthias Nienhaus, Andriy Luzhetskyy and Jan Eijkel.

Een hartelijke dank aan mijn familie die me altijd hebben bijgestaan in zowel mijn doordachte als ondoordachte keuzes. Ook ben ik erg dankbaar voor jullie vele bezoeken en de moeite die jullie hebben genomen om de Saarbrücken ervaring met me te delen. Dank jullie wel Adri, Gerard (ook voor je rol als paranymph) en Eric.

Men spreekt wel eens als de grote filter omtrent het universum en wat er allemaal overblijft nadat de tijd passeert, met vrienden is het net zo. In dit geval is de filter de afstand en maakt dat voor echte vriendschappen niet uit. Daarom wil ik jullie ook nog bedanken voor alle bezoekjes, gedeelde drankjes, pannenkoeken, bordspellen en natuurlijk goede gesprekken; Esmeralda, Berry, Remco, Edo, Wing, André, Ward, Esther, Tjerk, Pauline, Marjolein, Barend.

Tevens een speciaal bedankje voor de mensen van Campuslaan 71 is ook op zijn plaats. De oude en de nieuwe bewoners van Huize Schommelbank; Daniël, Lisanne, Joost, Floor, Ivo, Joyce, Gerben-Jan, Sam, Ellen, Fenna, Simon, Marloes, Steven, Vonne, Jelmer, Marjolijn. Bedankt dat jullie met zoveel die trip hebben gemaakt aan het begin van mijn tijd in Duitsland. Het was een hart onder de riem en betekende meer voor me dan jullie je kunnen voorstellen, vermoed ik. Ook wil ik de huidige bewoners bedanken voor hun gastvrijheid en gezelligheid over de afgelopen jaren. Het voelt nog steeds als een tweede thuis om bij jullie op bezoek te mogen komen.

To those making Saarbrücken such an amazing place to live, I miss hanging out with you guys a lot. The culinary exploration of the city, the city trips, the live music, the festivals, I am very grateful for having been able to share that with you guys; Henrique, Philip, Joanna, Lara, Samir, Pichelidoo's favorite German: Markus, Stefi, Maria, Sophie, Elidjona, Mohammad, Aleks, James, Dee, 'Welsh' Chris, Raveen, Dee, Kleo, Tim, Esther, Marouane, Monika, Sebastian, Valentina, Gloria, Bryan, Fraser, Johannes, Kap, Michael, Zhe and, last but not least, the epic Dhananjay!

I have had the pleasure and honour of sharing a house with Rüdiger, Jules, Sebastian, Mattieu, Marius and Minako over the years. Vielen Dank, for all for the evenings filled with games, movies, drinks and for updating my German vocabulary.

These four years have been filled with the joy of meeting and greeting more new people than I expected to meet. If I happened to have met you, but forgot

to mention your contribution, this is for you: Thank you.

Publications

Journal articles

Hageman T A G, Pichel M P, Hendrix J, Keizer H, Manz A, Abelmann L, 2018b
"Real-time monitoring of growth and magnetic properties of magnetotactic bacteria via optical density"
(in preparation)

Khalil I S M, Pichel M P, Abelmann L, Misra S, May 2013
"Closed-loop control of magnetotactic bacteria"
The International Journal of Robotics Research **32**, pp. 637–649, doi: 10.1177/0278364913479412

Pichel M P, Hageman T A G, Khalil I S M, Manz A, Abelmann L, 2018
"Magnetic response of magnetospirillum gryphiswaldense"
(under review) arXiv:1710.00405

Book chapters

Khalil I S M, Pichel M P, Zondervan L, Abelmann L, Misra S, 2013
"Characterization and control of biological microrobots"
In: *Experimental Robotics, Springer Tracts in Advanced Robotics*, volume 88, pp. 617–631, Springer Verlag, Bern, Switzerland

Conference contributions

Abelmann L, Pichel M, Hageman T, Manz A, 2016
"Response of magneto-tactic bacteria to a rotating magnetic field"
In: *Joint MMM-Intermag Conference*,

Hageman T, Pichel M, Altmeyer M, Manz A, Abelmann L, 2015
"Planar manipulation of magneto-tactic bacteria using unidirectional magnetic fields"
In: *MicroTAS 2015 - 19th International Conference on Miniaturized Systems for Chemistry and Life Sciences*, pp. 716–718,

Hageman T A G, Pichel M P, Altmeyer M O, Abelmann L, Manz A, 2014
"An integrated magnet array for trapping and manipulation of magnetotactic bacteria in microfluidics"
In: *Micromechanics and microsystems Europe workshop*,

Hassan H, Pichel M, Hageman T, Abelmann L, Khalil I S M, 2016

"Influence of the magnetic field on the two-dimensional control of magnetospirillum gryph-iswaldense strain msr-1"
In: *Proceedings of the IEEE International Conference on Intelligent Robots and Systems (IROS), Daejeon, Korea*, pp. 5119–5124,

Khalil I S M, Tabak A F, Hageman T, Ewis M, Pichel M, Mitwally M E, El-Din N S, Abelmann L, Sitti M, 2017
"Near-surface effects on the controlled motion of magnetotactic bacteria"
pp. 5976–5982, doi: 10.1109/ICRA.2017.7989705

Pichel M, Hageman T, Altmeyer M, Abelmann L, Manz A, 2014
"Magnetic manipulation of bacteria in microfluidics"
In: *MicroTAS 2014, 18th International Conference on Miniaturized Systems for Chemistry and Life Sciences*, pp. 721–723,

Pichel M, Hageman T A G, Manz A, Abelmann L, 2016
"Towards measuring motile magnetic fractions of magnetotactic bacterial cultures"
In: *Micromechanics and microsystems Europe workshop,*

Pichel M P, Hageman T A G, Altmeyer M O, Abelmann L, Manz A, 2014
"Dynamics and magnetic control of magnetotactic bacteria u-turn trajectories in micro-fluidics"
In: *Micromechanics and microsystems Europe workshop,*

Pichel M P, Hageman T A G, Altmeyer M O, Abelmann L, 2015
"U-turn trajectories of magnetotactic bacteria in microfluidics"
In: *Micromechanics and microsystems Europe workshop,*

Biography

Marc Pichel was born on the 21th of November 1982 in the city of Rotterdam, the Netherlands. He enjoyed an education at several schools in the Netherlands, Africa and Indonesia. In 2004 he started his BSc Biomedical Engineering at the University of Twente and formal education for the position of judo teacher. In 2008 he moved to Enschede and went on to receive his BSc in 2011 and his MSc in 2013 after finishing his thesis on closed-loop control of magnetotactic bacteria. During his study period he spent time on student boards and committees relating to sports, culture and non-profit organisations like the royal institute of engineers (KIVI) and Amnesty International. In this time he was part of the committee which organised the 2011 'KIVI NIRIA Wetenschapsquiz' in the wake and light of Twente University's 50-year anniversary, which brought national attention to the university. He also holds a third degree black belt in Jiu Jitsu and a first degree black belt in Judo. This paved the way for time spent as substitute teacher at the student martial arts organisation V.A.S. Arashi, making a martial arts movie set in Enschede, the hometown of the University of Twente, and attaining a 4th place in the national 'E-bo-no-kata' competition in 2008. In 2013 he started as a PhD candidate at KIST Europe in Germany under guidance of Prof. Dr. Ir. Leon Abelmann, which resulted in this thesis. During this period he supervised several students, taught practical courses for the University of Saarland and discovered a passion for creative writing and scuba diving.